AN ABSTRACT OF THE THESIS OF

YUAN-SHOU SHEN (Name) for the DOCTOR OF PHILOSOPHY (Degree)

in Mechanical Engineering (Materials Science) (Major) presented on September 28, 1967 (Date)

Title: THE PHASE DIAGRAM OF ZIRCONIUM AND CHROMIUM WITH SPECIAL REFERENCE TO THE TRANSFORMATION IN THE INTERMETALLIC COMPOUND $ZrCr_2$

Redacted for privacy

Abstract approved: O. G. Paasche

The zirconium-chromium phase diagram was investigated in the region between 40% and 85% chromium. The $ZrCr_2$ intermetallic compound which has been the source of some controversy was especially considered. It was found that $ZrCr_2$ transforms from the low temperature C-15 ($MgCu_2$, FCC) structure to the high temperature C-14 ($MgZn_2$, HCP) structure between 1550°C and 1600°C, just the opposite transformation from previously reported results.

X-ray diffraction and metallographic methods were used to determine that this transformation is a shear type transformation which occurs on the (111) plane along the $[1\bar{1}2]$ direction.

The shear mechanism involved in the transformation was determined as a sluggish martensitic transformation.

The Phase Diagram of Zirconium and Chromium with Special Reference to the Transformation in the Intermetallic Compound $ZrCr_2$

by

Yuan-Shou Shen

A THESIS

submitted to

Oregon State University

in partial fulfillment of
the requirements for the
degree of

Doctor of Philosophy

June 1968

APPROVED:

Redacted for privacy

Professor of Mechanical Engineering

in charge of major

Redacted for privacy

Head of Department of Mechanical Engineering

Redacted for privacy

Dean of Graduate School

Date thesis is presented September 23, 1967

Typed by Clover Redfern for Yuan-Shou Shen

ACKNOWLEDGMENT

The author is grateful to Professor O.G. Paasche of the Oregon State University Department of Mechanical Engineering for his kind guidance, valuable suggestions and patience in the preparation of this dissertation. He is further indebted to Mr. M.B. Siddell and Dr. C.J. Sandwith for their valuable assistances. He wishes to give his special thanks to Mr. S.A. Worcestor and Dr. B. Kieffer, both of Wah Chang Albany Corporation for their inspiring technical and philosophical discussions.

TABLE OF CONTENTS

LIST OF FIGURES

Figure Page

Figure Page

Figure Page

LIST OF TABLES

THE PHASE DIAGRAM OF ZIRCONIUM AND CHROMIUM WITH SPECIAL REFERENCE TO THE TRANSFORMATION IN THE INTERMETALLIC COMPOUND $ZrCr_2$

I. PURPOSE

The purposes of this investigation were (1) to explore and determine the manner of allotropic transformation of intermetallic compound $ZrCr_2$, which has been a dispute since 1942; (2) to find out whether there was any kind of solid state transformation within the region of the composition of intermetallic compound $ZrCr_2$; (3) to determine the habit plane of the allotropic transformation of $ZrCr_2$; and (4) to propose a postulation explaining the transformation mechanism from the C-15 structure to the C-14 structure.

II. THEORETICAL BACKGROUND

A. The Phase Diagram of Zirconium and Chromium

1. History and General Discussion

The first investigation of the zirconium and chromium system was reported by McQuillan in 1951 (29). The material used was magnesium reduced zirconium and electrolytic chromium, both relatively impure materials. All alloys were prepared by arc-melting under argon atmosphere. It was predicted that this diagram should be similar to the titanium and chromium diagram, because both zirconium and titanium are Group IVB materials. Figure 1 shows McQuillan's diagram. An intermetallic compound Cr_3Zr_2 formed by the reaction: $Zr(\beta) + L \rightarrow$ compound, occurs at 62 a/o of chromium (Note: In this thesis, a/o represents atomic percent and w/o, weight percent). McQuillan found that chromium dissolved in beta zirconium up to about 40 a/o. The complete diagram consists of one eutectoid between zirconium and the compound, and one eutectic between chromium and the compound.

Hayes, et al. (23) studied the zirconium and chromium alloy system up to 60 a/o of chromium. The alloys were also made by means of arc-melting magnesium reduced zirconium and electrolytic chromium under argon atmosphere. From Figure 2, it can be seen

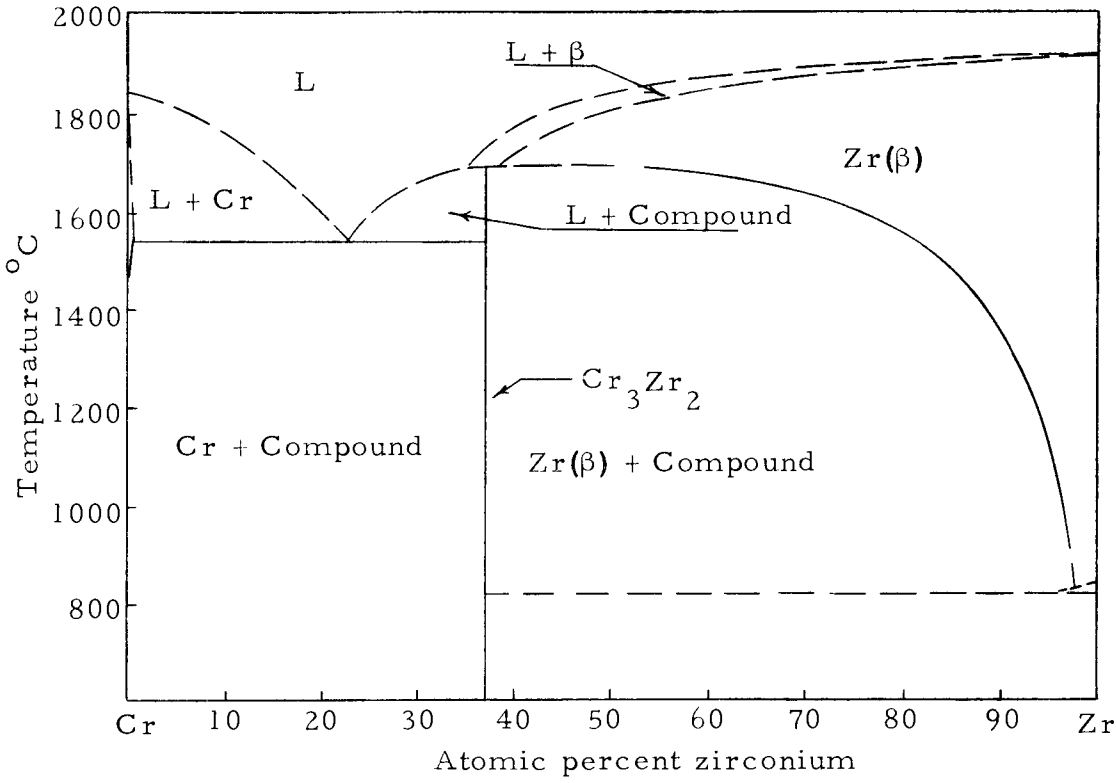

Figure 1. Phase diagram of the Zr-Cr system after McQuillan.

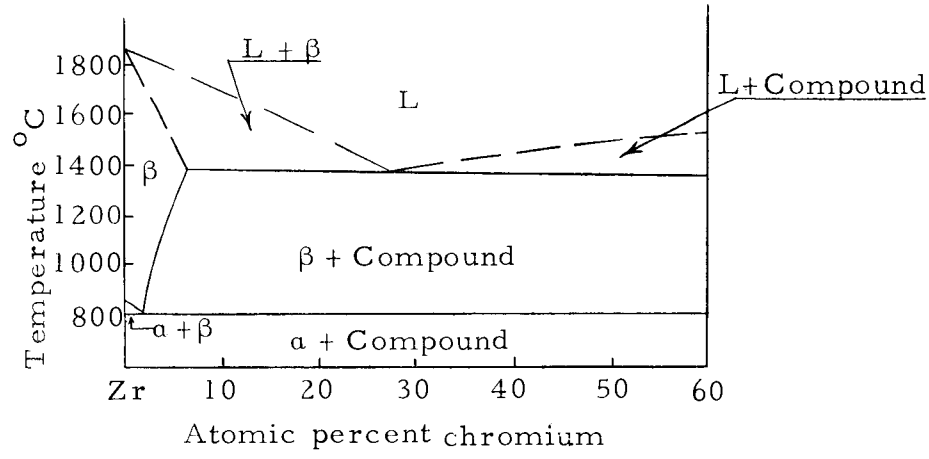

Figure 2. Phase diagram of the Zr-Cr system after Hayes.

that their results are quite different from McQuillan's. The region of solid solution of chromium in zirconium is limited to 4.5 a/o of chromium. There is one eutectoid and one eutectic between pure zirconium and the compound. In the discussion with McQuillan (23), Hayes argued that extensive solubility of chromium in zirconium is not likely, because the atomic dimensions of zirconium and chromium differ by considerably more than 15%.

Later in 1953, Domagala, et al. (11) presented results of their work on the complete diagram using iodide zirconium crystal bar of 99.8 w/o purity, and electrolytic chromium. Their phase diagram (Figure 3) agrees with Hayes' results on the zirconium rich side, and confirmed the existence of $ZrCr_2$ rather than Zr_2Cr_3. As shown in Figure 3, they proposed that the zirconium and chromium diagram consisted of one eutectoid $(Zr(\beta) \rightarrow Zr(\alpha) + ZrCr_2)$ at 1.7 a/o of chromium, two eutectics $(L \rightarrow Zr(\beta) + ZrCr_2$ and $L \rightarrow Cr + ZrCr_2)$ at 28 a/o and 80 a/o chromium, respectively, and the intermetallic compound at 66.67 a/o chromium. The solubility of chromium in alpha zirconium is nil, but is up to 5 a/o in beta zirconium. The solubility of zirconium in chromium is 1.5 a/o at $1630^{\circ}C$. This diagram has been accepted and published in Hansen's "Constitution of Binary Alloys" (22, p. 573).

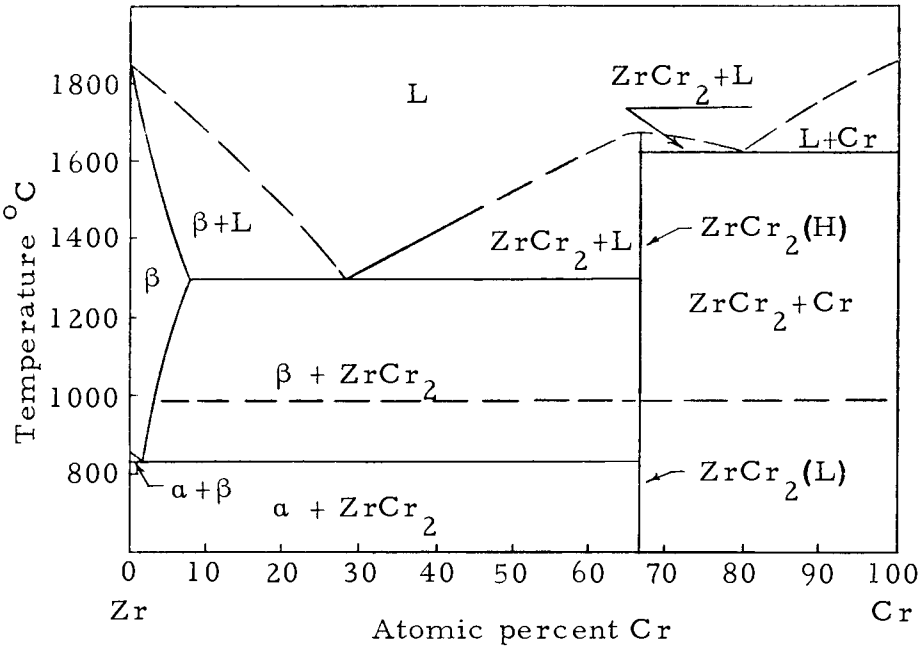

Figure 3. Phase diagram of the Zr-Cr system after Domagala.

2. The Transformation of $ZrCr_2$

a. The Contradictions of Previous Research. The region of the intermetallic compound $ZrCr_2$ in the zirconium-chromium diagram shows special interest and is worthy of further investigation because previous research has shown disagreement concerning crystal structures and the manner of transformation.

The crystal structure of $ZrCr_2$ was first determined to be hexagonal $MgZn_2$ (C-14) type structure by Wallbaum (36) as early as 1942. Hayes et al. (23) reported that the crystal structure of $ZrCr_2$ was a cubic $MgCu_2$ (C-15) type with $a = 7.21\text{Å}$. However, Domagala (11) supported Wallbaum's finding that the structure was hexagonal with a lattice parameter $a = 8.262\text{Å}$, and $c = 5.079\text{Å}$.

Rostoker (33) conducted a series of tests to determine the structure of $ZrCr_2$. He quenched a series of specimens from various temperatures and concluded that a polymorphic transformation took place in which $ZrCr_2$ transformed from the C-14 type at low temperature to the C-15 type at a temperature between 900° and $994^{\circ}C$.

Jordan, et al. (26) studied this transformation by long time (seven days and ten days) annealing of specimens at five different temperatures. He annealed two specimens above $980^{\circ}C$ and two below $760^{\circ}C$. One specimen was heated to $980^{\circ}C$ then heated to near

the melting point. He concluded that $ZrCr_2$ existed as C-15 type at low temperatures and C-14 at high temperatures, the opposite of the previous investigators. He did not determine the transformation temperature, but he said that the transformation temperature should be near the melting point.

Elliott (14) supported Rostoker's finding. In his experiments, he heated one specimen at 800°C for 48 hours, and another at 1000°C for 24 hours. From powder X-ray diffraction patterns, he determined $ZrCr_2$ to be C-14 structure below 800°C, and C-15 structure above 1000°C.

Hansen (22, p. 573), in his book, did not draw any conclusions on the allotropic transformation of $ZrCr_2$, although he seemed to favor Elliott's work. He indicated a transformation at 1000°C and identified the two structures as $ZrCr_2$(L) and $ZrCr_2$(H).

The disagreements mentioned above may result from sluggishness of the solid state tranformation. Jordan mentioned such a possibility in his work but did not verify it. The major objective of this thesis is to resolve these conflicts and to determine the nature and mechanism of the transformation.

b. Possible Occurrence of Phase Transformation in a Small Region in the Neighborhood of $ZrCr_2$. One method to investigate the possible occurrence of alloy behavior of one element is to compare

this element with another element with similar physical and chemical properties. This approach is now applied in this investigation by comparing the element titanium with the element zirconium.

Referring to Table 1, one can see that both zirconium and titanium are quite similar in many respects. They both belong to group IVB in the periodic table and have the same electron configuration (d^2s^2) outside of the inert gas core. The difference between their melting points is only 9.9%. The difference between their boiling points is even less: 8.8%. Other properties of these two elements such as heat of fusion, electronegativity, and first ionization potential are even closer. They have the same oxidation state, and the same allotropic crystal transformation: close-packed hexagonal structure at low temperature, and body-centered cubic structure at high temperature. Hence a review of the titanium and chromium alloy system is beneficial.

Table 1. Comparison of titanium and zirconium.

	Titanium	Zirconium
Group number	IVB	IVB
Electron configuration	(Ar)$3d^2 4s^2$	(Kr)$3d^2 4s^2$
Melting point ^oC	1668	1852
Boiling point ^oC	3260	3580
Oxidation state	4	4
Crystal structure	HCP & BCC	HCP & BCC
Atomic Radius Å	1.47	1.60
Electronegativity (Pauling's)	1.50	1.40
First ionization potential (Kcal/g-mol)	158	160

The phase diagram in Hansen's "Constitution of Binary Alloys" is shown in Figure 4 (22, p. 566). In this diagram, one can see that the region close to the intermetallic compound $TiCr_2$ is not well defined. $TiCr_2$ exists in the form of hexagonal C-14 type structure at high temperature, and in the form of C-15 structure at low temperature. The transformation takes place somewhere between 1000°C and 1300°C (22, p. 567).

In 1963, Farrar et al. (17) reinvestigated the titanium-chromium diagram, and concentrated their attention on the region close to the intermetallic compound. They discovered one peritectoid reaction and one eutectoid reaction within a narrow region between 65 to 68 w/o of chromium. Their findings are reproduced as shown in Figure 5.

Comparing the Zr-Cr phase diagram (Figure 3) and the Ti-Cr phase diagram (Figure 4), one can see the difference and the similarity between these two phase diagrams. The main difference between these two diagrams is that a continuous solid solution region occurs between beta titanium and chromium, whereas in the zirconium-chromium system only limited solid solubility is found in beta zirconium. Other than that, the general features of these two diagrams are quite similar. A pseudo-eutectic (or minimum melting) point which occurs at the left of the intermetallic compound in the Ti-Cr diagram corresponds to the eutectic point on the Zr-rich side of Zr-Cr diagram.

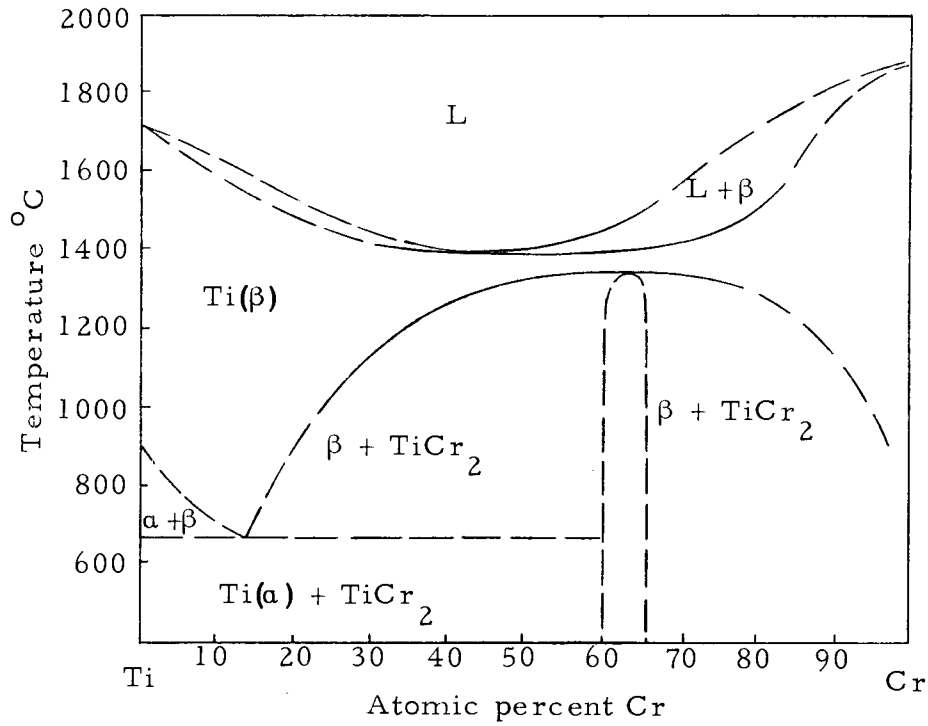

Figure 4. Ti-Cr phase diagram (Hansen).

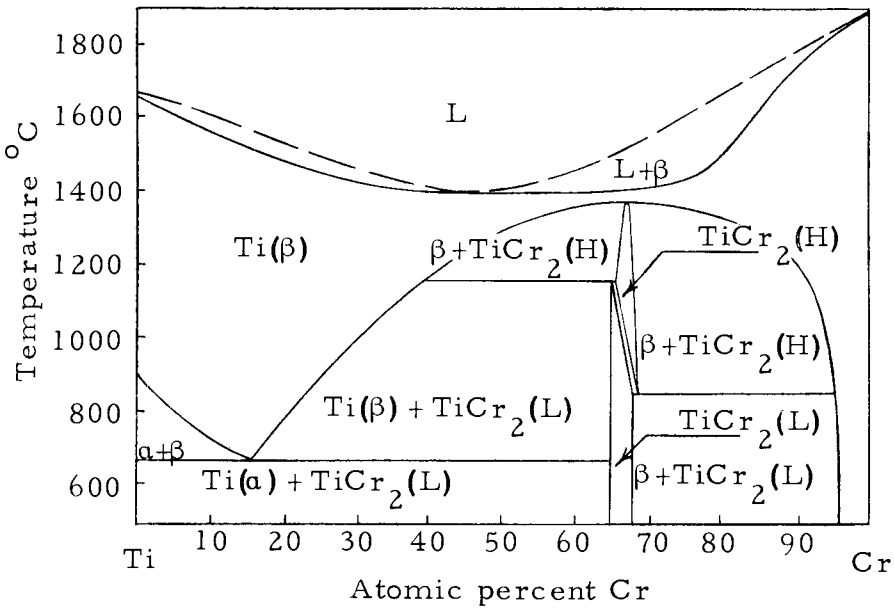

Figure 5. Ti-Cr phase diagram (Farrar).

Both diagrams have one eutectoid reaction to the left of 66.67% chromium. The solubility of chromium in either alpha-titanium or alpha-zirconium is very limited. An intermetallic compound occurs at about 67% of chromium in each diagram. Both intermetallic compounds have an allotropic transformation. In the case of $TiCr_2$, it exists in the C-15 type structure at low temperatures and C-14 type structure at high temperatures. $ZrCr_2$ similarly exists in either C-14 type structure or C-15 type structure, although the manner of transformation is yet to be decided.

The only difference between zirconium and titanium alloying behavior with chromium is due to the atomic size. The atomic diameters of zirconium, titanium and chromium are 3.19 Å, 2.93 Å, and 2.57 Å respectively. The atomic size difference between titanium and chromium is 12.3 percent, while that between zirconium and chromium is 19.4 percent. Therefore, the complete solubility shown by chromium in titanium is not expected in zirconium-chromium diagram. Other than that, the similarities of the other important characteristics such as electronegativity, valence, and crystal structure, lead us to expect that the allotropic transformation of $ZrCr_2$ might be C-14 at high temperature and C-15 at low temperature, and that some sort of transformation would occur in the neighborhood of $ZrCr_2$.

B. The Laves Phase

1. Definition

A Laves phase in a binary alloy system is a type of intermetallic compound whose crystal structure is limited to one of the crystal structures C-14 ($MgZn_2$, HCP), C-15 ($MgCu_2$, FCC), and C-36 ($MgNi_2$, HCP) (4, p. 256). Almost all of the previously discovered Laves phases are of the composition AB_2 where the size of atom "A" is greater than that of atom "B". Recent (30) research on the phase diagram of niobium and cobalt disclosed that the Laves phase exists in the composition of $NbCo_3$ as well as $NbCo_2$ with crystal structures C-36 and C-14 respectively. Therefore Laves phases might be found in more than one composition in binary alloy systems.

2. Crystal Structure

The three crystal structure types of Laves phases are closely related. Their only difference is in the stacking arrangement (7).

All "A" atoms, which are larger, are arranged in the form of a tetrahedron with one atom at the center. Each "A" atom is surrounded with four other "A" atoms, and twelve "B" atoms. Thus the coordination number of the "A" atom is 16. The "B" atoms are also arranged in tetrahedra but all "B" atoms are located at the corners only;

thus, each "B" atom is surrounded with six "A" atoms and six "B" atoms. Therefore, the coordination number of the "B" atom is 12. Elliott and Rostoker (16) averaged these two numbers and assigned the coordination number for the Laves phase as 13.33.

The ideal atomic radius ratio for the closest-packed structure of this kind of atomic arrangement should be 1.225 (21). It has been found that in Laves phases, the summation of R_A (radius of the large atom) and R_B (radius of the small atom) is less than the distance between the centers of atoms "A" and "B". Hence, atom "A" should not be in contact with atom "B", if we assume the atoms to be rigid spheres.

A brief description of the three different crystal structures of Laves phases is given as follows:

1) C-14, $MgZn_2$ type: The unit cell of this structure is of the hexagonal type and consists of 24 atoms. Friauf (17) determined the position of each atom in the space lattice. Its designation in the International Crystallographic Tables is $P6_3/mmc$ (24, p. 304). The tetrahedra, where all small "B" atoms are arranged at their corners join alternately, point to point and base to base to form the complete network (Figure 6). This type of array provides large holes in which the large magnesium atoms are fitted. With respect to magnesium atoms the atom layers stack in the

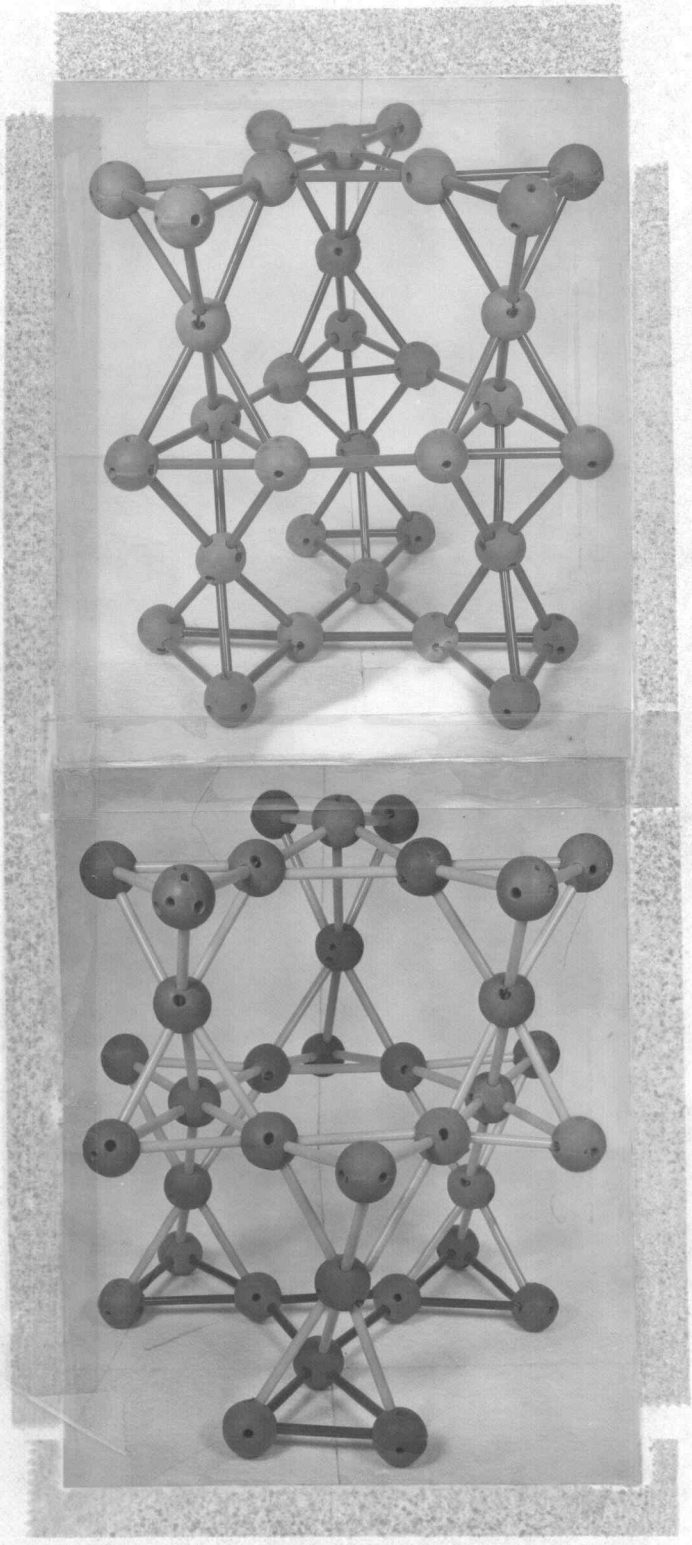

Figure 6. The arrangements of "B" atoms in the C-14 and the C-15 structures.

Top: C-14
Bottom: C-15

order of ABABAB.

2) C-15, $MgCu_2$ type: The unit cell of this structure is of cubic symmetry and consists of 24 atoms. The positions of the atoms were also determined by Friauf (18). The crystal symmetry is designated as Fd3m (24, p. 340) in the International Crystallographic Tables. The tetrahedra with "B" atoms at the corners join point to point throughout the whole network (Figure 6). As in the C-14 type, holes are also formed in this network to accommodate large magnesium atoms. With respect to magnesium atoms the atom layers stack in the order of ABCABC.

3) C-36, $MgNi_2$ type: The unit cell of this structure is of hexagonal symmetry. The atom layers, with respect to magnesium atoms, stack in the order of ABACABAC. It is generally recognized as a transition structure between the C-14 and C-15 structures (20).

3. The Formation of Laves Phases

a. The Size Factor. Based on Hume-Rothery's rules of alloying behavior of metals Laves (28) developed three general principles to explain the relationship of all elements between Groups IA and IIIA in the periodic table including all transition elements and their crystal structures. He also used these principles to explain the formation

of Laves phases. His principles may be stated briefly as follows:

1) Space principle: Metallic elements between Groups IA and IIIA generally tend to be close-packed. Therefore, each element tends to have a coordination number of 12. The coordination number generally decreases with increasing temperature. For example, 11 elements with closest-packed structures transform to body-centered cubic structures at higher temperatures.

2) Symmetry principle: Elements which do not have the closest-packed structure, usually follow the structure of highest symmetry. Thus, the coordination number, eight (body-centered cubic) prevails more than other coordination numbers 7, 9, 10 or 11.. Directed bonds with high strengths may form relatively low coordination structures. Rising temperature may weaken the directed bonds and eventually make the element follow the "space principle". Examples are chromium and iron. Their structures are body-centered cubic at room temperature and transform to close-packed structures at high temperature.

3) Connection principle: In a structural arrangement, each atom is connected with all the others. If only the shortest links are considered, those atoms which are connected with each other are said to form a "connection". The connections

can be finite or infinite, and can extend in one, two, or three dimensions, and accordingly can be categorized as islands, chains, (one-dimensional), nets (two-dimensional) and lattices (three-dimensional). It is a principle that the atoms tend to form connections of higher dimensions, i.e. all atoms tend to form lattices.

Applying these principles to the Laves phases, it can be seen that the C-14, C-15, and C-36 types of structures satisfy these three basic principles because they are close-packed (principle 1), highly symmetrical (principle 2), and form three dimensional lattices (principle 3). Laves (28) concluded that when the radius ratio (Goldschmitt's radius) of element A(R_A) and element B(R_B) is close to 1.225 and when low free energy of mixing occurs, these two elements should crystallize in one of the C-14, C-15, or C-36 types. The formation of the intermetallic compound is not necessarily dependent on a fixed ratio of valencies but rather on the geometric properties of the elements. When the radius ratio is different from 1.225, as in most Laves phases, "A" and "B" atoms will mutually adjust their size to meet the geometric requirement (19). When $R_A : R_B$ is greater than 1.225, the "A" atom demonstrates a size contraction, otherwise size expansion. The "B" atom behaves just the opposite. Owing to the radius adjustment, Laves phases can occur over a great range of size variations. Laves phases have been discovered occurring at the

values of $R_A : R_B$ between 1.049 ($TiZn_2$) (32, p. 877) and 1.668 ($BaRh_2$) (37).

b. The Electronic Structure Factor. Atomic size is not considered to be the only factor forming Laves phases, many combinations of elements having radius ratios falling in the proper range do not form Laves phases. For example, in the alloy systems, Hf and Cu, Hf and Ni, each radius ratio lies within the range 1.10 and 1.30, but do not form Laves phases. Investigators, therefore, concentrated their attention principally on electron configurations.

Elliott and Rostoker (16) postulated that the ratio between the numbers of valence electrons and atoms governed the formation and the crystal structure of Laves phases. They assume the critical electron-to-atom ratios of 1.80 and 2.32 govern the range of stability of C-14 or C-15 types of structure as follows:

if

$e/a < 1.4$, no Laves phases occur;

$1.4 < e/a < 1.8$, C-15 structure predominates;

$1.8 < e/a < 2.3$, C-14 structure predominates;

$2.3 < e/a$ C-15 structure predominates;

where "e" is the number of valence electrons and "a" is the number of atoms. Based on this postulation, they designated a valence electron number for each element. Their postulate appears applicable

to Laves phases formed from some of the titanium group elements, but they cannot explain the Laves phases formed by the scandium group such as $ScNi_2$ (e/a is less than 1.17 but forms C-14 type) and others. According to their theory, the valence electron numbers are assumed to be 3.92, 3.25, and 1.69 for the elements titanium, zirconium and chromium respectively. Thus the e/a value for $ZrCr_2$ and $TiCr_2$ would be 2.21 and 2.63. Therefore, they concluded that the structure of $ZrCr_2$ would be C-14 type, and $TiCr_2$ would be C-15 type at low temperatures. However, in this thesis, it has been found that $ZrCr_2$ exists in C-15 type at low temperature.

Dwight (13) postulated, based on the 164 known Laves phases, that the selection of the crystal structure of a Laves phase is governed by periodic table relationships. This could be described by a graph with "B" components arranged along the X-axis according to the sequence of the atomic number in each long period and a Y-axis scale in arbitrary units, representing the index of "electron : atom ratio" (essentially the same as that used by Elliott and Rostoker). The Y-axis is partitioned into three bands representing two zones of stability for the C-15 type and one zone in between for the C-14 type. A smooth curve can be plotted showing that the structure of a series of AB_2 compounds, each made from a fixed "A" component and different "B" component, changes from the C-15 type to the C-14 type and then again to the C-15 type. While this postulate can be

applied to most Laves phases, it can not explain why in most cases no Laves phase is formed when Au, Ag, or Cu is the "B" element.

Bardo et al. (3) postulated that the occurrence of the Laves phases depends on the total electron concentration outside of the inert gas core. Let N_e be the total number of electrons outside of the inert gas cores of the elements in the compound, and N_a be the total number of elements in the compound. If the ratio of N_e to N_a is less than eight, the Laves phases will occur. According to Bardo's theory, $TiNi_2$ does not exist in the form of a Laves phase because its $N_e:N_a$ ratio is eight. When nickel in this compound is replaced with 25% silicon, the compound $TiNi_{1.5}Si_{0.5}$ will exist in the form of C-14, because now the value of N_e/N_a becomes seven. Bardo verified this theory by making a series of the ternery Laves phases; however, this theory cannot explain the occurrence of the following Laves phases: $UNi_2(N_e:N_a = 8.67)$, $UIr_2(N_e:N_a = 8)$, $PuRu_2(N_e:N_a = 8)$ and some others.

In reviewing all the existing electron concentration theories concerning Laves phases, one tends to agree with Rundle's statement (34) that there is as yet no real theory of metals and alloys. Each theory has its limitations, because its conclusions are usually drawn from existing empirical data. A more complete theory can be developed when more data become available in the future.

III. EXPERIMENTAL WORK

A. Alloy Preparation

1. Material

Alloys employed for this experiment were prepared from zirconium supplied by the Wah Chang Corporation, Albany, Oregon, and chromium supplied by the United States Bureau of Mines (USBM). The description of the raw material is as follows:

1) Zirconium: Two different kinds of zirconium were used for preparing two different batches of alloys. Zirconium for the first batch was of reactor grade in sheet form. Zirconium crystal bar reduced through decomposition of zirconium iodide vapor was used for the second batch of alloys. Their analyses are shown in Table 2.

2) Chromium: Electrolytic ingot. Its analysis is shown in Table 2.

2. Equipment

The button furnace for preparing the alloys was built by United States Bureau of Mines in Albany, Oregon. Its major components consisted of a vacuum system, a furnace assembly, a power supply system, a water cooling system, and argon back-filling system. The

furnace-body assembly included a furnace chamber, a water-cooled hearth plate which was capable of holding seven buttons, and a water-cooled non-consumable tungsten electrode.

The pumping system, including a mechanical pump, could evacuate the furnace chamber to 15×10^{-3} torr.

The power supply system, a modification of the power system of a welding rectifier, was capable of supplying a direct current of 25 volts and 450 amperes.

Table 2. Analyses of material used.

	Zirconium		Chromium
	Reactor Grade	Crystal Bar	Electrolytic Ingot
Form	Sheet	Crystal bar	Ingot
	Impurities (percent)		
Al	0.0042	less than 0.003	
C	0.0070	0.003	
Cr	0.0077	0.003	
Fe	0.0410	0.028	0.001 - 0.01
H	0.0003	0.0003	
Hf	0.0076	0.0014	
N	0.0025	0.003	less than 0.0010
O	0.0630	0.005	0.0750
Si	0.0040	0.004	0.001 - 0.01
Ti	0.0033	less than 0.002	
Nominal purity	99.80	99.95	99.90

Note: Alloys which are made of zirconium sheet are designated with the prefix "I", and alloys which are made of zirconium crystal bar are designated with the prefix "WC".

3. Process

The as-received zirconium sheet and crystal bar were rinsed with acetone, then pickled in a mixed-acid solution of nitric acid (70%, 45 parts), hydrofluoric acid (48%, 10 parts), and water (45 parts). Then they were rinsed in water and dried in an oven at 90°C. The surface of the material thus treated appeared shiny, which indicated that no oxidizing film remained.

The chromium ingot was also rinsed with acetone and then pickled with concentrated hydrochloric acid, water rinsed and dried. The ingot was then crushed to chunklets of various sizes.

The zirconium was in the form of sheet or crystal bar, and was too ductile for making powder. It was cut into small pieces and chunklets. For each alloy composition, the zirconium was weighed approximately to the required weight. From this weight, the amount of required chromium was calculated. Because chromium was so brittle that it could be crushed to any required size, there was no difficulty in matching the required weight of chromium with the weight of zirconium.

During alloy melting, chromium usually suffered more loss because of its high vapor pressure. In order to keep this loss to a minimum, when loading the material in the hearth, chromium chunklets were placed in the center of the hearth first. Zirconium sheets were

set around the chromium. In the case of the crystal bar, the chunklets were put atop the chromium metal. This arrangement allowed the zirconium to melt before the chromium. The molten zirconium transferred heat to the chromium chunklet and formed alloys before the chromium chunklet encountered the high temperature arc which would cause excessive evaporation.

An oxygen getter button of titanium-zirconium alloy was loaded with the alloy-making materials in the furnace in a separate crucible. The furnace was closed and then evacuated to 15×10^{-3} torr. The furnace chamber was then back-filled with helium. The evacuating and back-filling process was repeated three to five times. The getter button was melted before alloy melting to eliminate, as far as possible, all traces of oxygen.

The alloys were arc-melted at 20 volts and 350 amperes. Each button was flipped and remelted twice after the first melting. This homogenized the button. Alloys with compositions near the compound $ZrCr_2$ were brittle. To avoid shattering of the button after solidification, the current of the arc was decreased gradually from 300 amperes to 100 amperes. Then the arc was moved slowly to the edge of the molten pool. This edge was maintained in the molten state until the remainder of the button gradually solidified. Thus the contraction occurring during solidification induced much less internal stress in the button and decreased the tendency of the button to shatter after

solidification.

The tungsten electrode was weighed before and after melting. No detectable loss was observed. This indicates that the alloys were not contaminated by the tungsten electrode.

Every finished button had a bright shiny surface which indicated that no oxidation occurred during or after melting.

All buttons were weighed after melting. The melting losses of most buttons were within 1.5% of the total input material weight (see Table 3). Hence it is felt that the actual composition of the alloy is probably within one percent of the intended composition. Nominal compositions are, therefore, used in referring to the alloys.

B. Heat Treatment

1. The Encapsulation of the Specimens

All heat treated specimens were encapsulated before being heat treated. Pure quartz tube capsules were used for heat treatments above 1000°C and Vycor tube capsules for heat treatments below 1000°C. All tubes were of 1/2 inch diameter.

Each specimen was first wrapped with paper and shattered with a hammer. A piece, 1-1/2 to 2 grams, was selected for heat treatment. The piece was always taken from the center of the button. This amount was found to be enough for both X-ray powder diffraction

Table 3. Alloy compositions and melting data.

Alloy Number	Nominal a/o Zr	Nominal a/o Cr	Nominal w/o Zr	Nominal w/o Cr	Actual input (gram) Zr	Actual input (gram) Cr	Actual input (gram) Total	Alloys Final Weight Total	Loss Weight	Loss %
I-1	60.0	40.0	72.4	27.6	18.19	6.89	24.98	24.93	0.05	0.23
I-2	50.0	50.0	63.6	36.4	15.90	9.11	25.01	24.90	0.10	0.40
I-3	40.0	60.0	53.9	46.1	13.48	11.56	25.04	24.44	0.60	2.46
I-4	37.5	62.5	51.2	48.8	12.30	12.20	24.50	24.40	0.10	0.41
I-5	35.40	64.60	49.0	51.0	12.25	12.76	25.01	Contaminated		
I-6	35.0	65.0	48.5	51.5	12.12	12.88	25.00	24.81	0.19	0.76
I-7	34.5	65.5	48.0	52.0	12.00	13.00	25.00	24.90	0.10	0.40
I-8	34.0	66.0	47.5	52.5	11.88	13.12	25.00	24.82	0.18	0.75
I-9	33.6	66.4	47.0	53.0	11.75	13.25	25.00	24.98	0.02	0.08
I-10	33.0	67.0	46.5	53.5	11.63	13.37	25.00	24.88	0.12	0.48
I-11	32.7	67.3	46.0	54.0	11.50	13.50	25.00	24.80	0.20	0.80
I-12	31.8	68.2	45.0	55.0	11.25	13.75	25.00	24.99	0.01	0.04
I-13	31.0	69.0	44.0	56.0	11.00	14.00	25.00	24.70	0.30	1.20
I-14	30.0	70.0	43.9	56.1	10.98	14.02	25.00	24.97	0.03	0.12
I-15	25.0	75.0	39.8	63.2	9.20	15.80	25.00	Contaminated		
I-16	20.0	80.0	30.50	69.15	7.63	17.37	25.00	24.10	0.09	0.36
I-17	15.0	85.0	23.6	76.4	5.90	19.10	25.00	24.72	0.28	1.12
WC-4	33.33	66.67	46.72	53.28	70.08	79.92	150.00	148.2	1.8	1.20

Note: Alloy I-5 and I-15 are contaminated by the getter during melting. These two alloys are omitted in this investigation.

and metallography.

Each specimen was wrapped with zirconium foil, then encased in a sheath of molybdenum sheet. The complete setup was inserted into a quartz or Vycor tube with one end sealed. The open end of the quartz tube was connected to a rubber hose which was connected to a vacuum pump, and to the argon source (25, p. 65-67). The quartz tube was evacuated to a pressure of a half inch of mercury then back-filled with argon. This process was repeated at least five times. A city gas-oxygen torch was used to seal the tube. The sealing was done with a residual pressure of argon in the tube which was adjusted so as to be one atmosphere at the heat treatment temperature.

Although the maximum allowable temperature for quartz suggested by Saybolt (35, p. 64) is 1100°C, it has been our experience that only slight deformations have been observed at 1250°C for a period of 24 hours. Eleven experiments have been conducted at various temperatures between 1400°C to 1600°C, with soaking periods varying from 45 minutes to four hours. Only at 1600°C was severe deformation of the quartz tube observed.

In Figure 7, the clear quartz capsule before being heat treated, is shown on the right, and the capsule after being treated at 1600°C for 45 minutes is shown on the left. One can see that the latter deformed badly after the heat treatment. Figure 8 shows two molybdenum sheaths for wrapping the specimens inside the capsules. The

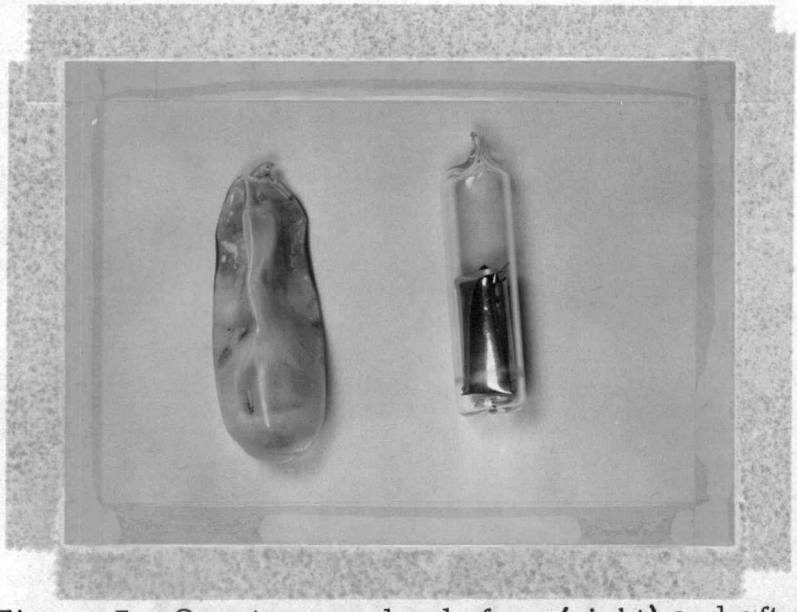

Figure 7. Quartz capsules before (right) and after (left) 1600°C annealing.

Figure 8. Molybdenum sheaths before (right) and after (left) 1600°C annealing.

newly made sheath is shown on the right. The sheath inside the deformed capsule in Figure 8 is shown on the left. There is no detectable oxidation on the sheath surface which indicates that there was no leak in the deformed capsule.

2. The Furnaces

Two different furnaces were used for heat treating the specimens.

1) Model G-07PT: The furnace was made by Hevi-Duti Electric Company, it was used for heat treating temperatures below 1300°C. It was an air furnace with maximum operating temperature of 1380°C. Its heating elements were made of silicon carbide.

2) Model KKK 5669: This furnace was made by Keith Furnace Company, and is owned by the Bureau of Mines in Albany, Oregon. It was used for heat treating specimens at temperatures above 1300°C. Argon was used for the furnace atmosphere. Its heating elements were made of molybdenum disilicide (Super Kanthal elements). The maximum operating temperature was 1650°C.

3. The Heat Treating Process

In the early stages of this experiment, two different batches of

specimens (each batch has 17 specimens) were treated at 900°C (Batch A) and 1250°C (Batch B) respectively. The soaking period for Batch A was 500 hours, and for Batch B, 24 hours. At the end of the soaking period, each specimen was taken out of the furnace and quenched in water. The capsule was then broken in ice water with a pair of tongs. In later long-time annealing experiments, all the specimens were cooled in the furnace.

C. Metallography

All alloy specimens were broken to a size with a cross-section from 0.5 to one centimeter in diameter for metallographic examination. Since most of the specimens were very brittle, comparatively low pressure (about 500 pounds) was used for molding the one inch diameter plastic mounts. The temperature used for the lucite mounts was 120°C, and the bakelite resin, 150°C.

Standard sample preparation technique (27, p. 1-57) was employed for polishing the specimens. Final polishing was done on a Vibromet automatic polishing unit with 0.05 micron alumina powder-water mixture as the abrasive.

For revealing grain boundaries, electro-etching was used. The etching solution consisted of five drops of base solution diluted with 100 ml of water. The base solution was composed of ten grams NaOH, ten grams $K_3Fe(CN)_6$, and 100 ml water. The etching voltage

was eight volts. The etching time was about 10 to 20 seconds. This procedure will be called the etching procedure A.

To reveal striations, the specimen was first etched on the polishing wheel. The etching solution consisted of 250 ml water, 20 ml HNO_3, and 3 ml HF. A very light force was applied to hold the specimen against the turning wheel for about 30 seconds. Then the specimen was electro-etched in a 10% oxalic acid solution for 10 to 15 seconds with a current of ten volts. This procedure will be called procedure B.

All photomicrographs were taken with a Bausch and Lomb Research metallograph. The light was filtered with a B and L No. 550 filter (green). Most pictures were taken with plain axial illumination. Oblique illumination was sometimes used to reveal the striations.

D. Powder Diffraction Photographs

X-ray diffraction experiments were performed with a Type 12045B-3 X-ray unit manufactured by Philips Electronics, Inc. For powder diffraction, mono-chromatic radiation from a copper target X-ray tube, filtered with a nickel filter, was used. Two different Debye-Scherrer cameras, (one with a diameter of 143.24 mm, the other 114.03 mm) were used. All "d" measurements were directly read from a Nies chart.

Each specimen was ground to fine powder in an agate mortar.

The fine powders used all passed a 325 mesh screen. The powdered specimen was encased in a small glass tube in vacuum and then annealed at 400°C for one hour to relieve the residual strains caused by grinding.

Powder from each specimen was mixed with Duco cement, then rolled into the shape of a thin rod of about 0.5 to 1 mm in diameter, and 10 to 15 mm long.

A total of 58 diffraction pictures were taken. Only 28 were selected for examination. ASTM X-ray diffraction data cards No. 6-0612 and 6-0613 were used for identification of the planes.

E. The Single Crystal Back-Reflection Patterns from Poly-Crystalline Specimens

Metallographic inspection revealed that striations occur in almost every grain of the specimen with face-centered structure. Further study from models (see paragraph IV, C) showed that the striations might be caused by the shear type movement of atomic planes during transformation. Hence it was necessary to find the orientation of planes represented by these striations.

$ZrCr_2$ is a very brittle intermetallic compound. It is very difficult, if not impossible, to make single crystal $ZrCr_2$ of such a size that the crystal can be handled for heat treatment. In this experiment a combination method was developed. It consists of the Laue method

and of the method to orient the plane from its trace in two surfaces as described by Barrett (4, p. 46).

The same specimen prepared for metallography was used for obtaining back-reflection-Laue patterns. Since the size of each grain in this polycrystalline specimen was very small (0.5 to 1 mm maximum), the following steps were followed to align the collimated X-ray beam with a particular grain to be studied.

To begin with, the instrument table with the camera track was disassembled from the X-ray unit. The collimator, whose pin hole size was 0.75 mm, was mounted in the ordinary position on the track. A telescope was mounted in the position of the goniometer. Then the cross hair of the telescope was adjusted so that it aligned with the center of the pin hole of the collimator.

The collimator was then dismounted. The telescope was turned around and mounted in the position where the collimator was. The goniometer, with the specimen, was installed on the track in the ordinary position and was opposite to the telescope. The specimen was first adjusted with a transit so that the surface of the specimen was perpendicular to the telescope's line of sight. The specimen was then adjusted either up and down or crosswise so that the grain to be examined centered on the cross hair of the telescope.

In the last step, the telescope was dismounted. The collimator, together with the film cassette, was set in place. The complete assembly was finally assembled on the X-ray unit. This complete process proved to be so successful that the collimated X-ray beam always impinged on the grain to be examined.

IV. RESULTS AND DISCUSSION

A. Confirmation of the General Features of the Zirconium-Chromium Diagram

In this investigation, a series of 15 alloys starting from 40 atomic percent to 85 atomic percent chromium was made in order to verify this particular section of the zirconium and chromium phase diagram. The photomicrographs of this alloy series confirm the general features of this section of the phase diagram as published by Hansen and shown in Figure 3 of paragraph II, A.

For convenience of discussion, the complete series of alloys is divided into three groups: the zirconium-rich group, the intermetallic compound group, and the chromium-rich group. These groups will be discussed in that order. Each group of alloys is considered in the as-cast condition and in the 1250°C annealed condition.

1. Zirconium-Rich Group: Alloys of three different compositions are included in the zirconium-rich group. They are designated as I-1, I-2, and I-3 whose chromium contents are 40 a/o, 50 a/o and 60 a/o respectively. This group of alloys shows that as the chromium content increases, the quantity of $ZrCr_2$ also increases.

a. As-cast condition: A typical hypereutectic structure consisting of primary $ZrCr_2$ embedded in the eutectic matrix is shown in alloy I-1 (40 a/o Cr), (Figure 9). The plate-like intermetallic

grains with sharp corners indicate that a relatively high anisotropy of interfacial energy existed between the growth nuclei of $ZrCr_2$ and the eutectic melt. The eutectic itself is of non-lamellar type. There is a clear evidence of eutectic divorcement around the intermetallic crystals.

Alloy I-2 (50 a/o Cr) reveals a larger proportion of $ZrCr_2$ crystals as shown in Figure 10. $ZrCr_2$ grains grow columnarly into eutectic colonies. The columnar structures remain in the plate shape.

The photomicrograph of alloy I-3 (60 a/o Cr) (Figure 11) does not reveal any eutectic structure due to more extensive divorcement. A part of the primary zirconium concentrates between the $ZrCr_2$ crystals and the rest of the primary zirconium is solidified and uniformly distributed in the $ZrCr_2$ matrices.

b. 1250°C annealed: After being annealed, the alloys I-1, I-2, and I-3 do not show any change in the proportions of $ZrCr_2$ and the eutectic or primary zirconium as shown in Figures 12, 13, and 14. Yet, the annealing process homogenized the alloys and caused a different appearance in the photomicrographs. Figures 12 and 13 show that the $ZrCr_2$ grains of alloys I-1 and I-2 become more rounded after being annealed. The eutectic structure becomes finer, and the eutectic divorcement band disappears. Figure 14 shows that the annealing process reveals clearer boundaries in alloy I-3 and agglomerates the eutectic colonies.

2. Intermetallic Compound Group: Ten alloys with designation numbers from I-4 to I-13 were made. The increment of chromium between each subsequent alloy varied from 0.5 to 1.0 atomic percent to establish the range of composition over which the compound is stable.

a. As-cast condition: The major component of each photomicrograph is the $ZrCr_2$ compound. Figures 15 (I-4, 62.5 a/o Cr) to 19 (I-9, 66.43 a/o Cr) show the alloys with the compositions slightly rich in zirconium. The second phase, the primary zirconium solid solution, gradually diminished as the chromium content increased. Figures 20 (I-10, 66.88 a/o Cr) through 23 (I-13, 69.0 a/o Cr) show the alloys with compositions slightly rich in chromium. The second phase, the primary chromium solid solution, gradually increases with the increasing chromium content.

b. 1250°C annealed: Figures 24 to 32 show the photomicrographs of I-4 to I-13 after a 1250°C annealing.

In the "as-cast" condition, degenerated eutectics and impurities are displayed in every photomicrograph of this intermetallic compound group. Nevertheless, during annealing the second phase in each alloy decreases considerably because the uncombined zirconium formed $ZrCr_2$. One can see the difference in the amount of the second phase by comparing the photomicrographs of the "as-cast" condition to that of the annealed condition of the same alloy in this group.

The stable composition range of the compound $ZrCr_2$ can be estimated from these photomicrographs by comparing the amount of second phase present in each case. In the ideal case, the photomicrograph of pure $ZrCr_2$ should display no second phase but should be entirely the compound. However, it is highly improbable that one will make an intermetallic compound completely free from second phase, if the range of the stable intermetallic compound is narrow. The reasons for this are twofold: First, the starting materials are not extremely pure. In the case of this thesis, the purity of zirconium is 99.8 w/o minimum, and the purity of chromium is 99.9 w/o minimum. These small amounts of impurities are always present as second phase either along the grain boundaries or dispersed in the compound matrices. Secondly, all the alloys were made under one atmosphere pressure of argon. The vapor pressures of zirconium (3×10^{-5} mm at 1900°C) and chromium (6 mm at 1900°C) are very different. Therefore, it is very difficult, if not impossible, to make the evaporation rate of these two elements equal. Consequently, the final compound always consists of a very small amount of excess element, either zirconium or chromium, which will appear as second phase in the pure compound structure.

In the series of photomicrographs of the annealed intermetallic compound group, one can see that none of these structures is free from the appearance of the second phase. This second phase, which

is formed from the impurities and from excessive zirconium or chromium, appears as small roundish shapes probably due to the fact that they form ternary or quaternary eutectics and have a lower melting point than the compound. Thus they always solidify along the grain boundaries, or form a chain of islands inside the grain.

Comparing this series of photomicrographs of the intermetallic compound group, one can see that the structures in Figure 27 (65.97 a/o Cr), Figure 28 (66.43 a/o Cr), Figure 29 (66.88 a/o Cr) and Figure 30 (67.32 a/o Cr) reveal the least second phase. The photomicrographs of the alloys with compositions falling outside the range 65.97 a/o to 67.32 a/o chromium show a considerable increase in the amount of the second phase. This would indicate that the pure compound $ZrCr_2$ exists within the range between 65.97 a/o to 67.32 a/o chromium. The range of stability of the compound is thus very narrow. This small region of composition presents extreme difficulty for detecting metallurgical reactions such as the peritectic or peritectoid within this region.

Another outstanding characteristic of this group is the appearance of the striations in every alloy after 1250^{o}C annealing. Such striations indicate that a phase transformation has occurred. The striations occur only after the alloy transforms from C-14 close-packed hexagonal structure to C-15 face-centered cubic structure. Moreover, the fact that all striations are parallel with each other

within each grain leads to the deduction that this solid state transformation occurs on a certain group of habit planes. The identification of these striations will be discussed together with X-ray work in later sections.

3. Chromium-Rich Group: Alloys of three different compositions are included in this chromium-rich group: they are designated as I-14, I-16, and I-17 whose chromium contents are 70 a/o, 80 a/o, and 85 a/o respectively. This group of alloys shows the hypoeutectic, eutectic, and hypereutectic structures between the compound and the primary chromium.

a. As-cast condition: The structure for the alloy of 70 a/o chromium shows the degenerated eutectic structure from the compound and primary chromium solid solution (Figure 33). This composition is very close to the compound, so the major portion of this structure is the $ZrCr_2$ compound. Alloy I-16 with 80 a/o chromium solid solution is a well developed non-lamellar type eutectic (Figure 34). The structure of the alloy with 85 a/o chromium shows the primary chromium dendrites embedded in a non-lamellar eutectic matrix (Figure 35). The primary chromium solid solution grains are rounded probably because chromium has a high surface tension. Eutectic divorcement also appears around chromium solid solution grains.

b. 1250°C annealed: The annealing process did not

change the appearance of the alloy with 70 a/o chromium except that striations occurred in the compound (Figure 36). These chromium solid solutions were affected by the annealing process in the eutectic structure (80 a/o chromium). They agglomerated into global form after the annealing as shown in Figure 37. In the alloy with 85 a/o chromium little change in appearance is produced by the annealing process other than a coarsening of the eutectic structure (Figure 38).

From this series of photomicrographs, the following facts can be enumerated:

1) No modification need be made in the general features of the zirconium-chromium phase diagram as published by Hansen.
2) The intermetallic compound $ZrCr_2$ exists in a very small region between 65.97 a/o to 67.32 a/o chromium.
3) Striations which occur in the photomicrographs of most of the alloys after 1250°C annealing indicate that the phase transformation has occurred on a certain group of habit planes.

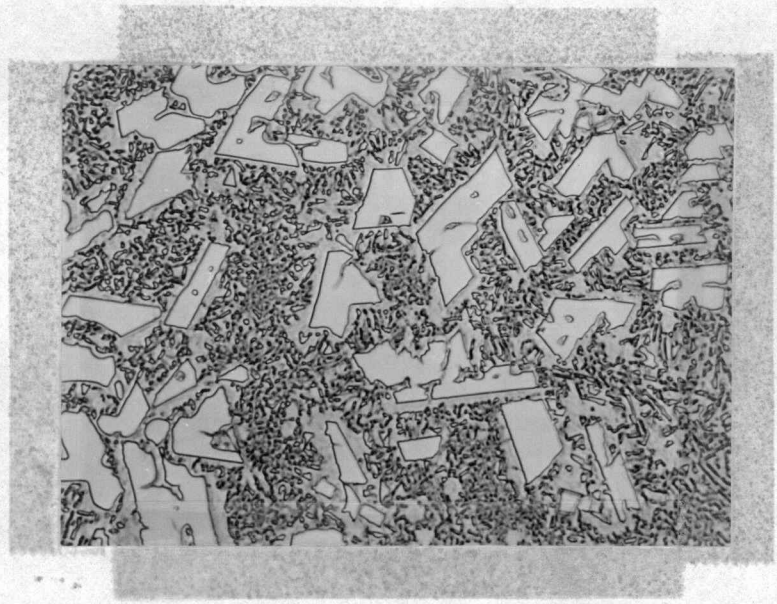

Figure 9. Specimen I-1, 40.0 a/o Cr, as-cast. $ZrCr_2$ and eutectic. Etching procedure "A". X 500.

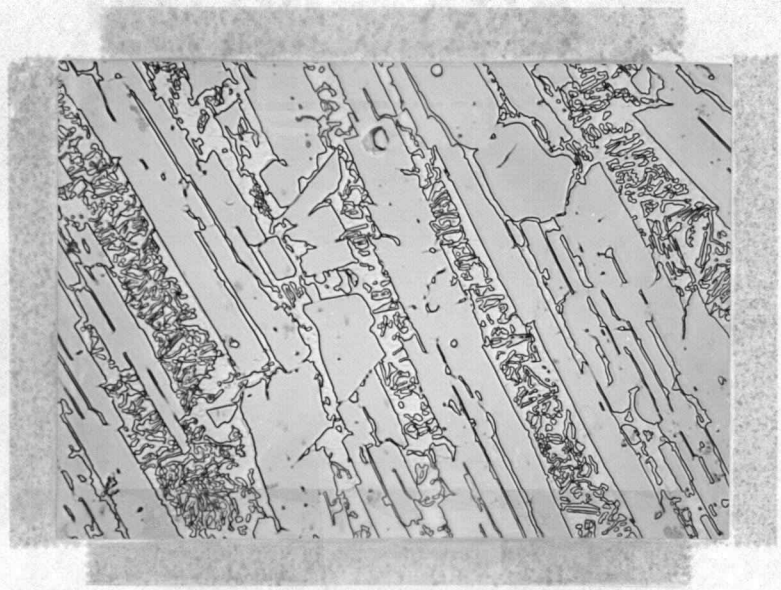

Figure 10. Specimen I-2, 50.0 a/o Cr, as-cast. $ZrCr_2$ and eutectic. Etching procedure "A". X 500.

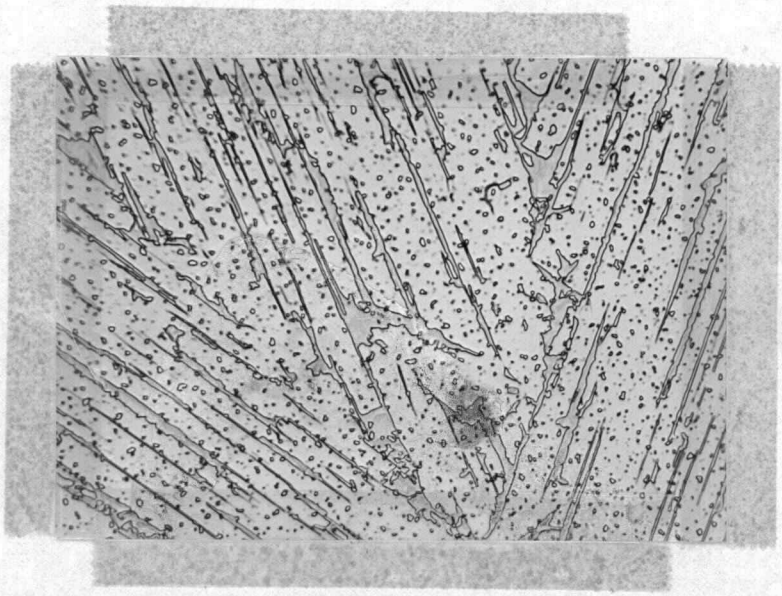

Figure 11. Specimen I-3, 60.0 a/o Cr, as-cast. $ZrCr_2$ and eutectic. Etching procedure "A". X 500.

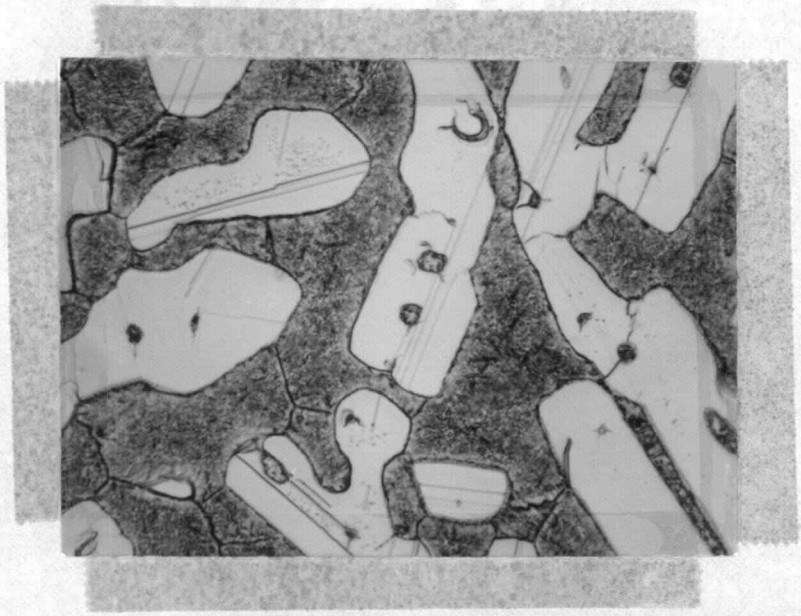

Figure 12. Specimen I-1, 40.0 a/o Cr, quenched after annealing at 1250°C. $ZrCr_2$ and eutectic. Etching procedure "B". X 500.

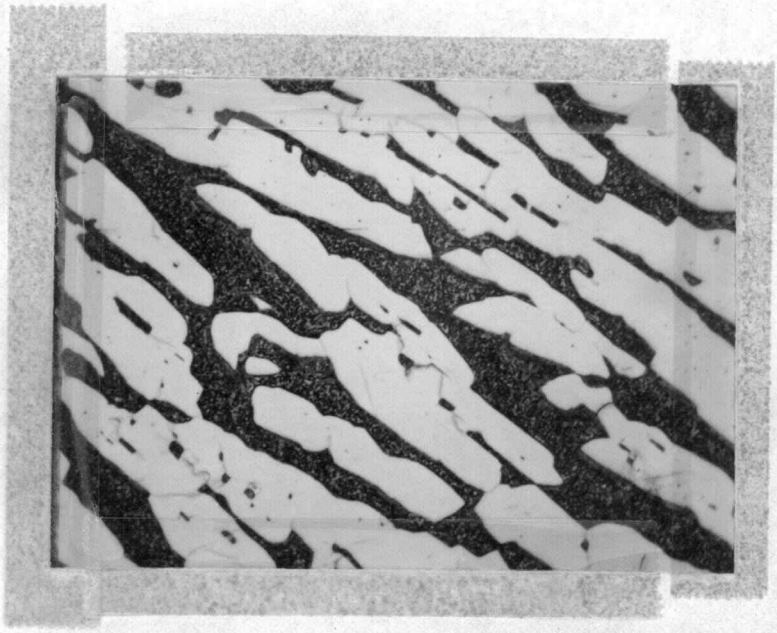

Figure 13. Specimen I-2, 50.0 a/o Cr, quenched after annealing at 1250°C. $ZrCr_2$ and eutectic. Etching procedure "B". X 500.

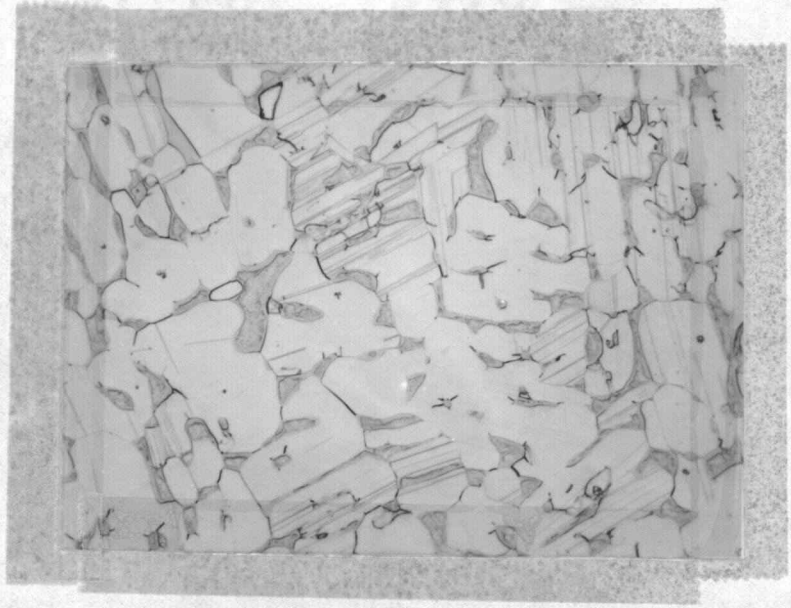

Figure 14. Specimen I-3, 60.0 a/o Cr, quenched after annealing at 1250°C. $ZrCr_2$ and second phase. Etching procedure "B". X 500.

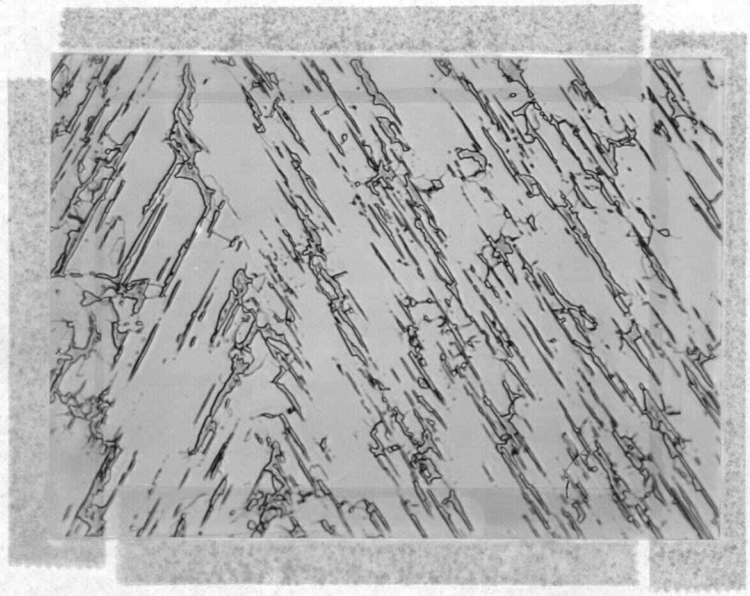

Figure 15. Specimen I-4, 62.5 a/o Cr, as-cast. $ZrCr_2$ and primary Zr solid solution. Etching procedure "A". X 500.

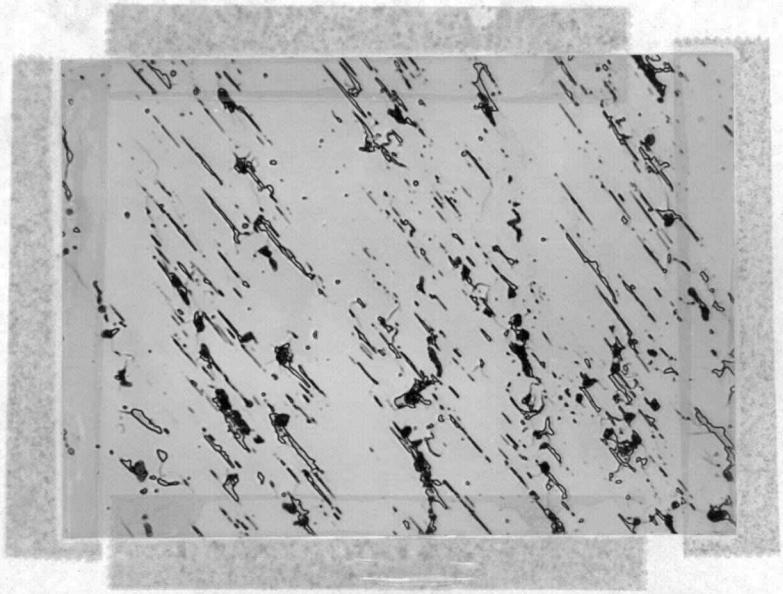

Figure 16. Specimen I-6, 65.07 a/o Cr, as-cast. $ZrCr_2$ and primary Zr solid solution and impurities. Etching procedure "A". X 500.

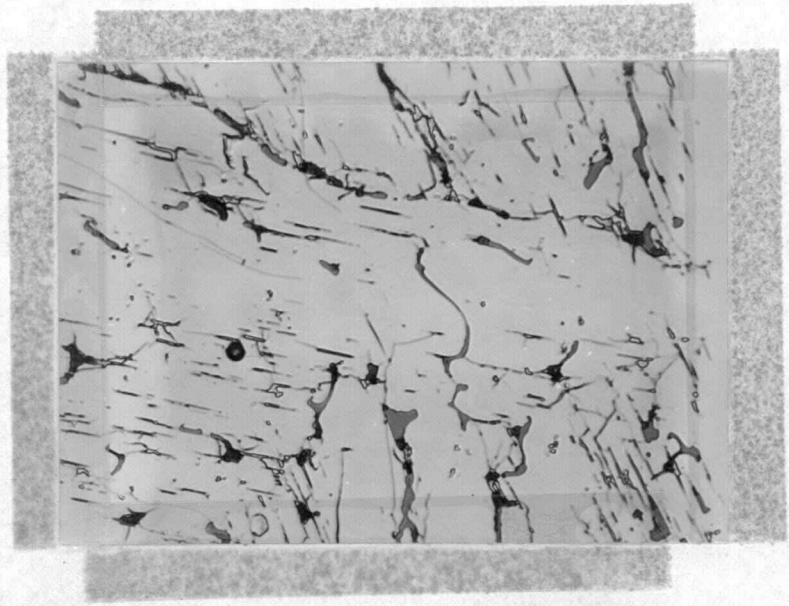

Figure 17. Specimen I-7, 65.53 a/o Cr, as-cast. $ZrCr_2$ and primary Zr solid solution and impurities. Etching procedure "A". X 500.

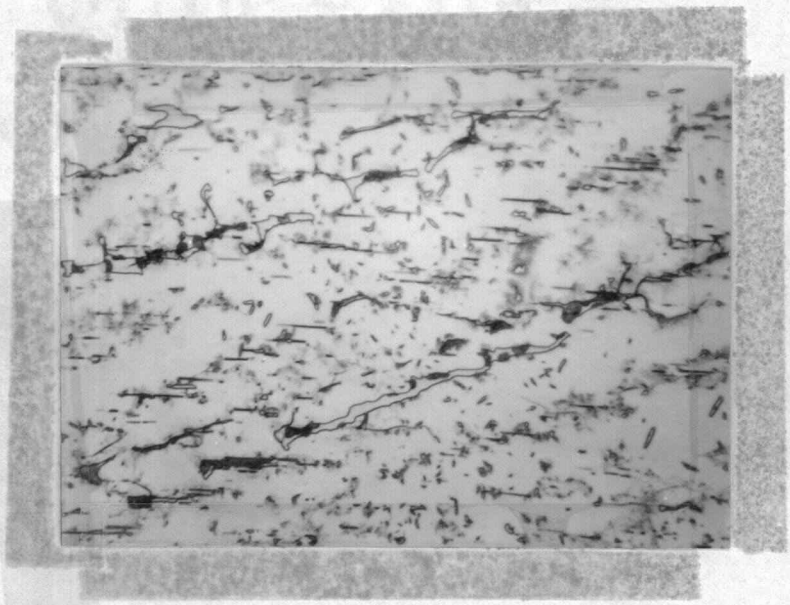

Figure 18. Specimen I-8, 65.98 a/o Cr, as-cast. $ZrCr_2$ and primary Zr solid solution and impurities. Etching procedure "A". X 500.

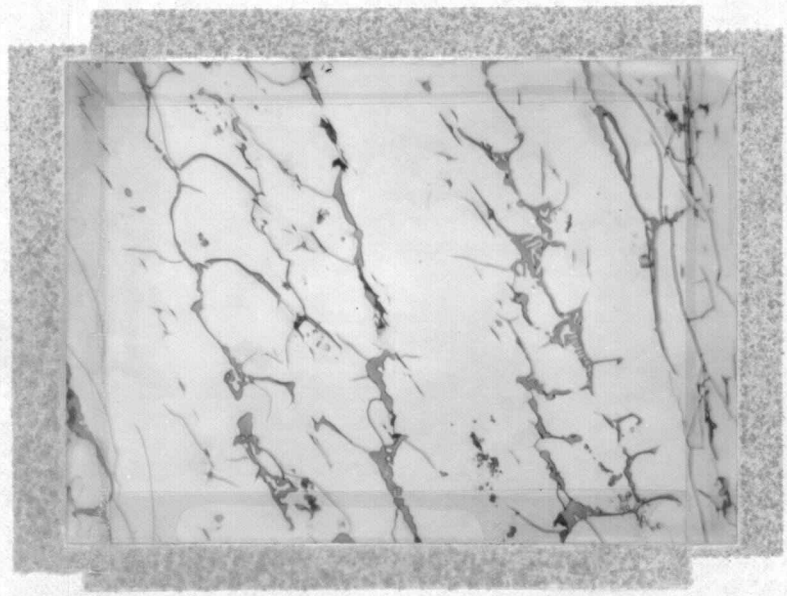

Figure 19. Specimen I-9, 66.43 a/o Cr, as-cast. $ZrCr_2$ and second phase. Etching procedure "A". X 500.

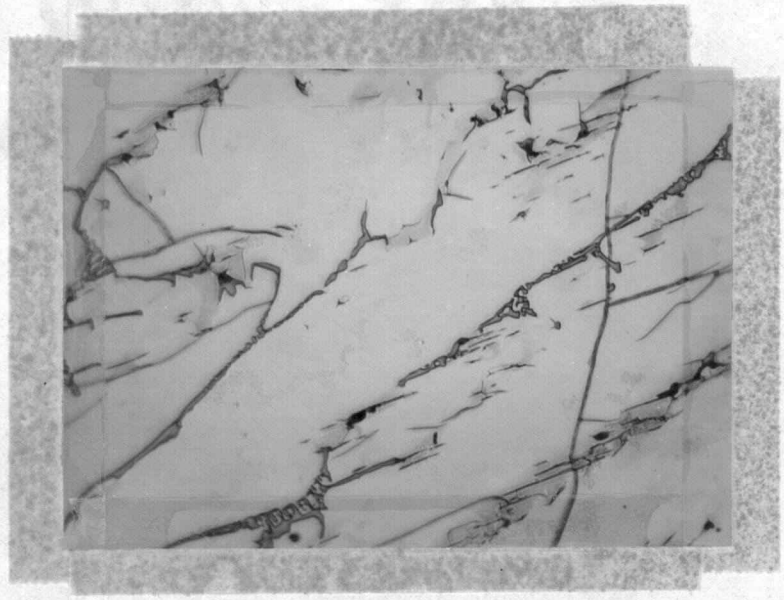

Figure 20. Specimen I-10, 66.68 a/o Cr, as-cast. $ZrCr_2$ and second phase. Etching procedure "A". X 500.

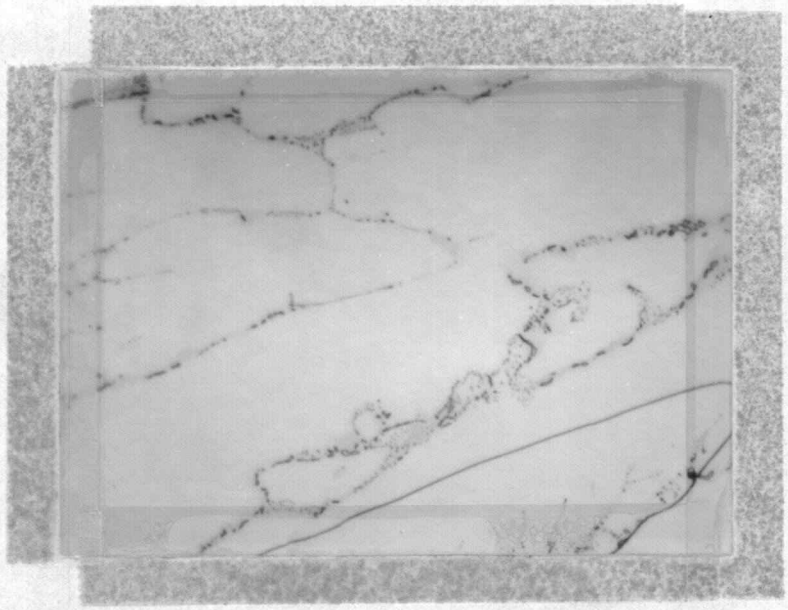

Figure 21. Specimen I-11, 67.32 a/o Cr, as-cast. $ZrCr_2$ and second phase. Etching procedure "A". X 500.

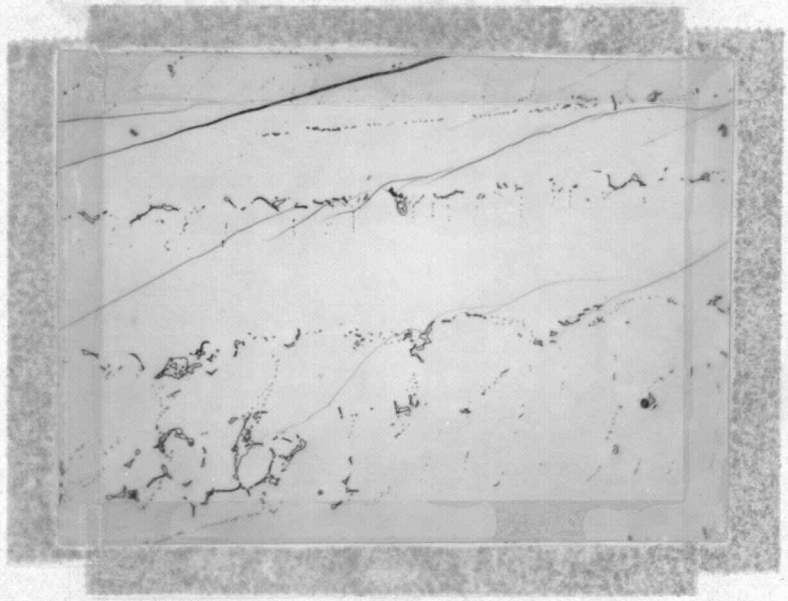

Figure 22. Specimen I-12, 68.20 a/o Cr, as-cast. $ZrCr_2$ and second phase. Etching procedure "A". X 500.

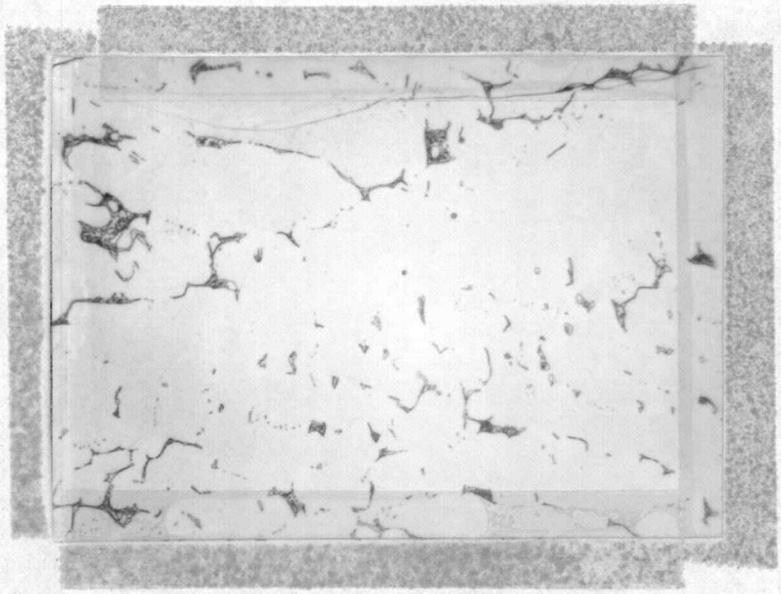

Figure 23. Specimen I-13, 69.0 a/o Cr, as-cast. $ZrCr_2$ and second phase. Etching procedure "A". X 500.

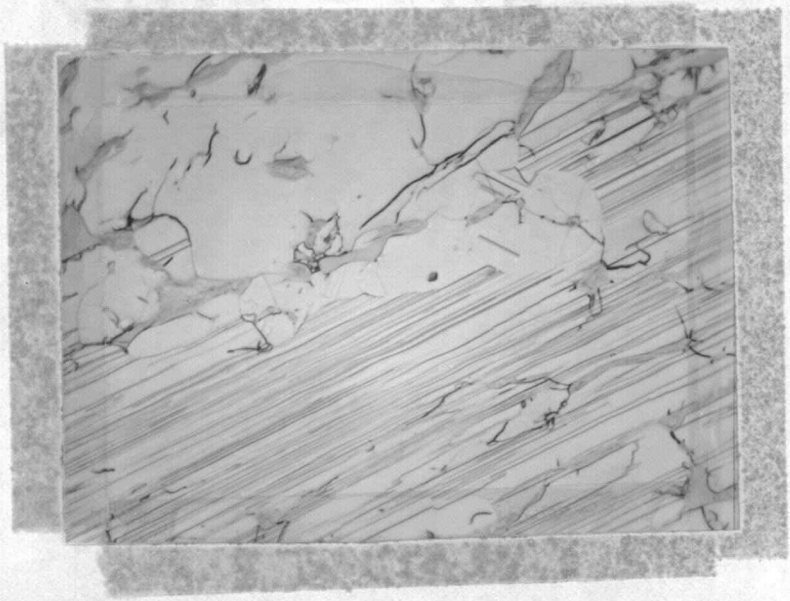

Figure 24. Specimen I-4, 62.5 a/o Cr, quenched after annealing at 1250°C. $ZrCr_2$ and second phase. Etching procedure "B". X 500.

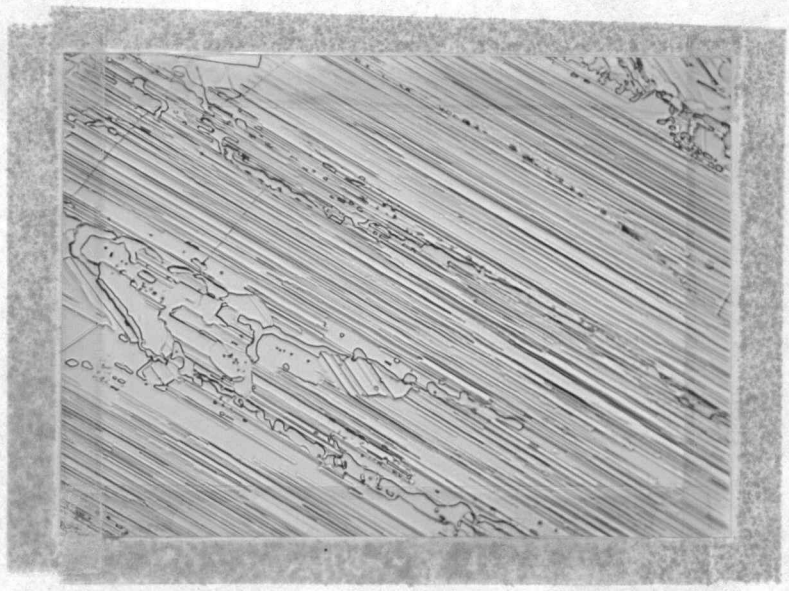

Figure 25. Specimen I-6, 65.07 a/o Cr, quenched after annealing at 1250°C. $ZrCr_2$ and second phase. Etching procedure "B". X 500.

Figure 26. Specimen I-7, 65.53 a/o Cr, quenched after annealing at 1250°C. $ZrCr_2$ and second phase. Etching procedure "B". X 500.

Figure 27. Specimen I-8, 65.98 a/o Cr, quenched after annealing at 1250°C. Nearly single phase $ZrCr_2$. Etching procedure "B". X 500.

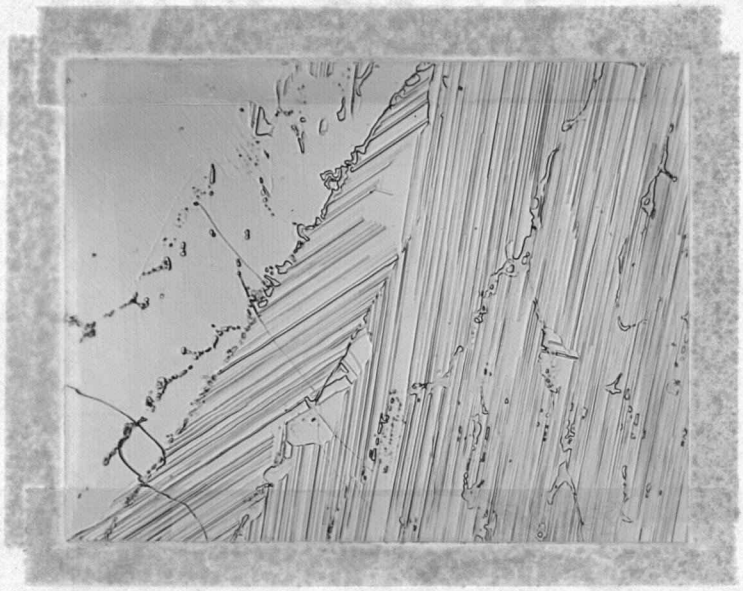

Figure 28. Specimen I-9, 66.43 a/o Cr, quenched after annealing at 1250°C. Nearly single phase $ZrCr_2$. Etching procedure "B". X 500.

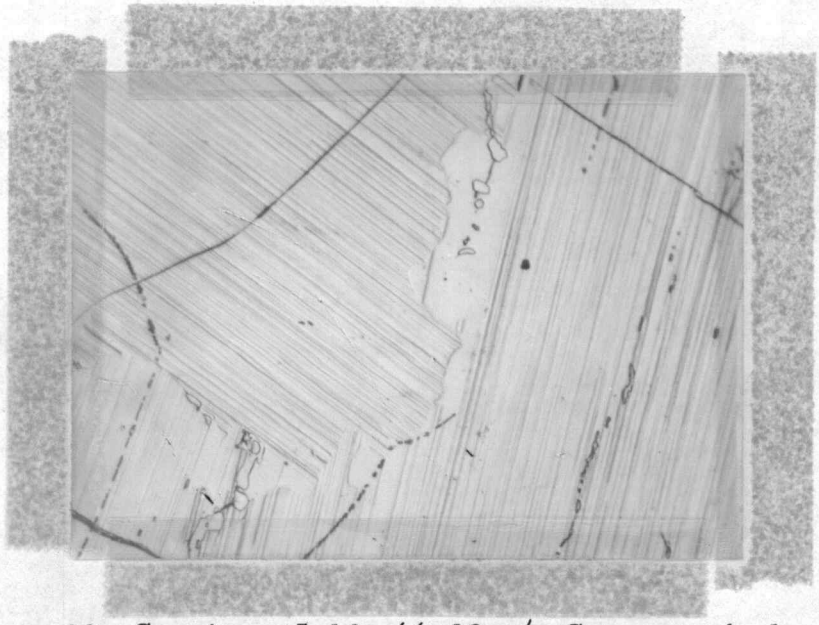

Figure 29. Specimen I-10, 66.88 a/o Cr, quenched after annealing at 1250°C. Nearly single phase $ZrCr_2$. Etching procedure "B". X 500.

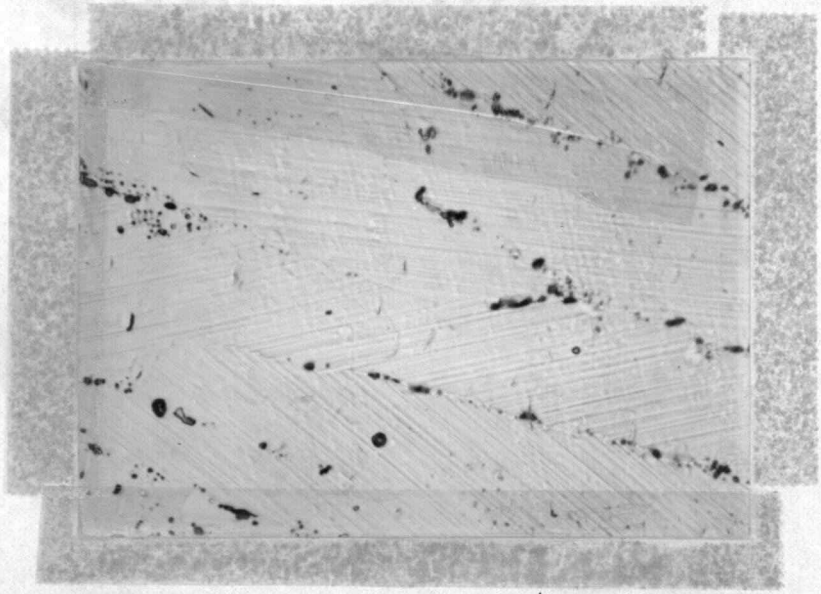

Figure 30. Specimen I-11, 67.32 a/o Cr, quenched after annealing at 1250°C. Nearly single phase $ZrCr_2$. Etching procedure "B". X 500.

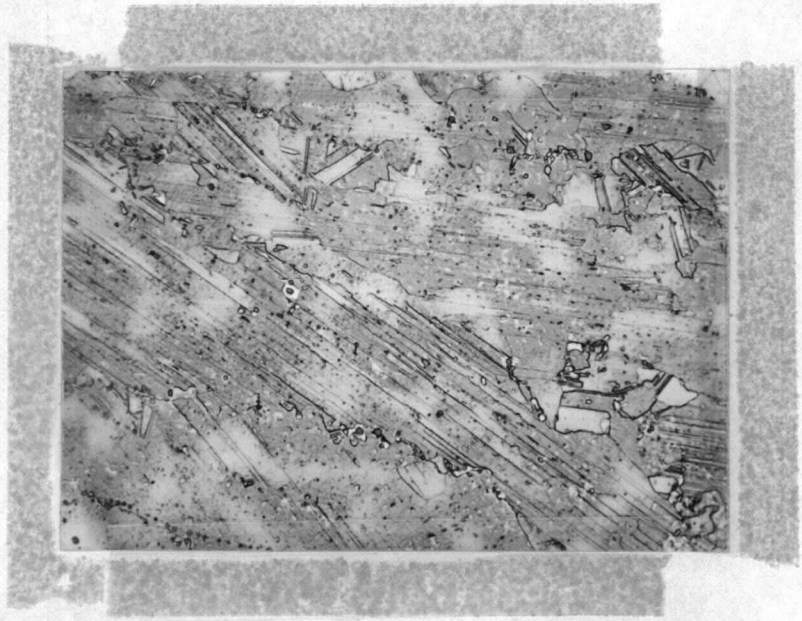

Figure 31. Specimen I-12, 68.20 a/o Cr, quenched after annealing at 1250°C. $ZrCr_2$ and second phase. Etching procedure "B". X 500.

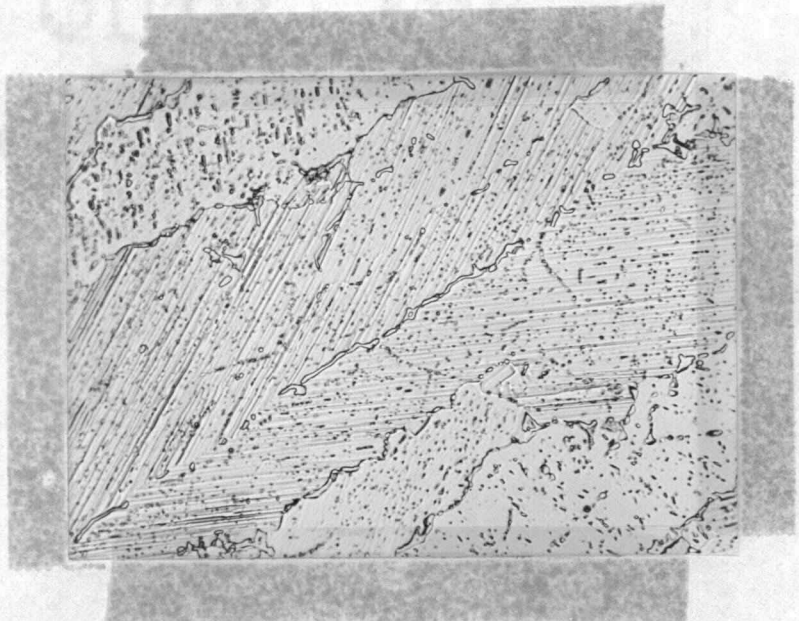

Figure 32. Specimen I-13, 69.0 a/o Cr, quenched after annealing at 1250°C. $ZrCr_2$ and primary chromium solid solution. Etching procedure "B". X 500.

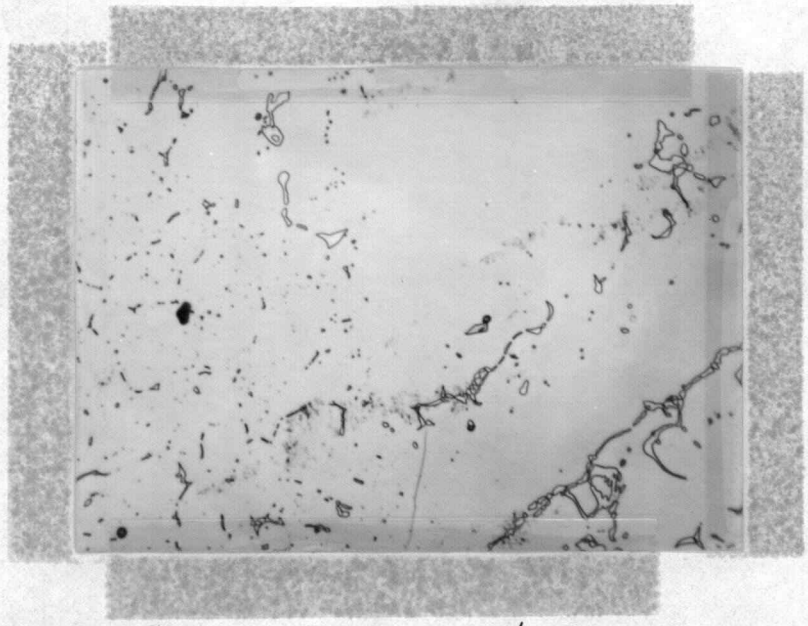

Figure 33. Specimen I-14, 70.0 a/o Cr, as-cast. $ZrCr_2$ and degenerated eutectic. Etching procedure "A". X 500.

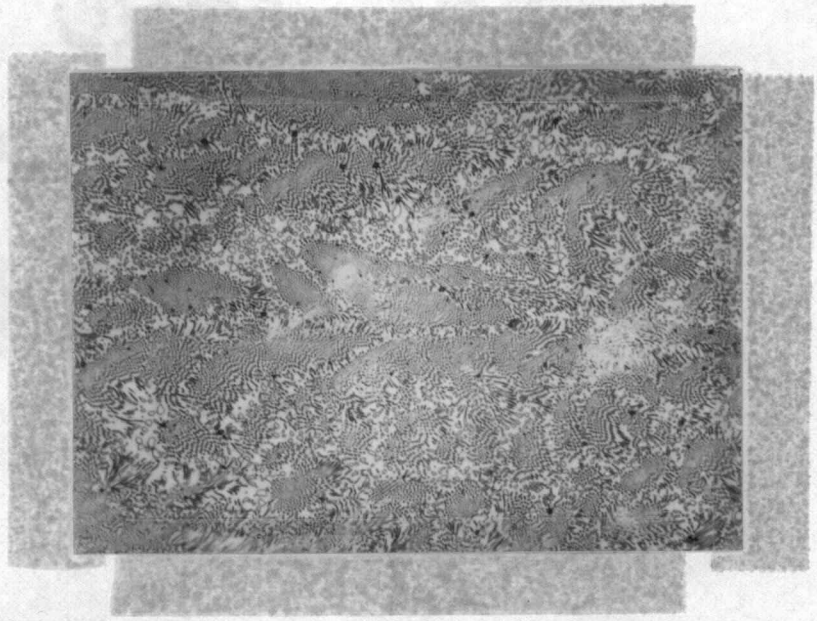

Figure 34. Specimen I-16, 80.0 a/o Cr, as-cast. Eutectic of $ZrCr_2$ and Cr. Etching procedure "A". X 500.

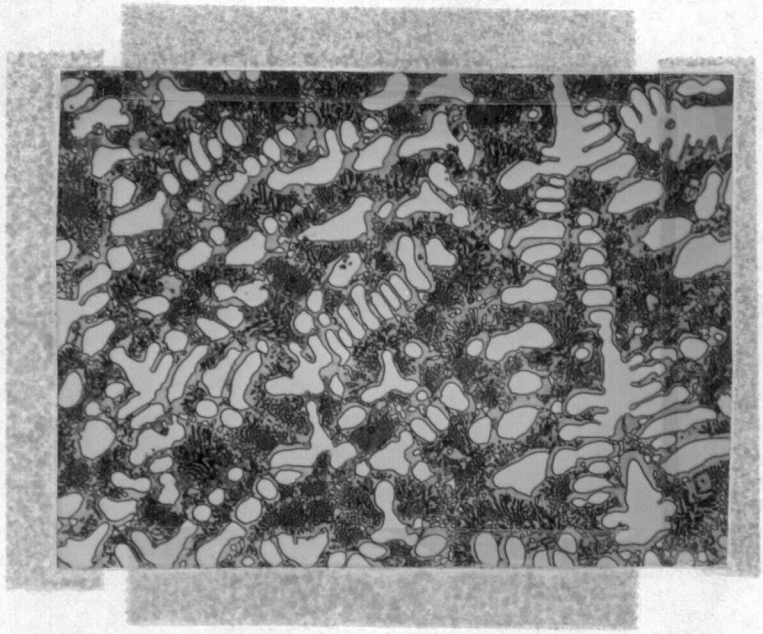

Figure 35. Specimen I-17, 85.0 a/o Cr, as-cast. Eutectic and primary Cr solid solution. Etching procedure "A". X 500.

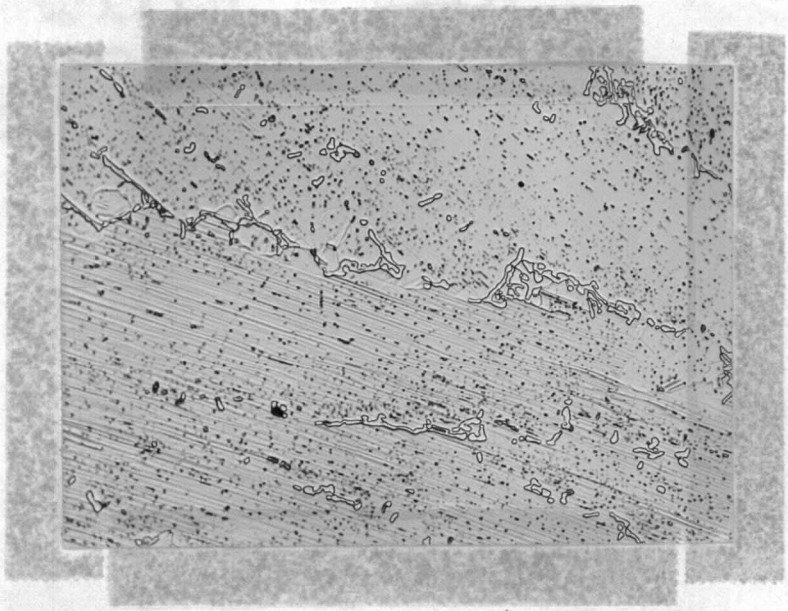

Figure 36. Specimen I-14, 70.0 a/o Cr, quenched from annealing at 1250°C. $ZrCr_2$ and primary Cr solid solution. Etching procedure "B". X 500.

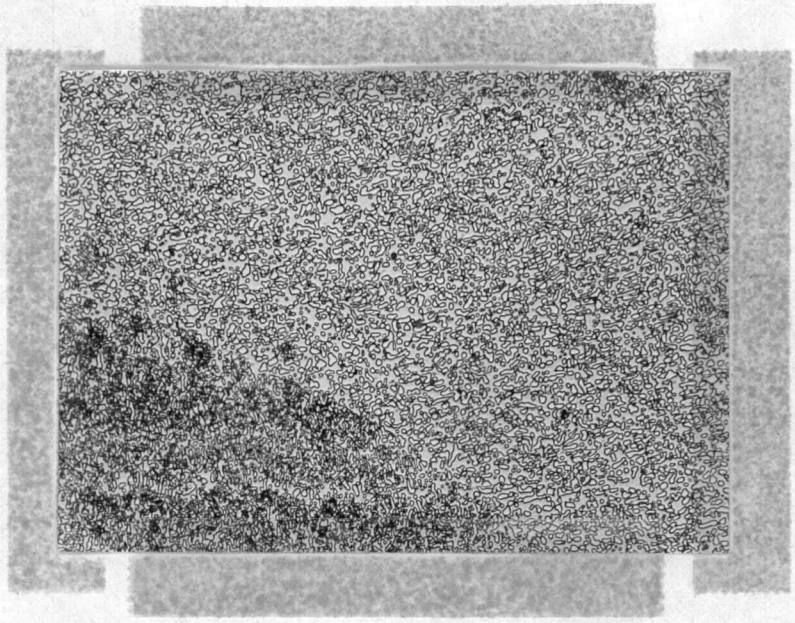

Figure 37. Specimen I-16, 80.0 a/o Cr, quenched from annealing at 1250°C. Eutectic of $ZrCr_2$ and primary Cr solid solution. Etching procedure "B". X 500.

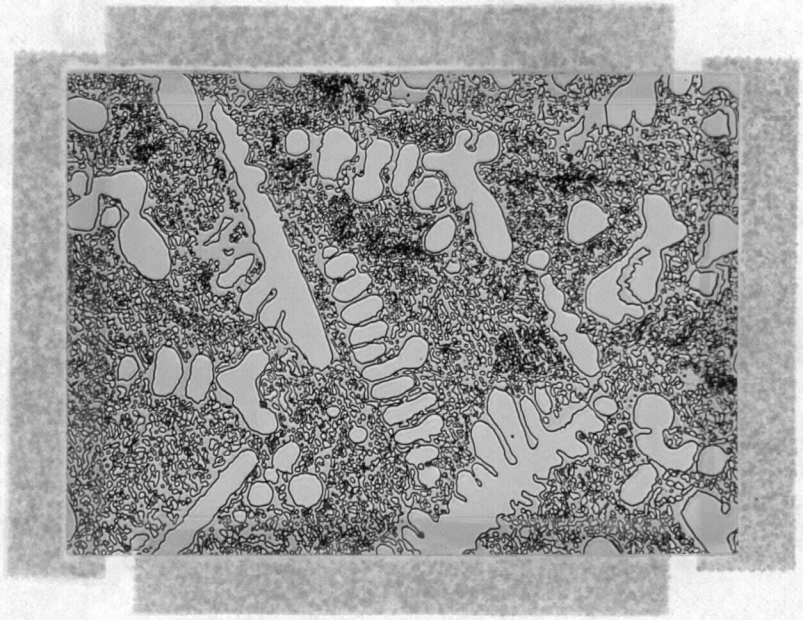

Figure 38. Specimen I-17, 85.0 a/o Cr, quenched after annealing at 1250°C. Eutectic and primary Cr solid solution. Etching procedure "B". X 500.

B. The Determination of the Transformation Temperature of $ZrCr_2$

In this investigation, the transformation temperature of $ZrCr_2$ was determined by two different means: the X-ray diffraction powder method and the metallographic method. The former was used for determining the crystal structure after high temperature annealings. The latter was used for verification. It has been shown in the photomicrographs of the previous section that striations across the grains appear when the compound transforms from the C-14 structure to the C-15 structure. The appearance of these striations is another criterion for structure determination.

1. The Diffraction Patterns of the C-14 Structure and the C-15 Structure

The powder diffraction patterns of the crystal structure of C-14 ($ZrCr_2$) and C-15 ($ZrCr_2$) were determined by Rostoker(33) and Hayes (23) respectively. Rostoker's data on the C-14 pattern are compared with Hayes' data of the C-15 pattern as shown in Table 4.

In this investigation, all X-ray diffraction data collected indicated that the structures and patterns reported by these authors are correct and no modification is necessary. Comparing these two patterns, one can see that the C-14 patterns have more lines than the C-15 patterns; and that the 'd' spacings of most of the lines in the C-15 pattern

are almost the same as those of certain lines of the C-14 pattern. Among the low angle diffraction lines, the most significant difference between the patterns is that C-15 has two more lines, d = 2.330 and d = 2.129, than C-14 has. In this investigation, the relative intensity of these two lines was used to determine the amount of C-14 structure appearing in a specimen with mixed structure.

Table 4. Powder diffraction line spacings and intensities of the two structures of $ZrCr_2$.

C-14($MgZn_2$ type HCP)			C-15($MgCu_2$ type FCC)		
hkl	Relative Intensity	d,Å	d,Å	Relative Intensity	hkl
002	20 vw	4.144	4.13	3 vw	111
003	20 vw	2.791			
110	80 s	2.543	2.54	63 s	220
103	80 s	2.330			
200	20 vw	2.201	2.17	100 vs	311
112	100 vs	2.166			
201	80 s	2.129	2.07	26 m	222
004	60 m	2.066			
202	20 vw	1.937			
104	40 m	1.867			
210	20 vw	1.681	1.654	1 vvw	331
212	50 w	1.545			
204	10 vvw	1.513	1.470	20 w	422
300	60 m	1.469			
213	80 s	1.427			
302	80 s	1.386	1.386	23 w	333
					511
205	80 s	1.323			
214	20 vw	1.299			
220	80 s	1.274	1.274	15 w	440
116	20 vw	1.214	1.140	? m	620

2. The Sluggish Transformation of $ZrCr_2$ from C-14 to C-15

The crystal structure of $ZrCr_2$ in the "as-cast" condition was determined to be the C-14 structure. Specimens in the as-cast condition were annealed at different temperatures and soaked at different times below 1250°C as shown in Table 5.

Table 5. Structure of $ZrCr_2$ at various temperatures below 1250°C.

Specimen Number	Structure Before Annealing	Annealing Temperature °C	Soaking Time Hour	Structure After Heat Treatment
I-9-as-cast	C-14	None		
I-9-760	C-14	760	284	C-14
I-9-810	C-14	810	240	C-14
I-9-810-850*	C-14	810 (850)	240 (480)	C-14
I-9-870	C-14	870	856	C-14
I-9-900	C-14	900	500	C-15
I-9-1250	C-14	1250	24	C-15

*This specimen was first annealed at 810°C for 240 hours and then annealed at 850°C for 480 hours.

From this table, the transformation temperature seems to fall between 870°C and 900°C, and crystal structure of $ZrCr_2$ at lower temperature seems to be of the C-14 type. Rostoker used almost the same procedure in his tests and concluded that the transformation occurred at some temperature between 900°C and 994°C, and the $ZrCr_2$ existed as C-14 structure at low temperatures. However, once the alloy transforms to C-15 structure, it is impossible to transform the alloy back to C-14 structure by annealing the alloy below 900°C as

shown in Table 6.

Table 6. The annealing of $ZrCr_2$ with the C-15 structure.

Specimen Number	Structure Before Annealing	Annealing Temperature	Soaking Time	Structure After Annealing
		°C	Hour	
I-9-1250-810	C-15	810	48	C-15
I-9-1250-850	C-15	850	220	C-15

A true transformation temperature is a temperature at which the transformation will take place reversibly. In other words, when a specimen is heated it will transform from one structure to another above the transformation temperature, and will return to the original structure, when the specimen is cooled slowly or annealed to just below the transformation temperature. From Table 5 and Table 6, it seems that the structure will transform from the C-14 structure to the C-15 structure when it is heated to above 900°C but will not transform from C-15 structure to C-14 structure when the specimen is annealed below 900°C.

In order to verify that a specimen with C-15 structure will not transform to C-14 structure around this pseudo-transformation temperature region, a long time annealing procedure was developed. One specimen with C-15 structure was placed in the furnace at 980°C. After 24 hours, the furnace temperature was gradually lowered to 870°C (see Table 7). At this temperature a specimen with the C-14

structure was placed in the furnace. Both specimens were soaked at this temperature for a long period of time. After this annealing process, X-ray diffraction tests show that the structure of both specimens remained the same as those before heat treatment.

Table 7. The long time annealing of $ZrCr_2$ with the C-14 structure and $ZrCr_2$ with the C-15 structure.

Specimen Number	Structure Before Annealing	Annealing Temperature	Soaking Time	Structure After Annealing
		°C	Hour	
I-9-1250-870*	C-15	980	24	
		950	24	
		900	133	
		890	24	
		870	1120	C-15
I-9-870	C-14	870	856	C-14

*The heat treatment of specimen no. I-9-1250-870 began at the annealing temperature of 980°C for 24 hours. As the temperature was decreased, longer soaking time was given. The continuous heat treatment stages for this specimen are as indicated in this table.

Photomicrographs taken of specimen I-9-1250-870 after the annealing process reveal clear striations which are the symptoms of transformation to the C-15 structure. I-9-870 remains single phase with unchanged grains (Figures 39 and 40).

The long time annealing of the specimen with C-15 structure has demonstrated that the C-15 structure is the stable structure of $ZrCr_2$ at lower temperatures. The C-14 structure is retained to room temperature because the transformation is very sluggish, and

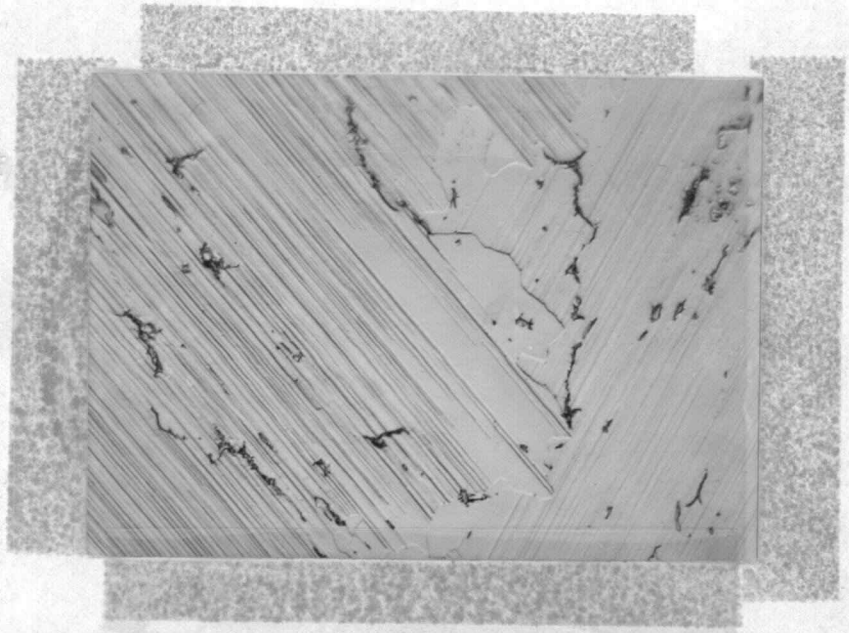

Figure 39. Specimen I-9, 33.57 a/o Zr and 66.43 a/o Cr, annealed at 1250°C for 24 hours, slowly cooled to 870°C then held for 1120 hours. C-15 structure as indicated by X-ray diffraction test. Etching procedure "B". X 500.

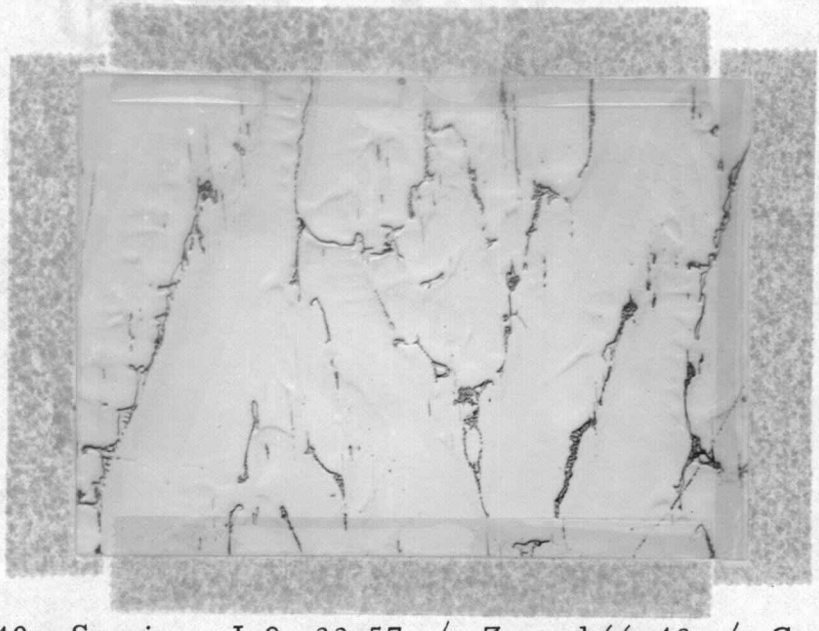

Figure 40. Specimen I-9, 33.57 a/o Zr and 66.43 a/o Cr, annealed at 870°C for 856 hours, homogeneous single $ZrCr_2$ phase and impurities. C-14 structure as indicated by X-ray diffraction test. Etching procedure "B". X 500.

fast cooling after melting does not allow enough time for the transformation. Additional energy is required to alter the metastable condition of the C-14 structure.

The sluggishness of this transformation was further demonstrated from another series of experiments. Four specimens were annealed at 900°C but each specimen was soaked for a different period of time (see Table 8). X-ray diffraction patterns of this group demonstrated that the C-14 structure gradually disappeared as the soaking period lengthened. The figures listed under the column of "% C-14 Structure" were estimated from the intensity of the d = 2.330 line of C-14 structure. The intensity of this line became weaker as the soaking period was extended.

Table 8. The transformation of $ZrCr_2$ with the C-14 structure at 900°C.

Specimen No.	Soaking Time Hour	% C-14 Structure
WC-as-cast		100
WC-900-36	36-1/2	80
WC-900-78	78	65
WC-900-192	192	75
WC-900-384	384	5

3. The Determination of the Transformation Temperature

To determine the transformation temperature of $ZrCr_2$, specimens with C-14 structure (as-cast condition) were annealed at 1300°C, 1400°C, 1500°C, 1550°C and 1600°C respectively, and subsequently

were examined by X-ray diffraction analysis. The result is shown in Table 9.

Table 9. Structures of $ZrCr_2$ at temperatures between 1300°C and 1600°C.

Specimen Number	Structure Before Annealing	Annealing Temperature °C	Soaking Time Hour	Final Structure
I-11-1300	C-14	1300	1	C-15
I-11-1400	C-14	1400	1	C-15
I-11-1500	C-14	1500	1	C-15
WC-4-1550	C-14	1550	3/4	C-15
I-11-1600	C-14	1600	1/4	C-14

From Table 9, one can see that the metastable C-14 structure transforms to stable C-15 structure at any temperature between 900°C and 1550°C. The structure of specimen WC-4-1600 which remains in the C-14 structure before and after the 1600°C anneal indicates two possible transformation behaviors: it may transform from metastable C-14 structure to stable C-15 structure in the temperature range between 900°C and 1550°C, then transform to the high temperature stable C-14 structure somewhere between 1550°C to 1600°C, or it may also indicate that C-14 is a stable phase over all the temperature range between room temperature and 1600°C. To clarify this point, another sequence of tests was conducted. Two specimens with C-14 structure were annealed at 1300°C and 1500°C and subsequently examined by X-ray diffraction. As shown in Table 10, both

transformed to C-15 structure after annealing. These same two transformed specimens were annealed at 1600°C again. X-ray diffraction analyses of these two specimens showed that both transformed to the C-14 structure (Table 10).

Table 10. Structure of $ZrCr_2$ with double annealing.

Specimen Number	Structure Before Analysis	Annealing Temperature °C	Soaking Time Hour	Final Structure
I-11-1300	C-14	1300	1	C-15
-1600	C-15	1600	1/4	C-14
I-11-1500	C-14	1500	1	C-15
-1600	C-15	1600	1/4	C-14

From the above series of tests, it is evident that a transition from C-15 structure at lower temperatures to the C-14 structure occurred at some temperature between 1550°C and 1600°C.

The metallographic evidence for the transition from the C-15 structure to the C-14 structure is just as conclusive as the X-ray diffraction analyses. Metallographically, as discussed in the paragraph IV, A, $ZrCr_2$ with the C-15 structure consists of a series of parallel striations within each grain. These features are also displayed in the microstructures of the specimens which are annealed just below and above the transition temperatures respectively. The microstructure of the 1550°C annealed specimen which was indicated as C-15 structure by X-ray analysis reveals the evidence of striations within each grain (Figure 41). On the other hand, the 1600°C annealed

specimen reveals a homogeneous structure (Figure 42) which was indicated as the C-14 structure by the X-ray diffraction analysis.

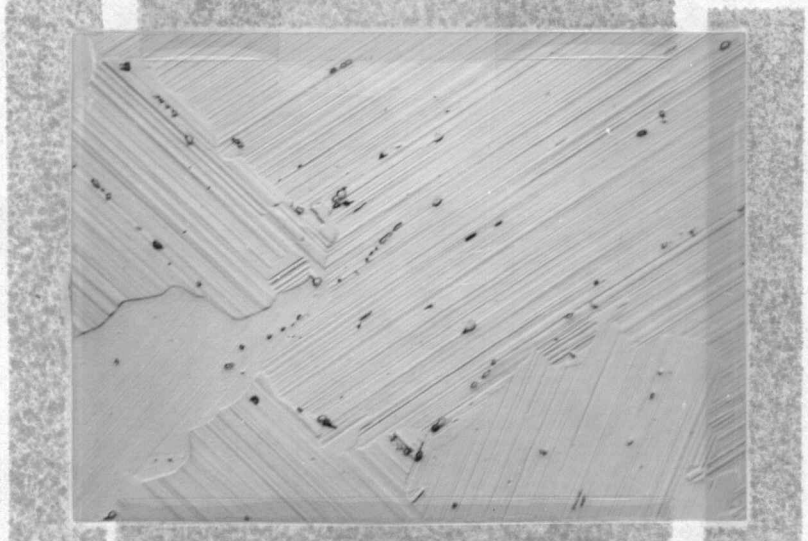

Figure 41. Specimen WC-4, 33.33 a/o Zr and 66.66 a/o Cr, annealed at 1550°C, single phase $ZrCr_2$ with impurities. C-15 structure as indicated by the X-ray diffraction test. Etching procedure "B". X 500.

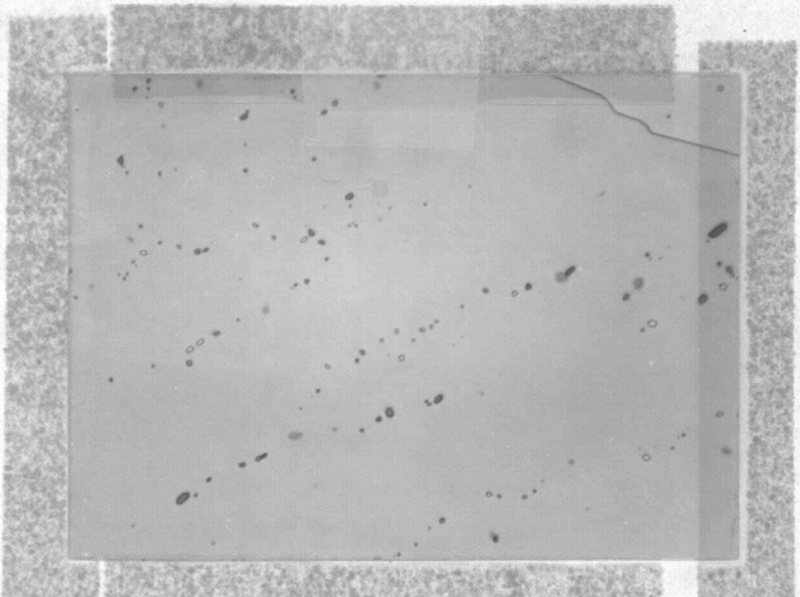

Figure 42. Specimen I-11, 32.68 a/o Zr and 67.32 a/o Cr, annealed at 1300°C and then 1600°C, single phase $ZrCr_2$ with impurities. C-14 structure as indicated by the X-ray diffraction test. Etching procedure "B". X 500.

C. The Determination of the Transformation Habit Plane of $ZrCr_2$

Because the intermetallic compound has a narrow range of composition, the assumption can be made that the transformation occurs in the same manner as that of a pure metal. This assumption can be further justified on the basis of the homogeneous nature of the compound and because it maintains its own crystal structure.

An allotropic change in the pure metal occurs through the movement of an interface consisting of a set of dislocations similar to the movement of dislocations postulated in theories of slip and twinning. Barrett (4) postulated that the atom leaves the lattice of the parent crystal and attaches itself to the lattice of a transformed crystallite as one of these dislocations passes an atom in a crystal. If the dislocation moves in the opposite direction, it has the opposite effect and transfers an atom back to the parent.

In the photomicrographs, it is clearly seen that the striations appear on most grains with C-15 structure. On the contrary, striations do not appear in specimens in the as-cast condition (C-14 structure). Moreover, striations disappear when a specimen with the C-15 structure transforms to the C-14 structure upon annealing at $1600^{\circ}C$ (Figures 41 and 42). The striations indicate that the transformation involves the shearing of certain sets of atomic planes. In order to find the planes represented by the striations, the crystal

orientation was determined. The plane represented by the striations was oriented by the method described in Structure of Metals by Barrett. The back-reflection-Laue diffraction method was used for this orientation.

The method used to determine the orientation of a particular grain in a polycrystalline specimen was described in Section III, E.

The first orientation picture revealed that the chosen grain with striations did not produce a single crystal pattern. After a few failures, the entire specimen surface was divided into fifty regions, each of which has an area of about one square millimeter. Back-reflection-Laue photographs were taken for every region in which a grain was located. However, none of the photographs disclosed a clear single crystal pattern, owing to the fact that the striations produced an effect similar to that which would be caused by a roughly abraded surface.

Finally a successful photograph was taken on a grain without striations on the surface. Some of the reflection spots in this graph are randomly distributed, but others lie on curves forming a good diffraction pattern.

The diffraction spots lying on any one curve were connected. A total of five curves were obtained and designated as A, B, C, D, and E in Figure 43. A Greninger chart for the solution of back-reflection-Laue patterns for a specimen-to-film distance of four

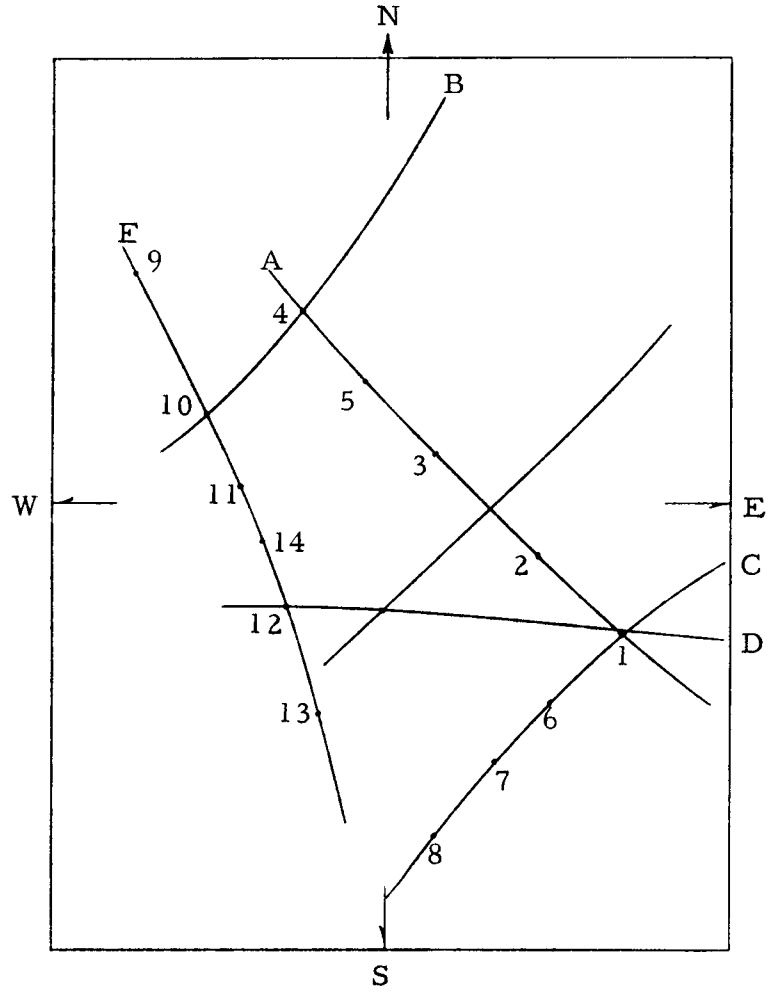

Figure 43. Back-reflection-Laue pattern of the "grain b" of Figure 50.

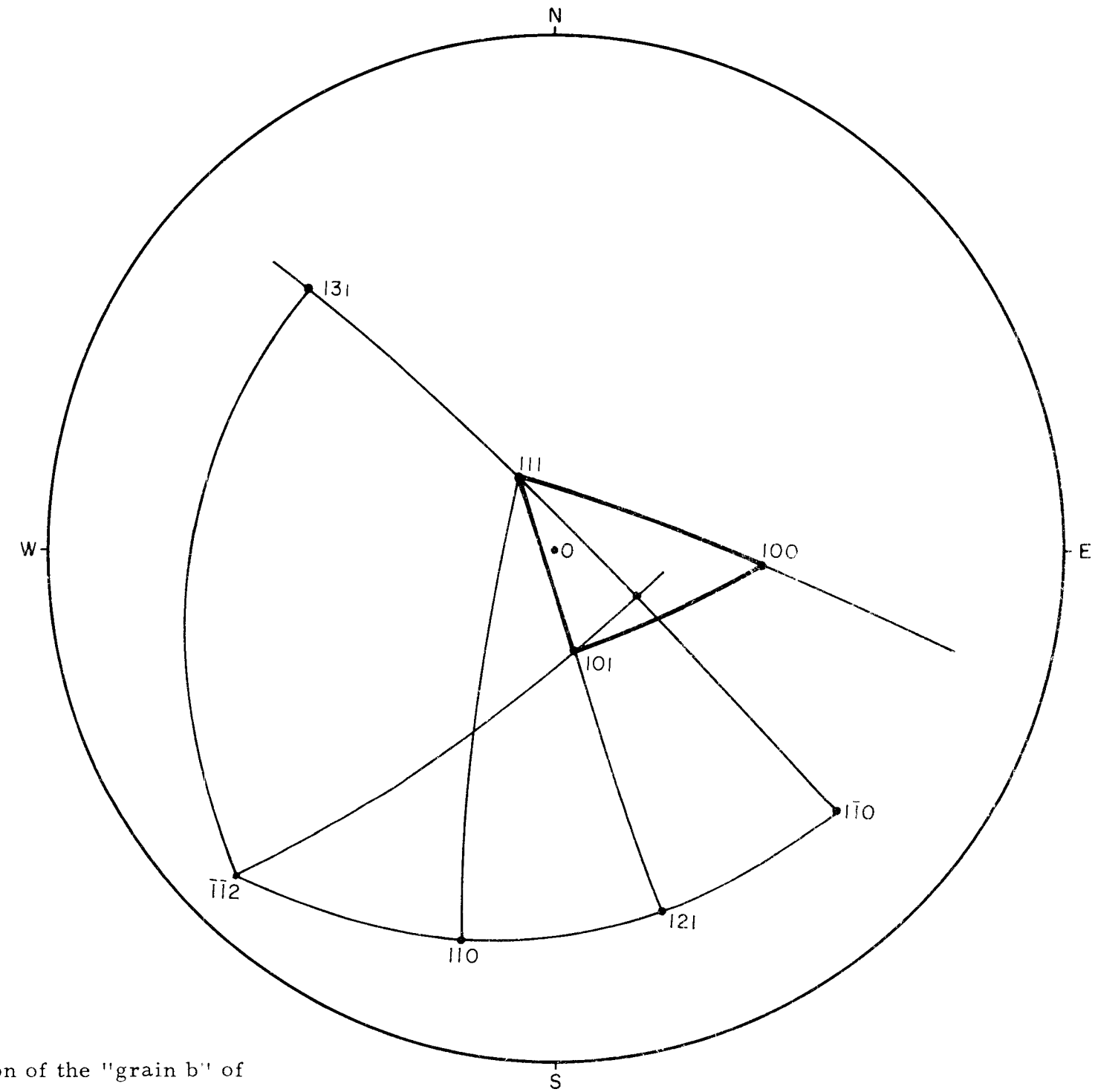

Figure 44. Orientation of the "grain b" of Figure 47.

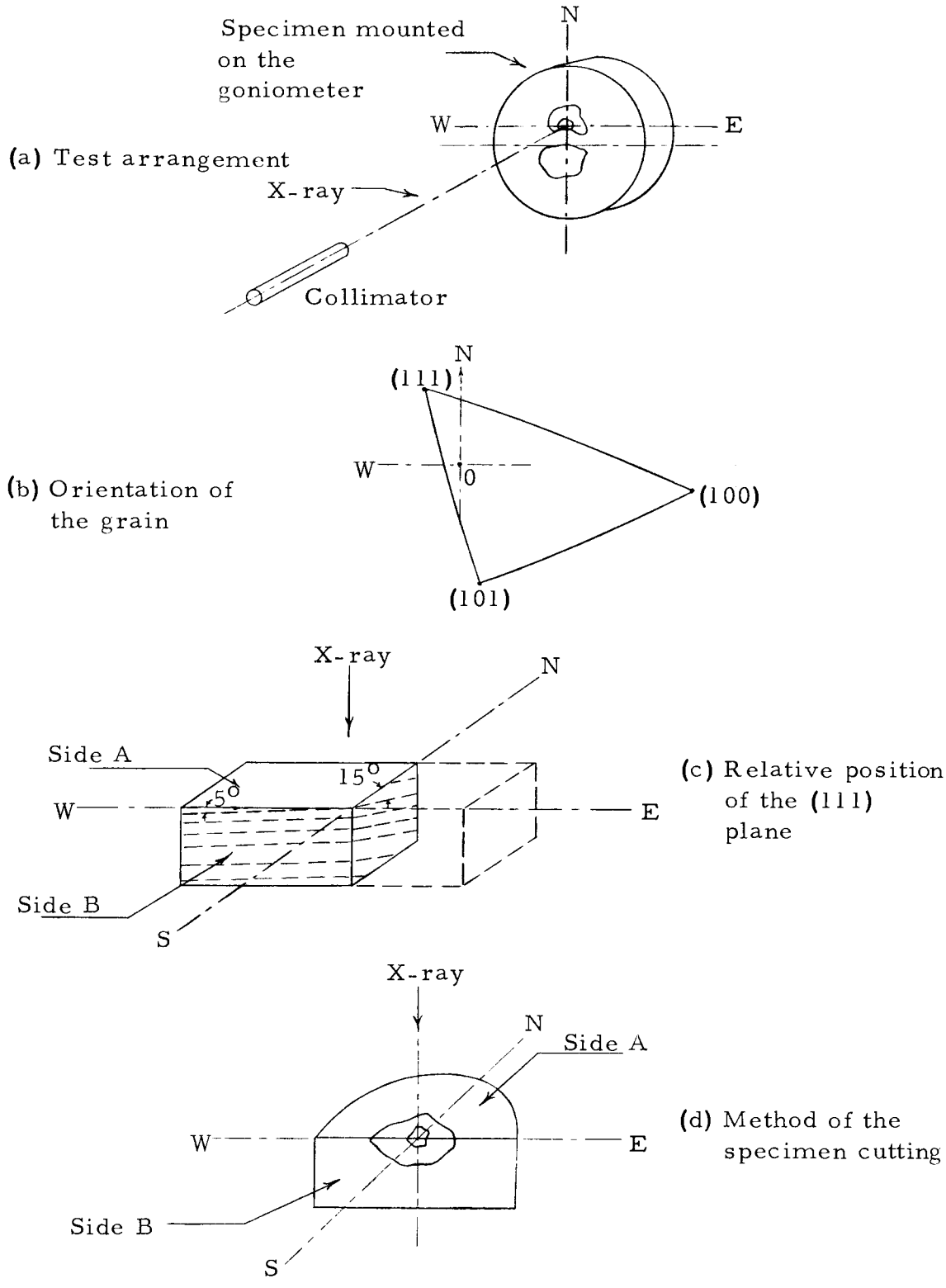

Figure 45. Sketches of the back-reflection-Laue method.

centimeters (D = 4 cm) is used for transferring the patterns to the stereographic projection. With the aid of a Wulff net, all zones and zone axes were plotted on a stereographic projection as shown in Figure 47 by following the standard method described in Cullity (10, p. 138-146).

The method of indexing each plane represented by each spot is essentially a trial and error method. One compares the measured angle between poles with a table of Angles Between Planes in Cubic Crystals (32) and with the aid of a "Standard (111) Projection for Face-Centered Cubic Crystal". Each plane revealed by the corresponding diffraction spot can be identified as shown in Figure 44. In this stereogram, the orientation of the grain is clearly shown by the unit stereographic triangle. The pole representing the (111) plane is about five degrees to the west of the N-S axis and 15^{o} to the north of the E-W axis.

The arrangement for taking the back-reflection-Laue photograph is shown in Figure 45a, where one can see the relative position between the incident X-ray beam and the specimen axes. The stereographic triangle (Figure 45b) showing the orientation of the grain is reproduced from Figure 44. The intersection of the N-S and E-W axes is located on the grain to be examined. Let one imagine that a rectangular slab is cut off from this grain. Figure 45c shows this imaginary slab and its relative orientation to the surface plane of the

specimen and to the incident X-ray beam and will be called "Side A" hereafter. A plane perpendicular to Side A and also perpendicular to the N-S axis is called "Side B". In Figure 45c, the (111) planes are represented by the dotted lines. The solution of the X-ray orientation photograph indicates that each (111) plane makes an angle of five degrees with the E-W axis and 15^{o} with the N-S axis. Therefore when the specimen shown in Figure 46 is cut in the manner as shown in Figure 45d, one can expect that the striations representing (111) planes will make a small angle with the E-W axis.

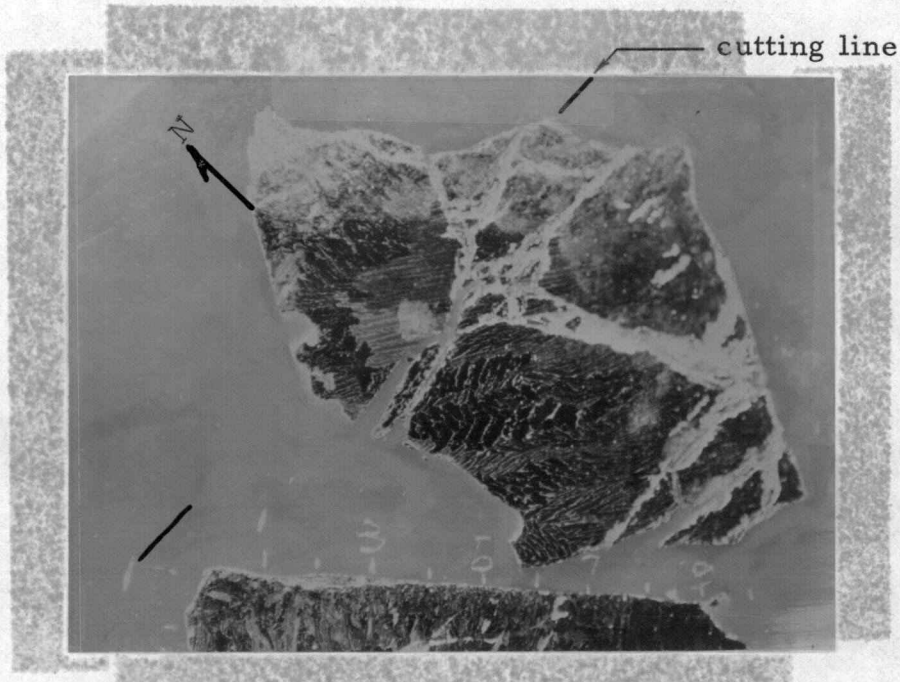

Figure 46. Specimen before cutting. N indicates the north direction for X-ray. X 10.

To prove this point the specimen was then cut and ground so that the surface of Side B of the oriented grain was exposed. Then Side B was polished and etched. Figure 46 shows Side A of the

specimen which was X-rayed before cutting. It also shows the directions of N-S and E-W axes. The specimen was then cut along the E-W axis. Figure 47 shows a photomicrograph of Side A after etching. Three grains along the E-W axis appear in the picutre; "grain b" is the grain which has been X-ray oriented. Striations appear in "grain a" but not in "grain b" or "grain c". Figure 48 shows the photomicrograph of Side B of the specimen after etching. Striations having different directions appear in all three grains. The striations appearing on "grain b" are of particular importance. They are almost parallel to the E-W axis which is also the cutting edge. This proves to be in agreement with the discussion in the previous paragraph.

Using the back-reflection-Laue method, it has been shown that the trace of the (111) plane on Side B is nearly parallel to Side A (Figure 45c). Here a cut on the specimen has been made to expose the Side B. The striations on Side B follow the direction of the (111) plane. It is evident therefore that the striation plane is in the (111) plane.

Since the striations appear only after C-14 to C-15 transformation as displayed in the photomicrographs in the previous sections, it is concluded that the transformation takes place due to shearing on the (111) plane.

It is interesting to note that the set of striations on Side B of "grain c" makes an angle of 10^{o} to 15^{o} with the cutting edge (E-W

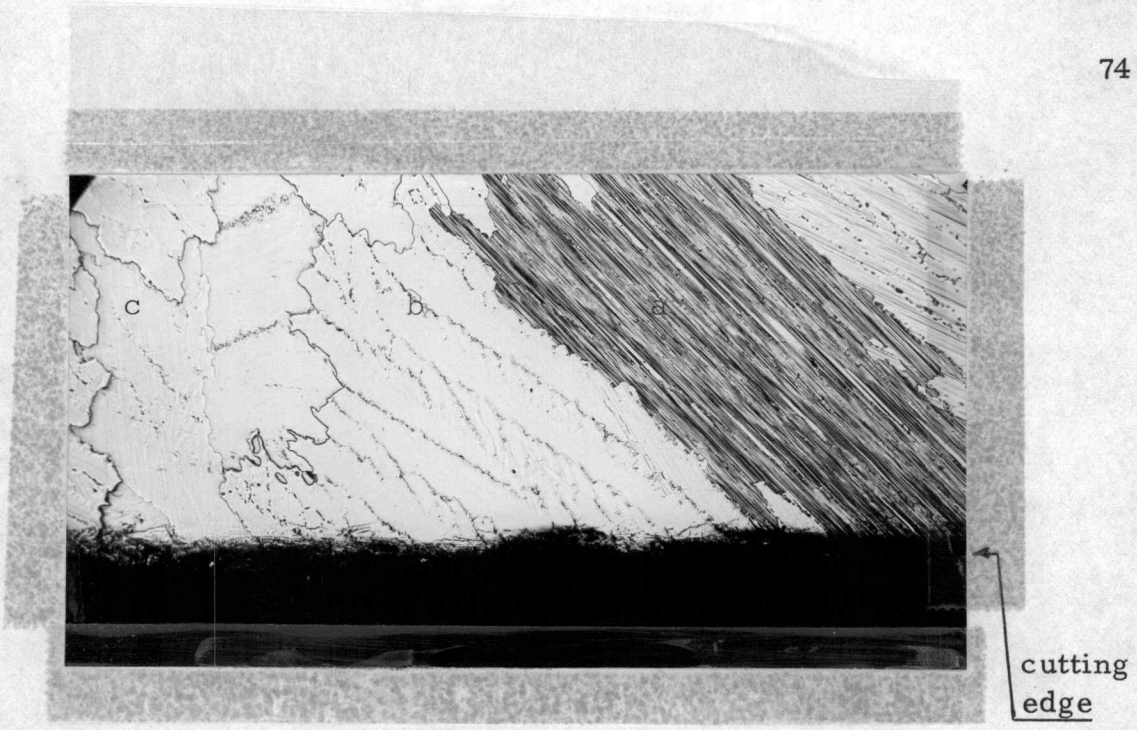

Figure 47. Specimen after cutting. Side A. X 50.

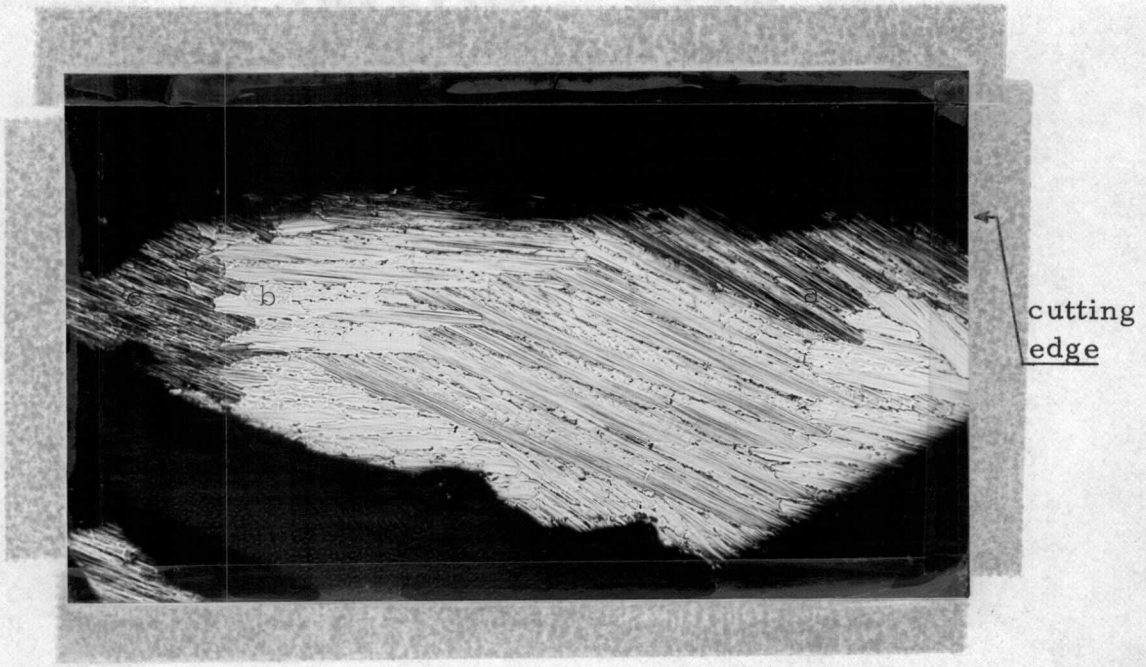

Figure 48. Specimen after cutting. Side B. X 50.

axis). There are also no striations observed on Side A of "grain c". From the low angle striations of "grain b" and "c", one can see that striations due to etching are not likely to occur on Side A if the shear plane makes a small angle to the surface of Side A. It would be quite reasonable to expect that a set of striations making 15^{o} to the N-S axis would appear on the surface perpendicular to E-W axis, if "grain b" were cut along N-S axis.

D. The Proposed Transformation Mechanism of $ZrCr_2$

Previously, it was experimentally demonstrated that the transformation from the C-15 structure to the C-14 structure occurs on the (111) planes of the C-15 structure. In this section models are developed to test the transformation coherency. The complete deduction is based upon the hard sphere approximation (i.e. assume that both zirconium and chromium atoms are hard spheres, but of different sizes) and upon considering the glide of rigid planes of atoms over one another during transformation.

To visualize the transformation easily two physical models were built. One depicts a unit cell of C-14 structure (HCP), and the other depicts a unit cell of C-15 structure (FCC) as it would appear projected on the (111) planes such that these planes are parallel to the (0001) planes of the C-14 structure (Figures 49 and 50). In these models the light-colored spheres represent zirconium atoms and the

dark-colored spheres represent chromium atoms. However, they indicate only the positions not the sizes of atoms. Figure 52 and Figure 53 are sketches to show the positions of these atoms.

The model of the C-14 structure with zirconium at each corner of the cell was built according to the following data: $c = 8.22$ kX, $a = 5.092$ kX, and $(c/a) = 1.615$. The scale is 5.092 kX = 6-inch.

The mode of transformation of the C-15 unit cell from cubic orientation to the orientation with (111) planes parallel to the (0001) planes of the C-14 unit cell is derived as follows: in Figure 54a, the plane (111) is parallel to the plane of the paper. The arrangement of the zirconium atoms in the (111) plane is a consolidation of many equal-sided parallelograms, one of which is outlined and designated ARSQ in Figure 54a. Each parallelogram forms a base of a transformed C-15 unit cell and is very similar to the arrangement of the base of the C-14 unit cell. The parameter of the C-15 structure is: $a = 7.193$ kX. Hence the distance "a_{equ}" between two zirconium atoms on the (111) plane is:

$$a_{equ} = (\sqrt{2}/2)a = 5.085 \text{ kX}$$

In Figure 54b, the (110) plane of the cubic oriented C-15 unit cell is parallel to the paper. The (110) plane is labelled as plane FEOB. In this figure the [110] direction represents the abcissa and

[001] direction, the ordinate. The (111) plane which is perpendicular to the paper projects as a line making an angle of $\theta = \tan^{-1}\sqrt{2}$ with the abcissa. The direction $[11\bar{2}]$ of Figure 54a also makes an angle of $\theta = \tan^{-1}\sqrt{2}$ with the abcissa in Figure 54b. The direction $[\bar{1}10]$ in Figure 54a is perpendicular to the paper at the point "0" of Figure 54b. Therefore, the projection of plane ARSQ in Figure 54a becomes a line shown as "AS" in Figure 54b. The height "h" of the transformed C-15 cell represented by "FO" is

$$h = \sqrt{3}a = 12.458 \text{ kX},$$

where "a" is as above.

It is shown in Figures 52 and 53 that there are eight layers and 12 layers of atoms in the C-14 and C-15 structures respectively. Since the stackings of these two cells are both closely packed, the parameter "c" of the C-14 unit cell approximately equals (2/3)h, i.e. 8.306 kX, of the C-15 unit cell. The value of (2/3)h will be called "c_{equ}". Figure 52 shows the model which demonstrates a complete unit cell with the value "h" as its height. Figure 51 shows the bottom two-thirds of the C-15 unit cell with "c_{equ}" as its height.

The features of these two kinds of structures are as follows:

1) Figure 55 shows the atomic arrangements of the vertical cross-sections of the two unit cells. Both cross-sections

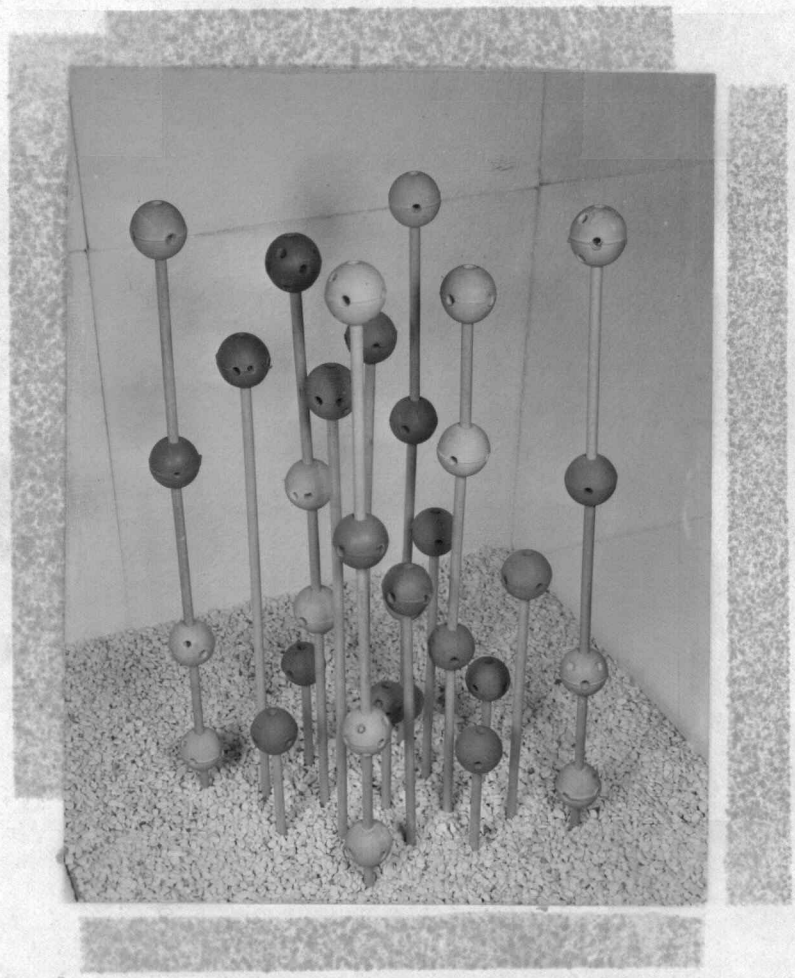

Figure 49. Sphere model to show the positions of atoms in the unit cell of the C-15 structure of $ZrCr_2$ projected on the (111)planes. Light-colored balls represent zirconium atoms; dark-colored balls, chromium atoms.

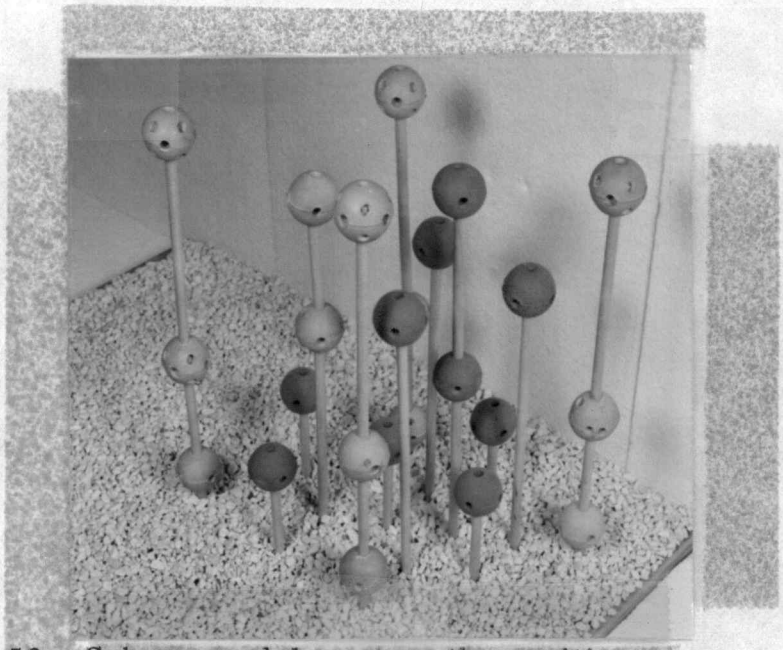

Figure 50. Sphere model to show the positions of atoms in the unit cell of the C-14 structure of $ZrCr_2$.

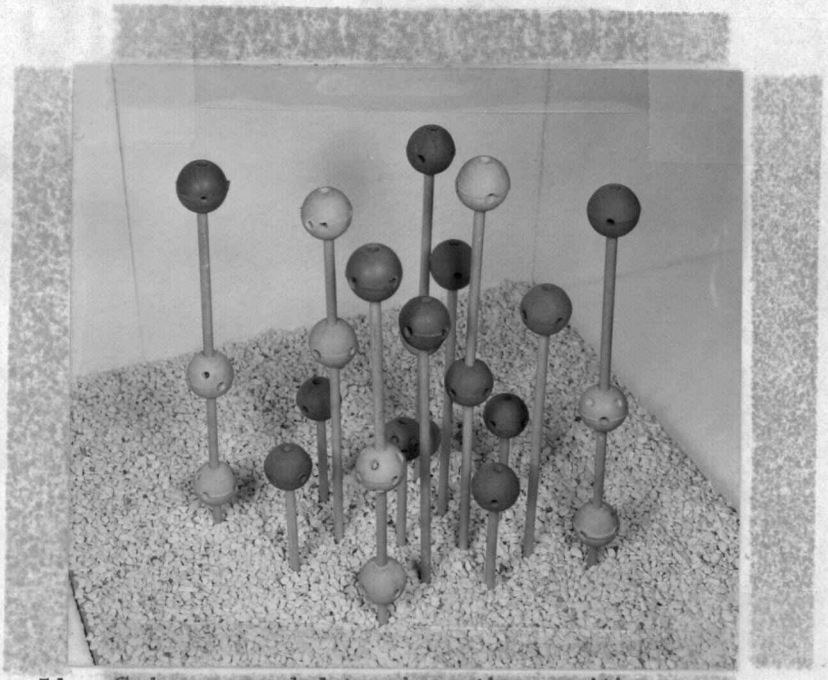

Figure 51. Sphere model to show the positions of atoms in the unit cell of the C-15 structure of $ZrCr_2$.

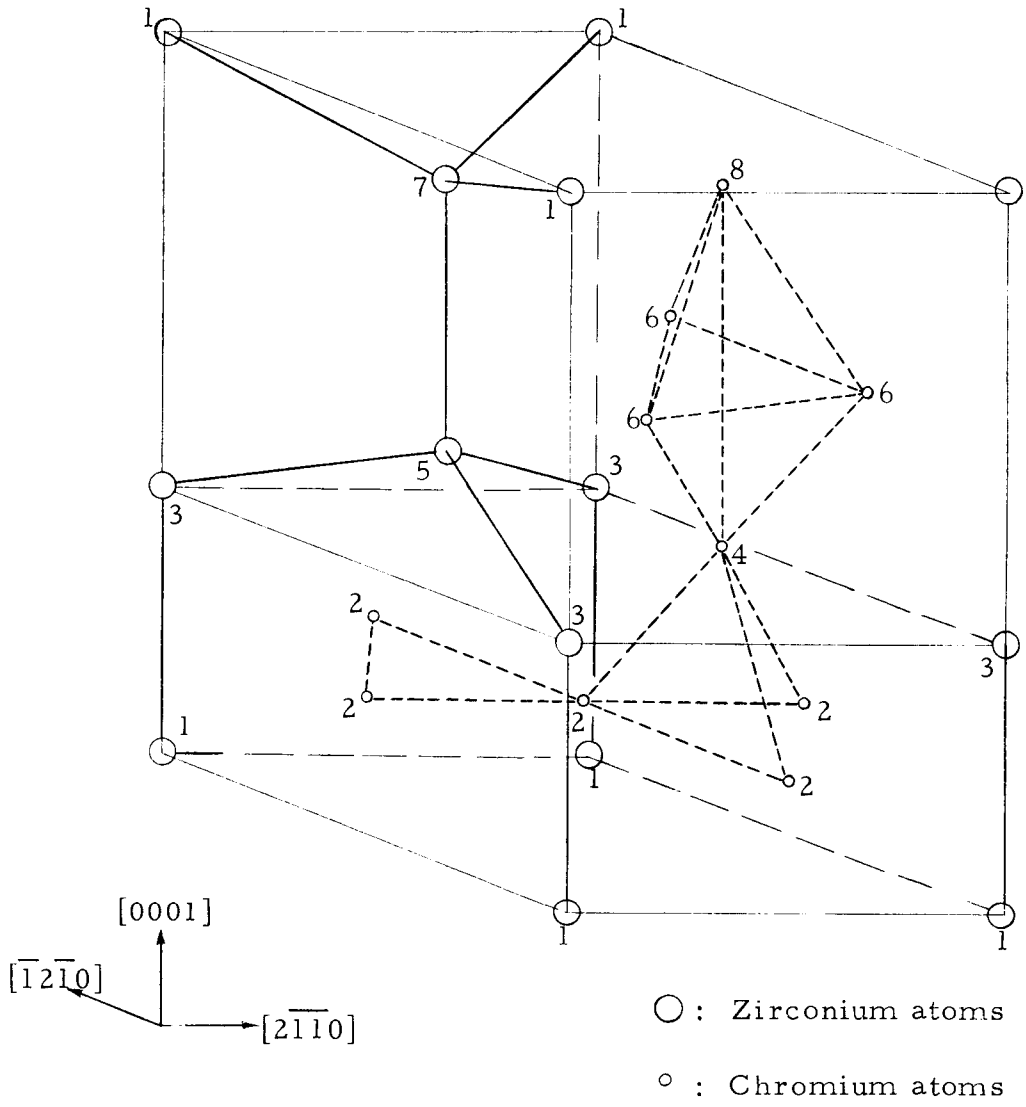

Figure 52. Arrangement of atoms in the unit cell of C-14 structure of $ZrCr_2$. Numerials denote the atomic layer numbers.

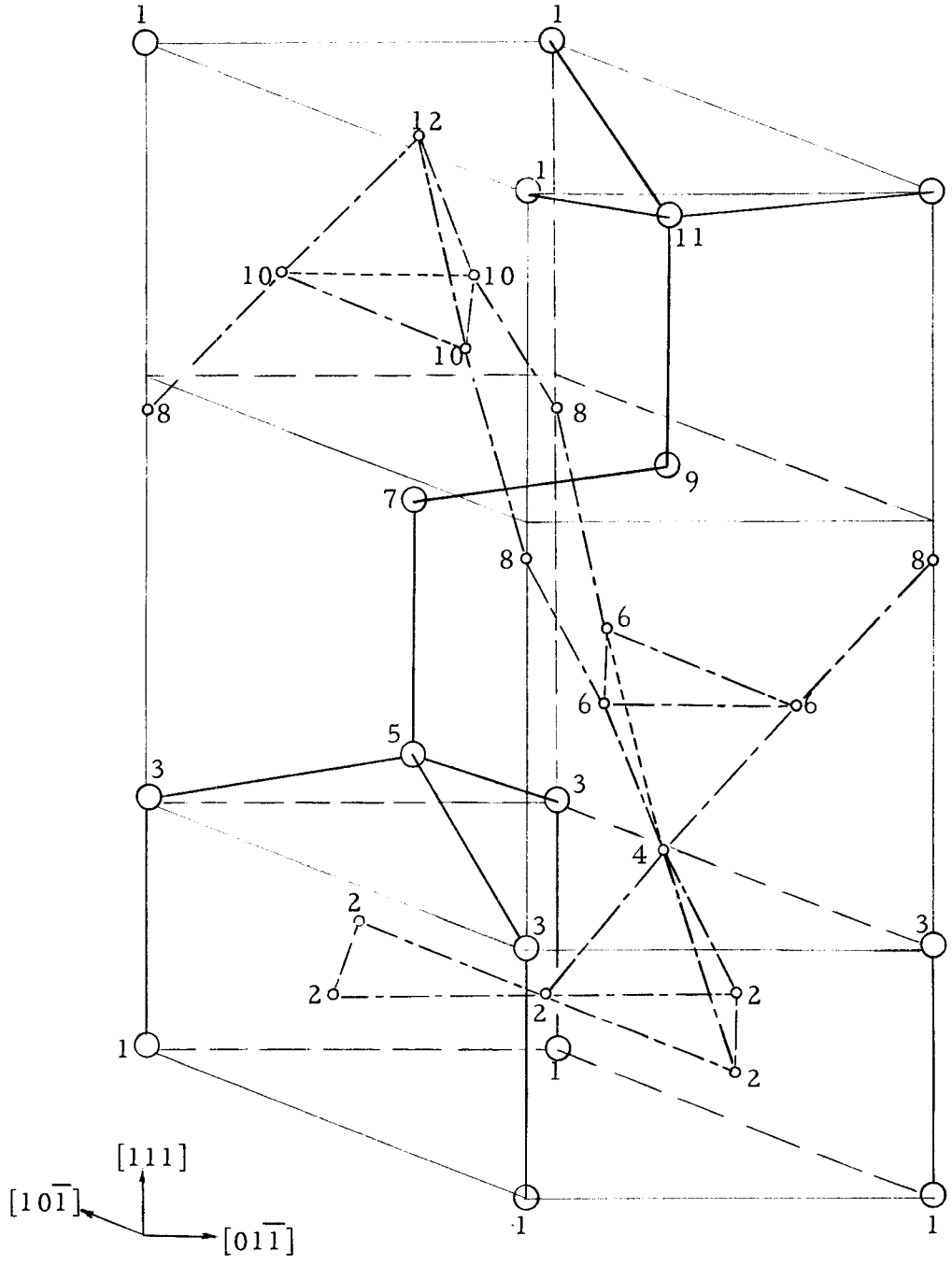

Figure 53. Arrangement of atoms in the unit cell of C-15 structure of $ZrCr_2$. Numerals denote the atomic layer numbers.

○: Zirconium atoms ∘: Chromium atoms

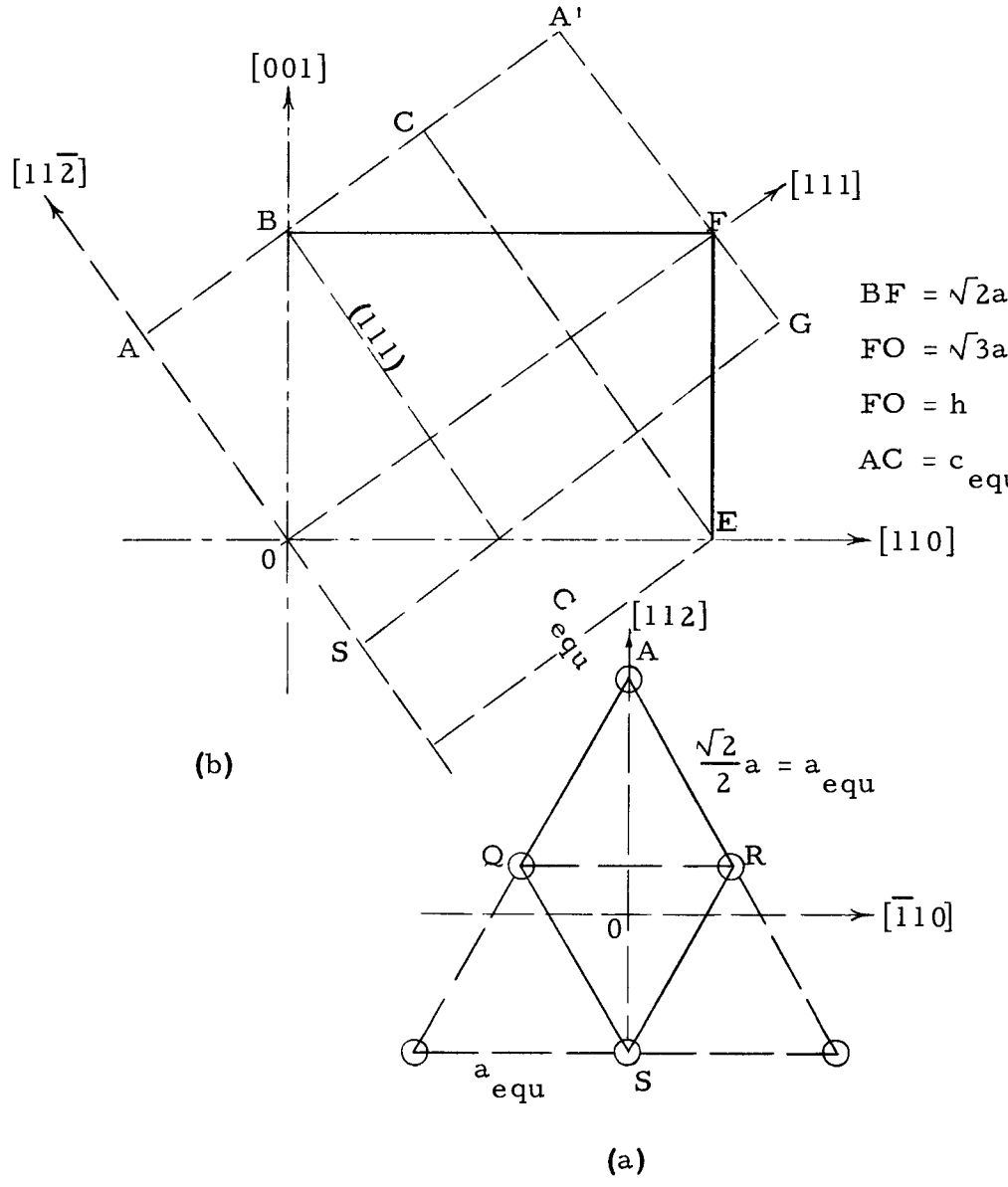

Figure 54. (a) The arrangement of atoms on the (111) plane, and (b) the dimensions of the (110) plane of the C-15 structure.

are made along the major diagonal of the cell bases. The lengths of the major diagonals are $(\sqrt{7}/2)$ "a" and $(\sqrt{7}/2)$ "a_{equ}" for the C-14 and C-15 structures respectively. All the atoms and the lattice parameters are in the same scale. The two figures in Figure 55 clearly show that the complete cell of the C-15 structure consists of 12 layers of the atoms with zirconium and chromium atoms alternately stacked. And the complete cell of the C-14 structure consists of eight layers of atoms with zirconium and chromium atoms alternately stacked. Therefore the height of the C-15 unit cell is about 1-1/2 times of the height of the C-14 structure.

2) Comparing the actual size of "c_{equ}" of the C-15 structure and the "c" of the C-14 structure, and "a_{equ}" and "a", one can see that the size differences are very small:

$$c_{equ} - c_{14} = 0.084 \text{ kX};$$

and

$$a_{equ} - a_{14} = -0.006 \text{ kX}.$$

In transforming from C-15 to C-14, the height will contract slightly and the base will expand by a much smaller amount. For practical purposes these trivial changes can be neglected.

3) When the 24 planes in two consecutive C-15 cells are

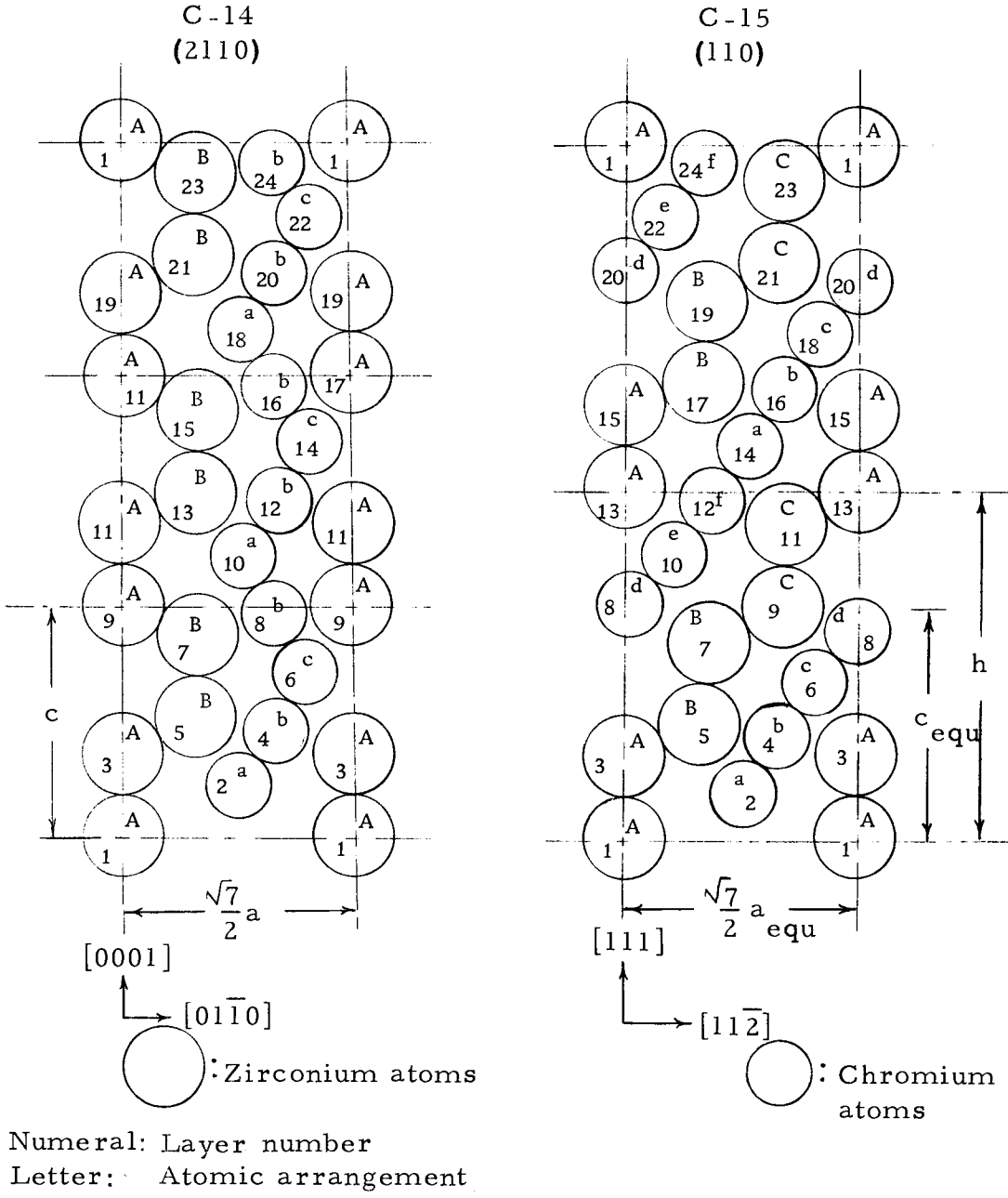

Figure 55. Vertical diagonal sections of the unit cells of the C-14 and C-15 structures.

sequentially numbered as 1, 2, 3, 4, ..., 24, and the 24 planes in the three consecutive C-14 cells are also numbered in the same manner (referring to Figures 52, 53 and 55), one can see that the same planes have the same number of atoms of the same kind, but the locations of atoms are different.

4) All the zirconium layers consist of one atom per unit area. All the chromium layers consist of either one or three atoms. If each layer is treated separately, the two-dimensional void area of each layer can be calculated as shown in Table 11.

Table 11. Calculation of the void area in the two-dimensional unit cell.

	Atomic Distance, d = kX	
	C-15 Structure	C-14 Structure
Zr-Zr	3.115	3.083
Cr-Cr	2.543	2.985

Structure Plane	Equation	Calculation kX^2	
		C-15 (111)	C-14 (0001)
(1) Area of cell*	$c^2 \sin 60^\circ$	22.401	22.454
(2) Area of Zr	$(1/4)\pi d^2$	7.625	7.471
(3) Area of Cr	$(1/4)\pi d^2$	5.082	5.091
(4) Void of the plane with Zr	(1)-(2)	14.776	14.983
(5) Void of the plane with one Cr	(1)-(3)	16.319	16.363
(6) Void of the plane with three Cr	(1)-3x(3)	7.115	7.181

*The term "c" represents the "c_{equ}" of the C-15 structure or "c" of the C-14 structure.

This table compares the two-dimensional void areas in the two corresponding planes of the C-15 structure and the C-14 structure respectively. Lines (4), (5), and (6) show the area of the two-dimensional void areas in the planes with one zirconium atom, one chromium atom, and three chromium atoms respectively. The results indicate that there is negligible space incoherency when C-14 transforms to C-15 or vice versa.

5) Referring to Figure 55, which is a vertical diagonal section of Figure 52 and Figure 53, one can see that C-15 is stacked in the manner of AaAbBcBdCeCf and C-14 in the manner of AaAbBcBb, where the capital letters represent the zirconium atom layers, and the lower-case letters represent the chromium layers. Layers with same letters have the same atomic arrangement. It will take 24 layers to complete one cycle of transformation as shown in Table 12.

Table 12 shows how the atoms change their arrangement in each layer. The table demonstrates that the transformation can be accomplished by merely rearranging the atoms in each layer. This is possible as the corresponding layers have the same number of atoms of each kind.

Table 12. The rearrangement of atoms during transformation.

Layer Number	C-15 transforms to C-14 (C-15→C-14)	
1	A	A
2	a	a
3	A	A
4	b	b
5	B	B
6	c	c
7	B	B
8	d	b
9	C	A
10	e	a
11	C	A
12	f	b
13	A	B
14	a	c
15	A	B
16	b	b
17	B	A
18	c	a
19	B	A
20	d	b
21	C	B
22	e	c
23	C	B
24	f	b

Bearing the above five features in mind, one can analyze the transformation movements of atoms by first isolating one layer of atoms at a time and then comparing the relative positions between the atoms and the space lattice in the C-15 and C-14 structures.

In each figure from Figure 56 to Figure 67, the movement of atoms in each of the 24 corresponding layers is shown as described in Table 12. In every figure four unit cells are shown. Zirconium in

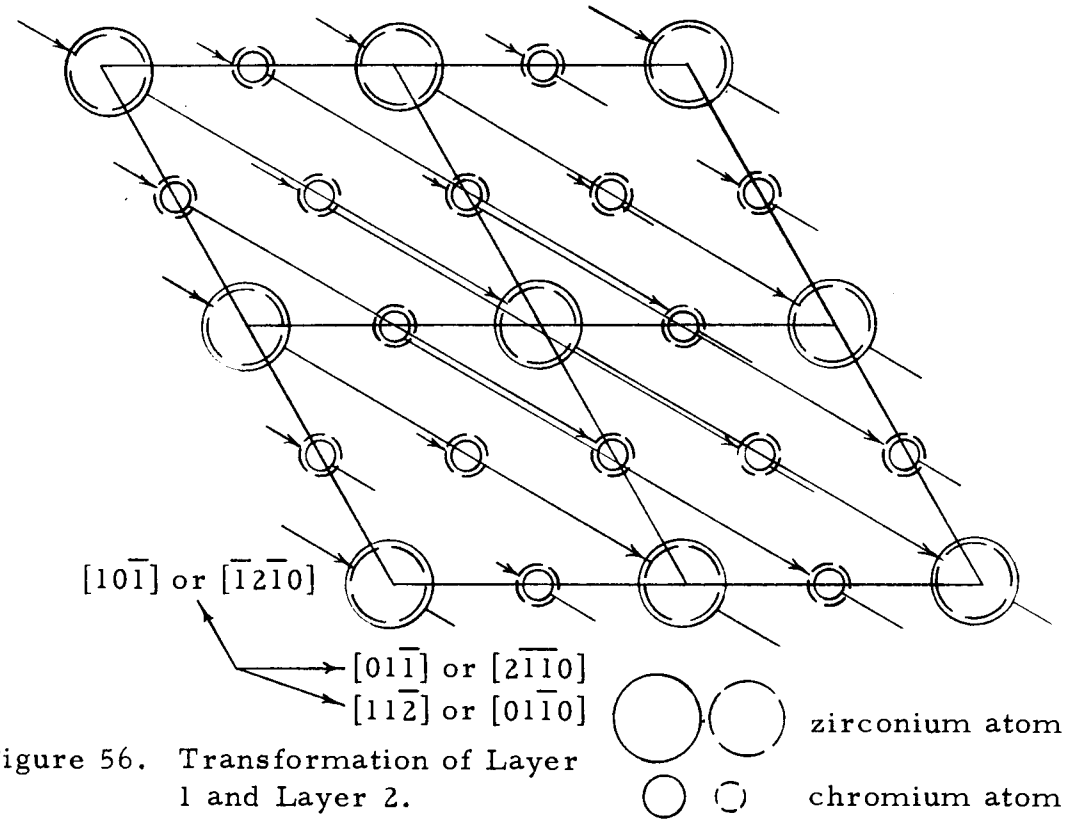

Figure 56. Transformation of Layer 1 and Layer 2.

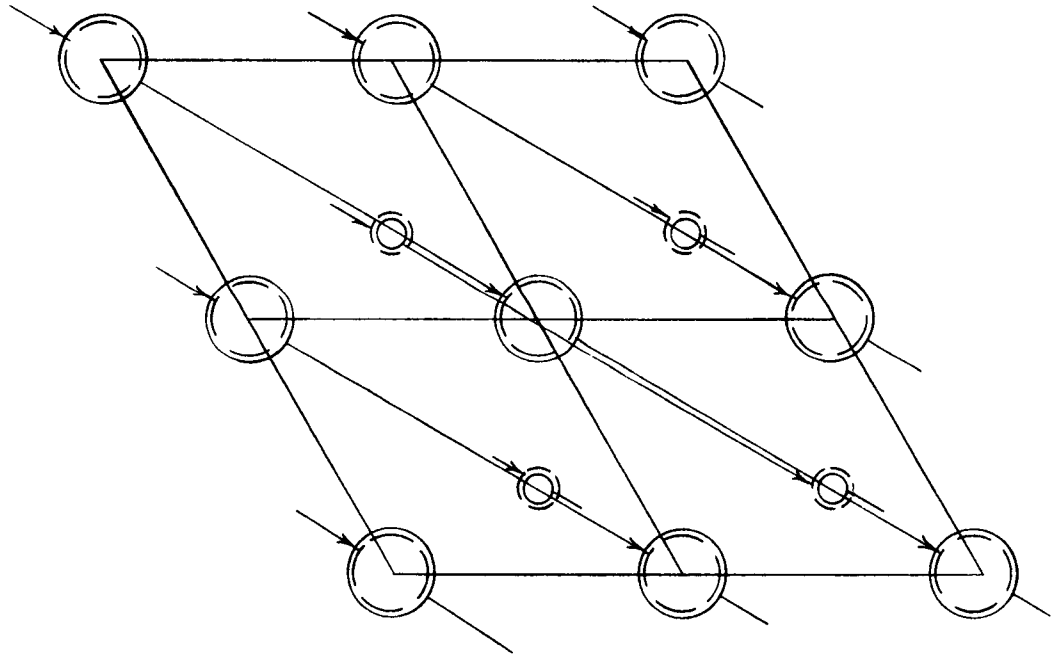

Figure 57. Transformation of Layer 3 and Layer 4.

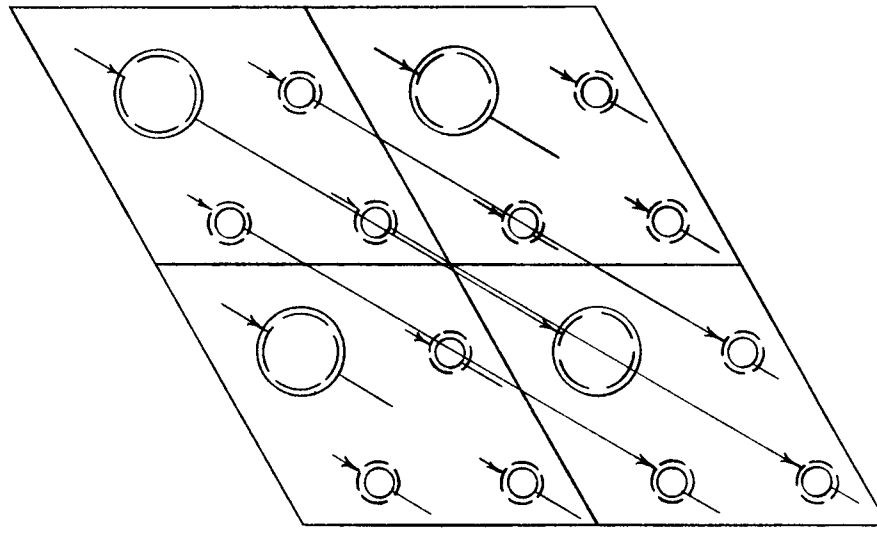

Figure 58. Transformation of Layer 5 and Layer 6.

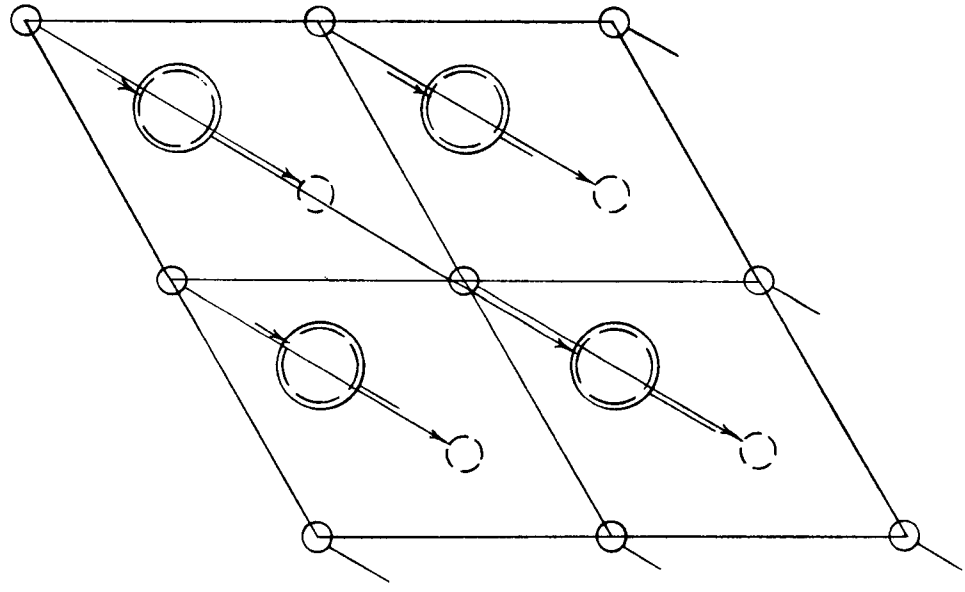

Figure 59. Transformation of Layer 7 and Layer 8.

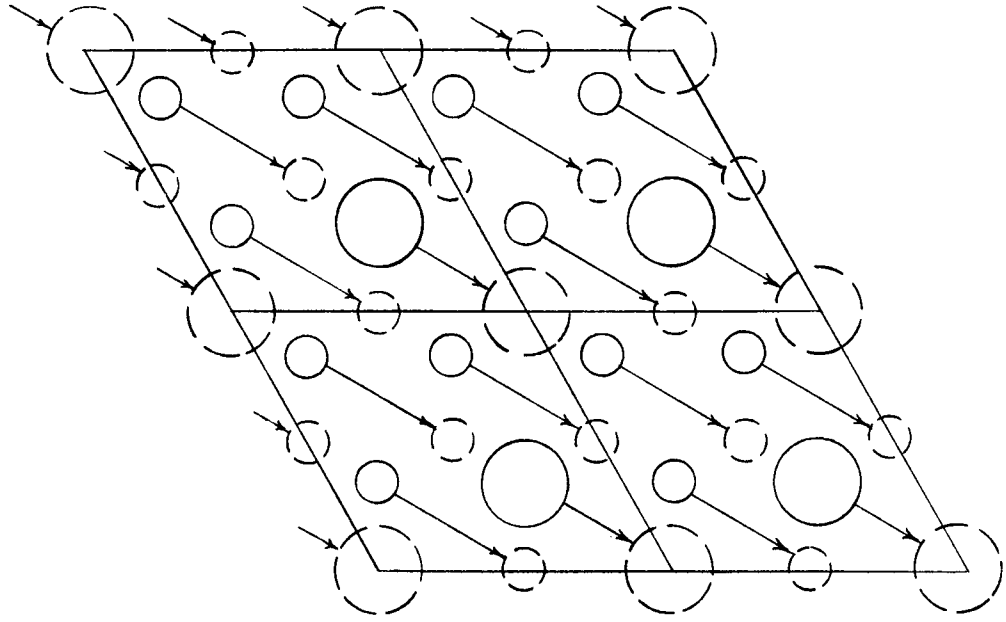

Figure 60. Transformation of Layer 9 and Layer 10.

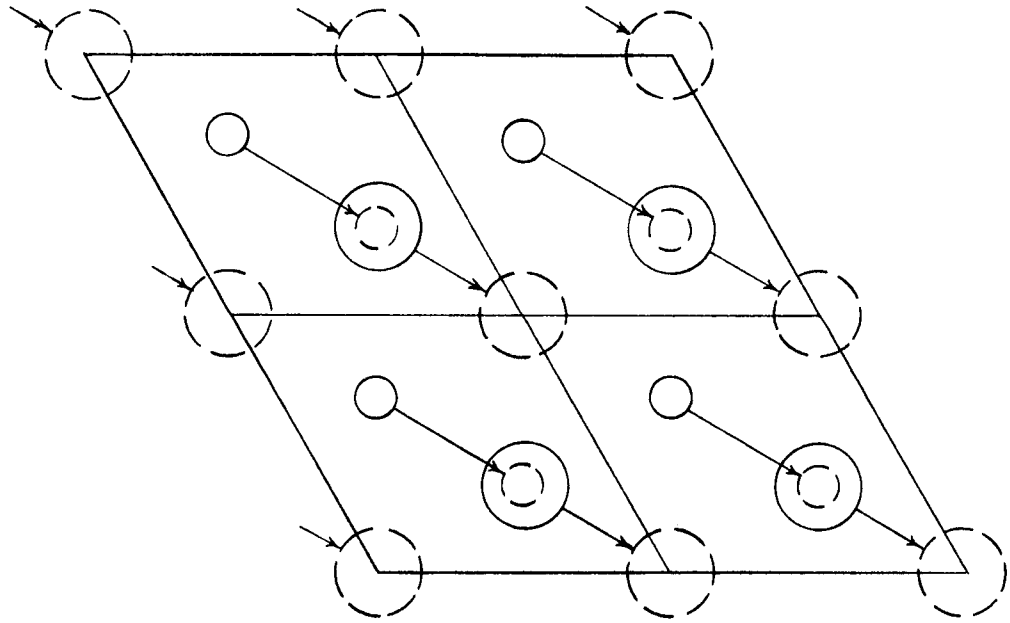

Figure 61. Transformation of Layer 11 and Layer 12.

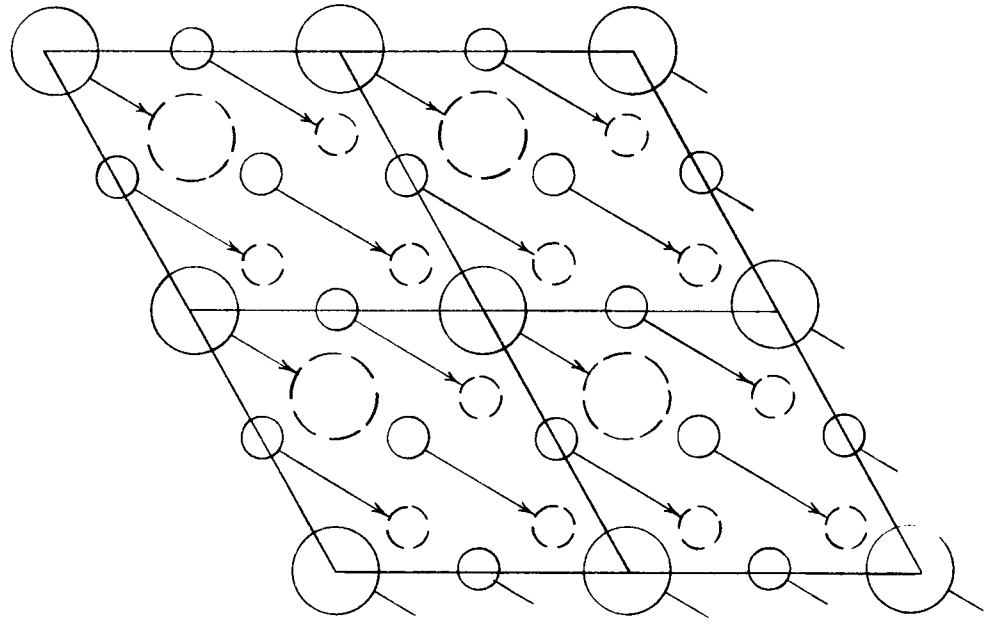

Figure 62. Transformation of Layer 13 and Layer 14.

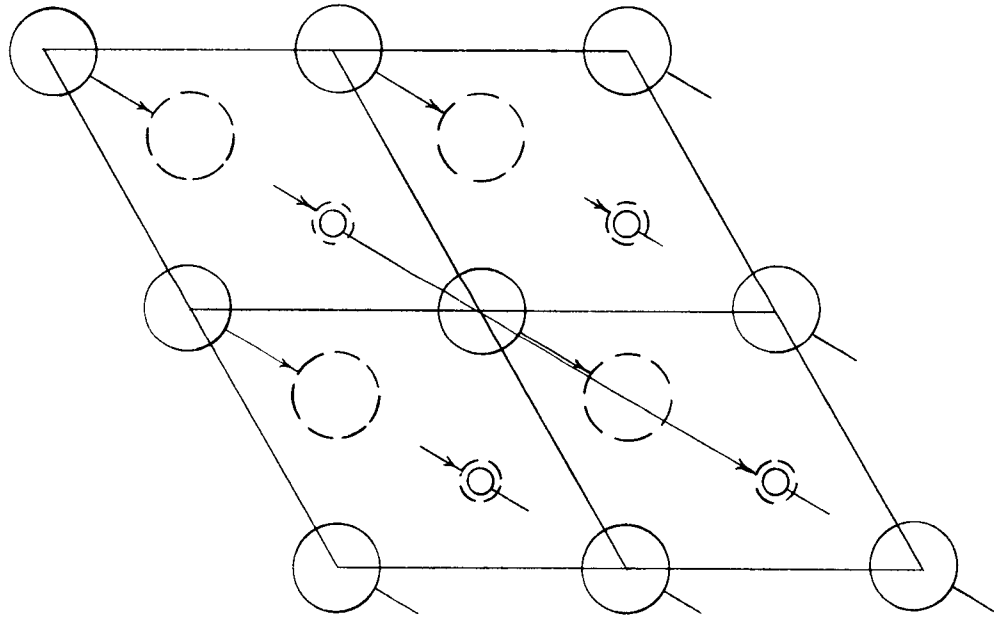

Figure 63. Transformation of Layer 15 and Layer 16.

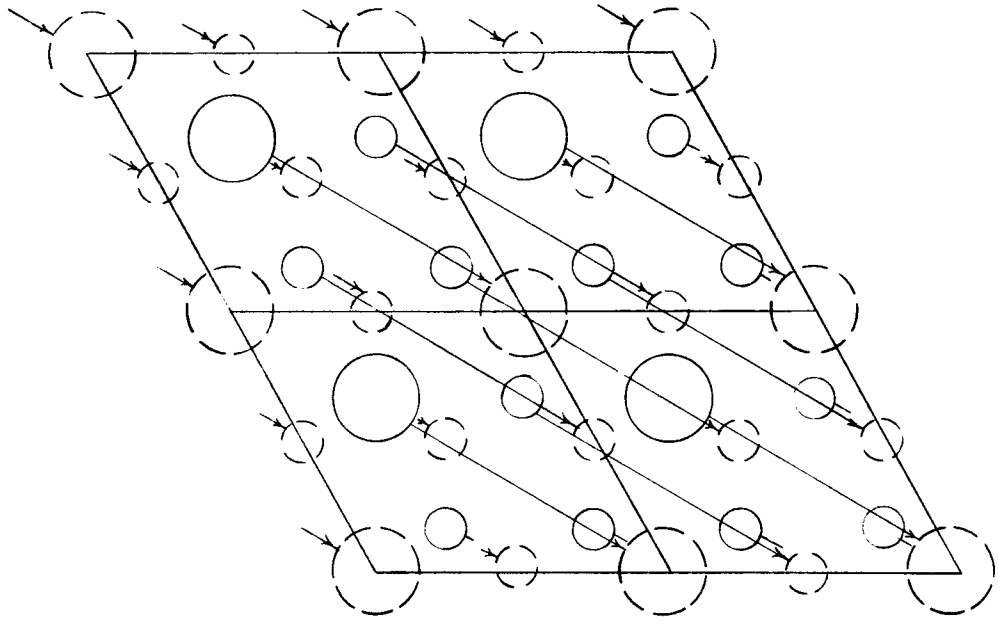

Figure 64. Transformation of Layer 17 and Layer 18.

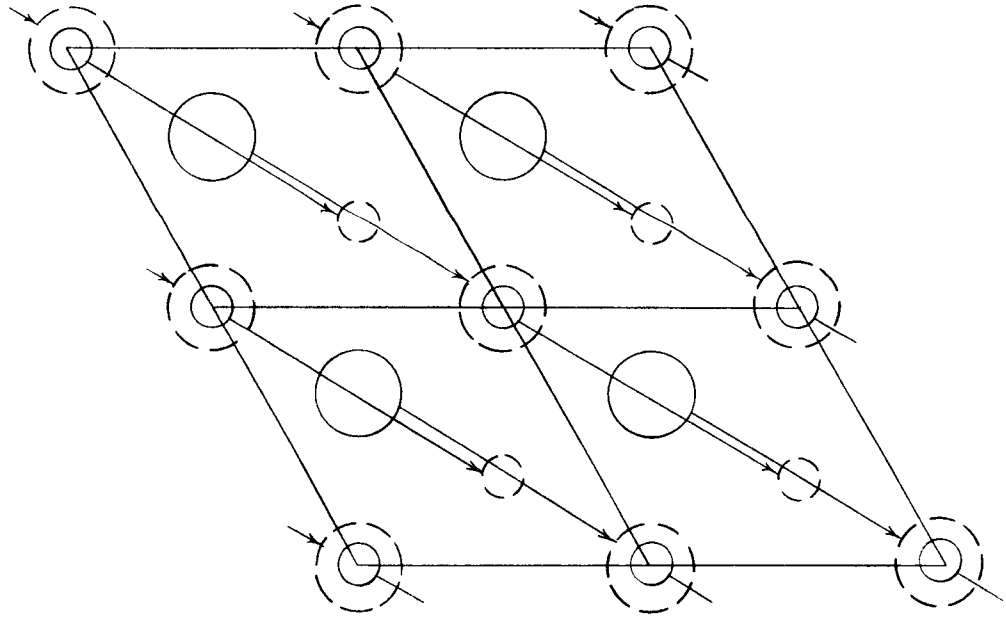

Figure 65. Transformation of Layer 19 and Layer 20.

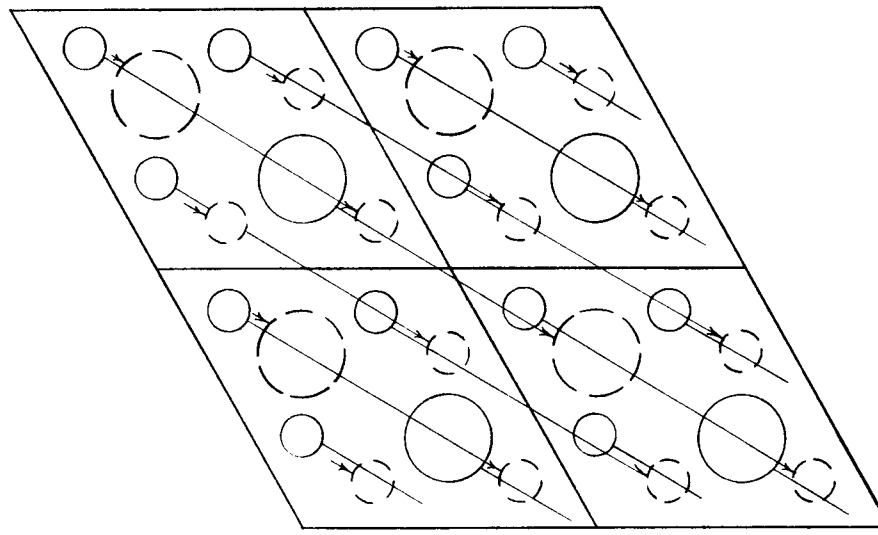

Figure 66. Transformation of Layer 21 and Layer 22.

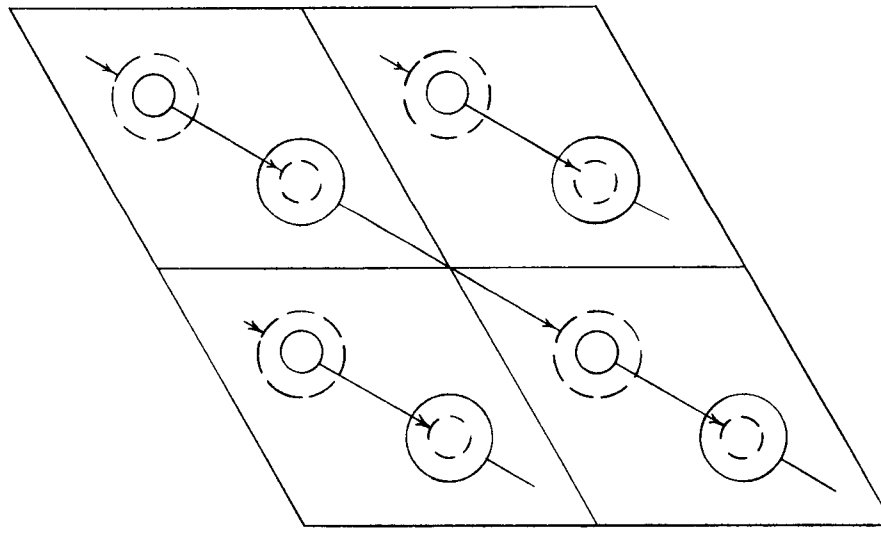

Figure 67. Transformation of Layer 23 and Layer 24.

the C-15 structure is represented by large solid circles, chromium by small circles, zirconium in the C-14 structure by large broken circles, and chromium by small broken circles. The direction and the amount of movement required of each atom during transformation from the C-15 to the C-14 structure within these four space lattices is indicated by solid arrows; the movements of the atoms to and from lattices other than these four are represented by incomplete short arrow heads or tails. Again one should notice that these circles only represent the locations of the atoms and not their sizes. Should each atom be drawn to the same scale as the lattice parameter, very little room would be left in the lattice as shown in Figure 68 which shows the scaled graph of Layers 13 and 14.

For convenience of discussion, it is assumed that one-third of the major diagonal of the lattice base is one unit of movement. The arrow between any two atomic positions indicates the initial and the final positions.

These 24 layers of atoms in two unit cells of the C-15 structure can be divided into three groups: Group 1, from Layer 1 to Layer 8; Group 2, from Layer 9 to Layer 16; and Group 3, from Layer 17 to Layer 24.

In Group 1 the atomic arrangement in every layer except Layer 8 in the C-15 structure is identical with that in the C-14 structure. Since the dimension of the major diagonal of the parallelogram is three

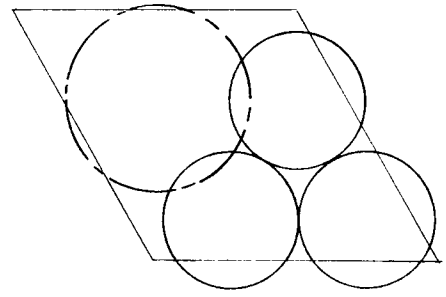

C-14

Big circle: Zirconium atom
Small circle: Chromium atom

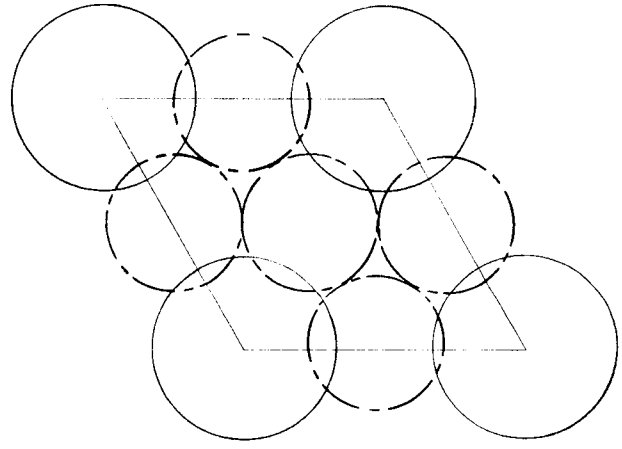

C-15

Figure 68. Scaled sketches of Layer 13 and Layer 14 in the C-14 and the C-15 structures.

units, a three-unit movement of atoms will leave the arrangement of atoms unchanged relative to the lattice. Therefore, as shown in Figure 56 to Figure 59, the amount of displacement of each layer from Layer 1 to Layer 7 is 3n, where "n" is an integer chosen sequentially from 0, 1, 2,...n, and the movement is in the direction of $[11\bar{2}]$ of the C-15 structure or $[01\bar{1}0]$ of the C-14 structure. The amount of displacement of Layer 8 is (3n-1) as shown in Figure 59.

Using the same method, and comparing each different layer of atoms in Group 2, one can see that the amount of displacement caused by the transformation from Layer 9 to Layer 15 is (3n + 1), as shown in Figure 60 to Figure 63. The amount of movement of Layer 16 is 3n, all in the $[11\bar{2}]$ direction. In Group 3 the amount of displacement of each layer from Layer 17 to Layer 23 is (3n + 2), and that of Layer 24 is (3n + 1) (Figure 64 to Figure 67).

Figure 69 represents a consolidation of all of the movements of atomic layers required to transform the C-15 structure into the C-14 structure. In this figure the $[11\bar{2}]$ direction in C-15 (corresponding to $[01\bar{1}0]$ in C-14) is the horizontal axis while the stacking sequence is represented by the vertical direction. It can be seen that the transformation of C-15 to C-14 is completed by means of shearing each group of the planes in the $[11\bar{2}]$ direction. The magnitude of displacement is one-third of the major diagonal of the lattice base relative to the neighboring group of planes. The difference between the movements of any two neighboring groups is proportional to one-third of the major

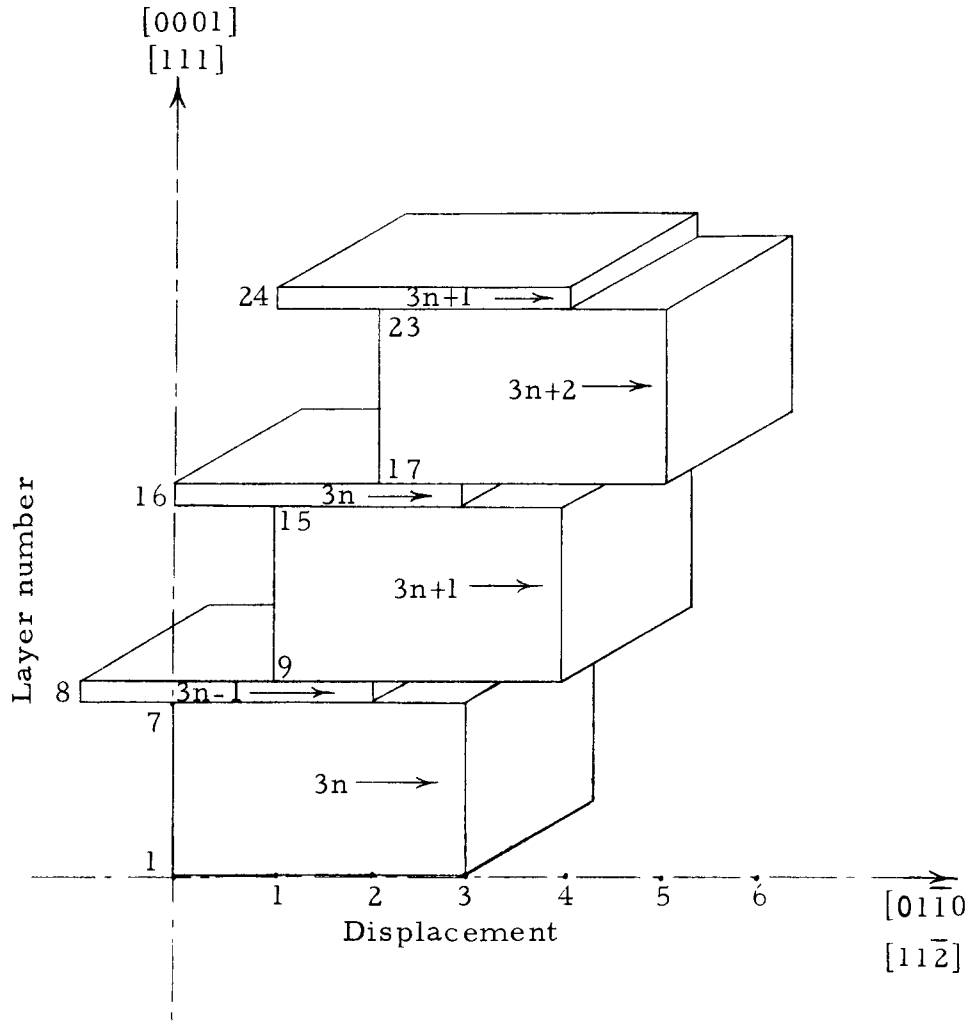

Figure 69. Schematic representation of shear transformation from C-15 to C-14.

diagonal of the parallelogram base of the unit cell. There is no relative motion between any two layers of the first seven layers within each group.

Layers 8, 16, and 24 are always displaced one unit less than the other layers of each corresponding group. This is due to the fact that the stable arrangement of chromium atoms in both crystal structures requires that a single fixed relation be maintained with respect to the tetrahedron. The abnormal movement makes it possible for the chromium atom in any one of these three layers to fit into the apex of one particular tetrahedron. Any other movement will distort the stable tetrahedral arrangement.

In conclusion the C-15 to C-14 transformation is a shear movement on the (111) plane along the $[11\bar{2}]$ direction but with a restraint of the 8th, 16th and 24th layers due to the overriding necessity to maintain the same tetrahedral lattice structure of the chromium atoms in these layers.

E. Summary Discussion

This research has demonstrated that, while most of the features of the Zr-Cr system may be accepted as essentially correct, the features having to do with the compound $ZrCr_2$ are incorrect. In this case, while crystal structures have been identified correctly, they have been assigned ranges of stability opposite to the correct ranges,

and furthermore the transformation temperature is in error.

These errors have been made because of the sluggishness of the transformation. It has been shown that the transformation temperature proposed by Rostoker (33) (about 1000°C) is not a true transformation temperature but an irreversible change from a metastable to the stable state. It also is not a single temperature because the transformation can be made to occur at a lower temperature if the time at temperature is increased. The transformation temperature, in the sense of a truly reversible reaction temperature, has been shown to be about 1600°C.

Because of the shearing mechanism involved in the transformation, one is tempted to classify the transformation as martensitic transformation. In the following paragraphs, the generally recognized (5, p. 487) characteristics of martensitic transformation as proposed by Christian (8) (9) and Troiano (1, p. 264) are compared with the characteristics of $ZrCr_2$ found in this investigation.

1) The transformation is independent of time: At constant temperature a fraction of the volume transforms very rapidly especially in carbon steel. It would appear that this characteristic is not applicable in the present case. Isothermal annealing experiments indicate that the transformation is strongly time dependent. This, however, is not a universal characteristic of all martensitic

transformations; some have been shown to be completely isothermal (5, p. 488).

2) The transformation is diffusionless: It is shown in this investigation that the transformation of $ZrCr_2$ is a kind of shear movement and no diffusion is necessary.

3) The product crystal has definite crystallographic planes and lattice orientation relationship with respect to the parent phase: The crystallographic relation between the C-14 and C-15 structures of $ZrCr_2$ has been shown as:

$$(111)_{C-15} \parallel (0001)_{C-14}$$

$$[11\bar{2}]_{C-15} \parallel [01\bar{1}0]_{C-14}$$

4) The transformation is reversible: The transformation of $ZrCr_2$ is reversible at the temperature of $1600^{\circ}C$. That the striations appear when C-14 transforms to C-15, and disappear when the reaction reverses is another proof of the reversibility of the transformation.

5) The composition remains unchanged after transformation: Metallographically, it is shown that one uniform single phase appears in both C-14 and C-15 phases. The fact that there is no occurrence of two-phase colonies (such as those that appear in the photomicrograph of eutectoid) indicates

that the same composition has been maintained before and after the transformation.

Based upon the above analyses, one concludes that the transformation of $ZrCr_2$ can be classified as a sluggish martensitic transformation. Generally speaking, the transformation of $ZrCr_2$ is very similar to the martensitic transformation of cobalt (2, 6). Two facts support this analogy: first, cobalt also has the polymorphic transformation from HCP to FCC; secondly, its movement is also along the (111) plane. The only difference is that the transformation of cobalt is in simple shear whereas that of $ZrCr_2$ is a partially restrained shear transformation.

Probably the difference in type of shear is the major cause of the sluggishness of the $ZrCr_2$ transformation. It is hypothesized that much more energy is required to complete the partially restrained shear transformation than the simple shear transformation since the motion of the former is much more complicated.

A review of Laves phases disclosed that including the Laves phase in this investigation, there are only eight among the 223 known Laves phases that have polymorphic transformations. So far as the exact manner of transformation is concerned, investigators of each of the other seven Laves phases held a different and, sometimes contradictory, conclusion as shown in Table 13. In view of the fact that the transformation of $ZrCr_2$ from C-14 to C-15 in this investigation

Table 13. Review of polymorphic transformations of some Laves phases.

Laves Phase		Summary of structure findings of different investigators	Heat treating range: Temp. °C	Soaking time, hr.	References
$HfCr_2$	(A)	C-36 with possible transformation to	600	312	(31, p. 539)
		C-14	1400	0.5	
	(B)	C-14 "as-cast" and at 1400°C	1400	4	(15)
		C-15 at 1200°C	600	48	
$HfMn_2$	(A)	C-36 at high temperature	600	312	(31, p. 681)
		Possibly C-14 at low temperature	1600	0.1	
	(B)	C-14 below 1200°C	1000	24	(15)
		Uncertain above 1400°C	1400	4	
$HfMo_2$	(A)	C-36 between 600°C and 2200°C	600	312	(31, p. 681)
		Duplex C-36 and C-15 at 1200°, 1400°, & 1600°C	1600	0.1	
	(B)	C-15 at all temperature	500	84	(15)
		Possibly C-14 below 800°C	1400	4	
$HfFe_2$	(A)	Duplex C-14 & C-15 between 600° to 1400° C	600	84	(31, p. 628)
		C-14 at 1600°C	1600	0.1	
	(B)	C-36 without transformation	600	84	(15)
			1400	4	
$TaCr_2$	(A)	C-15 above 1375° C	1375	-	(12)
		C-14 above 1375° C	1590	4	
	(B)	C-14 without transformation	600	312	(16)
			2000	0.1	
$TaCo_2$	(A)	$TaCo_2$: C-15 without transformation	600	312	(14)
		$Ta_{0.81}Co_{2.19}$: C-15 at 800°C	1200	7	
		Duplex C-14 and C-15 at 1000°C			
		C-14 at 1200°C			
$TiCr_2$	(A)	C-15 at low temperature	600	312	(14)
		C-14 at high temperature	1400	0.5	
	(B)	C-15 at low temperature transforms to C-14	800	864	(17)
		at high temperature through a two phase region	1375	5	

Note: For each compound, the summaries of two different investigators are listed, they are designated as (A) and (B) respectively.

The "Heat treating range" explains the highest and lowest temperatures as well as the longest and shortest soaking periods adopted by each investigator in his experiment. Most of the investigators made more than two heat treatments. Those temperatures in between are not listed in this table.

was completed in an extremely sluggish manner, the reason for these contradictions could possibly be that none of the investigators had any prenotion of the likelihood of a very sluggish transformation process and therefore did not develop a proper experimental procedure.

As a result of these experiments a new phase diagram for a Zr-Cr system is proposed as shown in Figure 70. The only modification is the transformation temperature of the compound $ZrCr_2$.

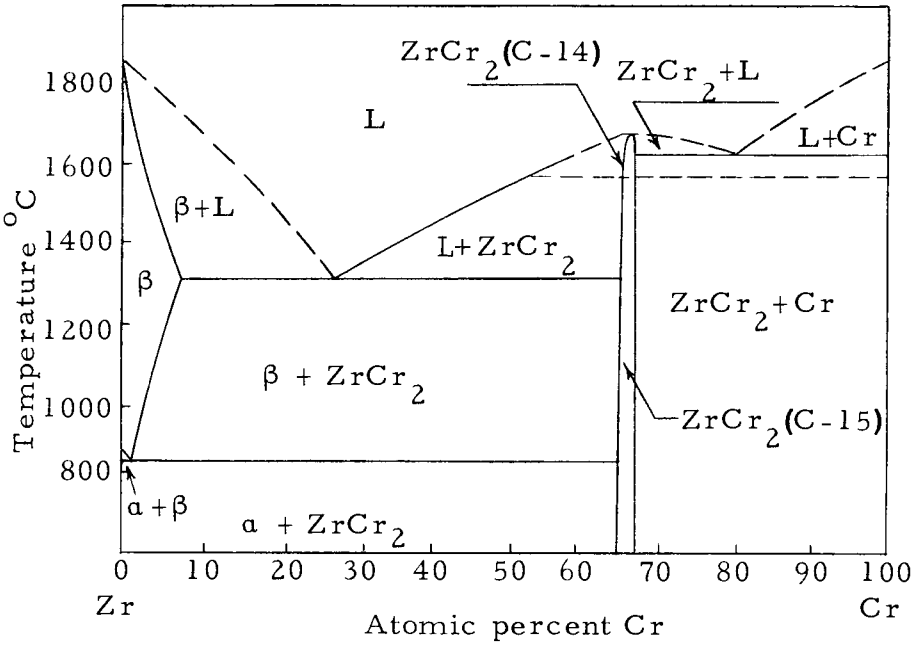

Figure 70. Proposed zirconium and chromium diagram.

V. CONCLUSIONS

A. Conclusions from the Research

1) No modification on the general features of the zirconium and chromium phase diagram is necessary. However, transformation temperature of $ZrCr_2$ should be about 1550°C as shown in Figure 70.

2) The photomicrographs indicate that a relative high anisotropy of interfacial energy seems to exist between the growth of the nuclei of $ZrCr_2$ and eutectic melt between $ZrCr_2$ and Zr.

3) Both the eutectic structures from the reaction $L \rightarrow ZrCr_2 + Zr$ and from the reaction $L \rightarrow ZrCr_2 + Cr$ are of non-lamellar type.

4) The $ZrCr_2$ compound occurs in the region between 65.97 a/o Cr to 67.32 a/o Cr. This is a very narrow composition range.

5) Other metallurgical reactions such as eutectoid and peritectoid are not likely to occur at the neighborhood of $ZrCr_2$.

6) Striations that occur in each grain after the transformation from C-14 to C-15 structure indicate that a shear type mechanism may occur in this transformation.

7) The chromium grain appears to have a higher surface tension as compared to the eutectic melt between $ZrCr_2$ and Cr.

8) A polymorphic transformation occurs in the intermetallic compound $ZrCr_2$. This transformation occurs between the

temperatures of 1550°C and 1600°C.

9) The intermetallic compound $ZrCr_2$ exists as the C-14 structure when it is above the transformation temperature and as the C-15 structure when it is below the transformation temperature.

10) The transformation from C-14 to C-15 is a very sluggish one. Ordinary cooling after alloy preparation will arrest the transformation and maintain the C-14 structure at room temperature.

11) The C-14 structure transforms gradually to C-15 at 900°C. It requires about 384 hours to complete the transformation.

12) The transformation is completed by means of rearranging atom positions through shearing mechanism. The shearing action occurs on the (111) plane of the C-15 structure or the (0001) plane of the C-14 structure. During shearing, eight layers of atoms behave as one unit. There is no relative movement between any two layers of the first seven layers. The movement of the eighth layer is restrained to maintain the stable arrangement of the crystal structure.

13) The transformation of the intermetallic compound from C-14 to C-15 can be classified as martensitic type.

14) It would appear that some modification in the electron atom theory of Elliott and Rostoker is required if the findings herein are to be included. It has been shown that the crystal structures of $ZrCr_2$ have temperature ranges of stability opposed to those used

by Elliott and Rostoker in the formulation of their theory.

B. Conclusions from the Experimental Process

1) The melting loss of the high-vapour-pressure element can be minimized if the element with low vapour pressure is melted first. The arc should be kept from striking the high-vapour-pressure element directly. The alloying should be performed in such a way that the high-vapour-pressure element gradually diffuses into the fused low-vapour-pressure element.
2) Shattering of the alloy button can be avoided if the button is made to cool off progressively from one side to the other. To achieve this, one may move the arc sideways across the button and then gradually decrease the current of the arc.
3) The quartz capsule for heat treatment can stand a temperature as high as 1600^{o}C for 45 minutes when the gas pressure inside the capsule is properly maintained.
4) To reveal grain boundaries in $ZrCr_2$, the following etching solution for electro-etching was developed: 10-gm NaOH, 10-gm $K_3Fe(CN)_6$, 100-ml water.
5) To reveal the transformation striations inside the grain of $ZrCr_2$, the following solution was developed: Swab etcing: 20-ml HNO_3, 3-ml HF, 250-ml water. The specimen is then electro-etched in 10% oxalic acid.

6) Back-reflection-Laue photographs can be taken from a grain about one square millimeter in a polycrystalline specimen by means of telescope alignment.

7) The phase distribution in Zr-Cr alloys is determined only after high temperature homogenization.

BIBLIOGRAPHY

1. American Society for Metals. Metals handbook. 8th ed. Metal Park, Ohio, 1948. 1332 p.

2. Anantharaman, T.R. and J.W. Christian. The existence of a macroscopic shear in the transformation in cobalt. The Philosophical Magazine 43:1338-1342. 1952.

3. Bardos, D.I., K.P. Gupta and P.A. Beck. Ternary Laves-phases with transition elements and silicon. Transactions of the American Institute of Mining, Metallurgical, and Petroleum Engineers 221:1087-1088. 1961.

4. Barrett, C.S. Transformation in pure metals. In: Phase transformation in solids; symposium held at Cornell University, under the auspices of the Committee on Solids of the National Research Council, August 23-26, 1948, ed. by R. Smoluchowski. New York, Wiley, 1951. p. 353-365.

5. Barrett, C.S. and T.B. Massalski. Structure of metals. 2d ed. New York, McGraw-Hill, 1966. 654 p.

6. Basinsk, Z.S. and J.W. Christian. The martensitic transformation in cobalt. The Philosophical Magazine 44:791-792. 1953.

7. Berry, R.L. and G.V. Raynor. The crystal structures of Laves phases. Acta Crystallographica 6:178-186. 1953.

8. Christian, J.W. The theory of transformation in metals and alloys. London, Pergamon, 1963. 973 p.

9. Christian, J.W., Thomas A. Read and C.M. Wayman. Crystallographic transformations. In: Intermetallic compounds, ed. by J.H. Westbrook. New York, Wiley, 1966. p. 428-449.

10. Cullity, B.D. Elements of x-ray diffraction. Reading, Mass., Addison-Wesley, 1956. 514 p.

11. Domagala R.F., D.J. McPherson and M. Hansen. System of zirconium and chromium. Transactions of the American Institute of Mining, Metallurgical, and Petroleum Engineers 197: 279-283. 1953.

12. Duwez, Pol and Howard Martens. Crystal structures of $TaCr_2$ and $CbCr_2$. Journal of Metals 4:72-74. 1952.

13. Dwight, A.E. Factors controlling the occurrence of Laves phases and AB_5 compounds among transition elements. Transactions of the American Society for Metals 53:479-500. 1961.

14. Elliott, Rodney P. A study of a family of Laves type intermediate phases. Chicago, 1954. 63 numb. leaves. (Illinois Institute of Technology. Armour Research Foundation. Technical Report no. 1. OSR-TN-247)

15. _____. Laves-type phases of hafnium. Transactions of the American Society for Metals 53:321-329. 1961.

16. Elliott, Rodney P. and W. Rostoker. The occurrence of Laves type phases among transition elements. Transactions of the American Society for Metals 50:617-632. 1958.

17. Farrar, P.A. and Harold Margolin. A reinvestigation of the chromium rich region of Ti-Cr system. Transactions of the American Institute of Mining, Metallurgical, and Petroleum Engineers 227:1342-1345. 1963.

18. Friauf, J.B. The crystal structures of two intermetallic compounds. Journal of the American Chemical Society 49:3107-3109. 1927.

19. _____. The crystal structure of magnesium dizincide. Physical Review 29:34-40. 1927.

20. Gebhardt, E. and J. Rexer: Der Aufbau des Systems $ZrCr_2$-$TaCr_2$. Journal of the Less Common Metals 11:295-296. 1966.

21. Hahnert, Von Manfred. Zur Kristallchemie intermetallischer AB_2-Verbindungen, specziell Laves-Phasen. Wissenschaftliche Zeitschrift des Humboldt-Universitat zu Berlin 24:756-770. 1962.

22. Hansen, Max. Constitution of binary alloys. New York, McGraw-Hill, 1958. 1135 p.

23. Hayes, E.T., A.H. Roberson and M.H. Daves. Zr-Cr phase diagram. Transactions of the American Institute of Mining, Metallurgical, and Petroleum Engineers 194:304-306. 1952.

24. Henry, N.F.M. and Kathleen Lonsdale. International tables for x-ray crystallography. Vol. 1. Birmingham, England, Kynoch, 1965. 558 p.

25. Hume-Rothery, W., J.W. Christian and W.B. Pearson. Metallurgical equilibrium diagrams. London, Chapman and Hall, 1953. 330 p.

26. Jordan, Charles B. and Pol Duwez. The structures of some alloys of Zr with Fe, Co, and Cr. Pasadena, Calif., 1953. 13 numb. leaves. (California Institute of Technology. Report 20-196)

27. Kehl, George L. The principles of metallographic laboratory practice. New York, McGraw-Hill, 1949. 520 p.

28. Laves, F. Crystal structure and atomic size. In: Theory of alloy phases. Cleveland, Ohio, American Society for Metals, 1956. p. 124-198.

29. McQuillan, Marion K. Surveys of the constitutional diagram of chromium-zirconium system. Melbourne, Australia, 1951. 19 numb. leaves. (Australia. Department of Aeronautical Research Laboratories. Report no. A.M. 165)

30. Pargeter J.K. and W. Hume-Rothery. The constitution of niobium-cobalt alloys. Journal of the Less Common Metals 12:366-374. 1967.

31. Pearson, W.B. A handbook of lattice spacing and structures of metals and alloys. New York, Pergamon, 1958. 1044 p.

32. Peavler, R.J. and J.L. Lenusky. Angles between planes in cubic crystals. New York, American Institute of Mining, Metallurgical, and Petroleum Engineers, n.d. 28 p.

33. Rostoker, W. Allotropy in the phase $ZrCr_2$. Journal of Metals 5:304. 1953.

34. Rundle, R.E. Theories of bonding in metals and alloys. In: Intermetallic compounds, ed. by J.H. Westbrook. New York, Wiley, 1966. p. 17-37.

35. Saybolts, A.U. and J.E. Burke. Experimental metallurgy. New York, Wiley, 1953. 339 p.

36. Walbaum, H.J. Ober weitere Zirconiumverbindungen mit Uberganselementen. Naturwissenschaften 30:149. 1942.

37. Wood, A. Elizabeth and Vera C. Campton. Laves-phase compounds of alkaline earths and noble metals. Acta Crystallographica 11:429-433. 1958.

APPENDIX

APPENDIX A

After this thesis was completed, an abstract in the Chemical Abstracts (Abstract no. 2704a, Vol. 63, 1965) was reviewed. It is an abstract of the article entitled "Equilibrium Diagram of $TiCr_2$-$ZrCr_2$", written by I.I. Kornilov, P.B. Budberg, K.I. Shakhova, and S.P. Alisova, published in the Russian magazine Doklady Akademii Nauk SSSR 161(6).

The abstract states that the equilibrium diagram "shows the formation of a continuous series of solid solutions (both with low-temperature and high-temperature modifications of title compounds)".

The article lends additional support to the finding of this investigation that the polymorphic transformation of $ZrCr_2$ exhibits C-15 at low temperature and C-14 at high temperature. According to the Hume-Rothery rules of solid solution, identical crystal structure of the components is one of the major conditions for complete solubility.